Stefan-Signorini Moving Boundary Problem Arisen From Thermal Plasma Cutting: Mathematical Modelling, Analysis and Numerical Solution

von Arsen Narimanyan

Dissertation

zur Erlangung des Grades eines Doktors der Naturwissenschaften

- Dr.rer.nat. -

Vorgelegt im Fachbereich 3 (Mathematik & Informatik)

der Universität Bremen

12. Juni 2006.

Datum des Promotionskolloquiums: 25.07.2006

Gutachter: Prof. Dr. Alfred Schmidt (Universität Bremen)
Prof. Dr. Gurgen Hakobyan (Staatliche Universität Jerewan, Armenien)

Acknowledgments

I feel most fortunate to have had the opportunity to do my PhD in the University of Bremen and enjoy the company of wonderful people I have met there.

Completing this doctoral work has been a wonderful and often overwhelming experience. I have been very privileged to have a smart and supportive supervisor and teacher, namely Prof. Dr. Alfred Schmidt. He has an ability to cut through reams of numerical PDEs that I will always admire. With his help I have learned a great deal of numerical analysis and gained a lot of programming skills. I thank Alfred Schmidt also for his invaluable time that he provided for discussions.
Many thanks goes to Prof. Dr. Michael Böhm for his remarks and advises concerning the aspects of the mathematical analysis of the present study.

I appreciate all my friends and colleagues for their kindness and support, in particular Ronald Stöver, a really nice person and an excellent friend. It is Ronald's contribution that I have got integrated in the German society very fast and learned how one should speak correct German. It has also been my pleasure to work with (and hang out with) Jenny Niebsch, Jorg Benke, Bettina Suhr, Thilo Moshagen, Serguei Dachkovski and Adrian Muntean. I thank Thilo and Bettina for their tips on the improvement of my program. The fun that we experienced with Adrian while writing our first joint paper has been one of the greatest ones during my stay in Bremen.

Last, but not least, I would like to thank my entire family, especially my parents, for their love and support. My wife, Astghik, has been my guiding light and big love over all these years. She has seen my best and my worst, and provided support, hugs and patience. Even when my emotional and research brains became so hopelessly entwined that I dreamed that the two of us have no common edges on the huge triangulation of the world, she still forgave me. Thank you, honey. I thank also my two sweet children Tatevik and Mane, who are always at my side to share my joys and sorrows and without whose patience this work would have remained just a dream.

Contents

Chapter 1

Introduction

1.1 General: the plasma cutting process

There is a wide range of thermal cutting techniques available for the shaping of materials. One example is the *plasma cutting*. The origin of plasma-arc process goes back to 1941. In an effort to improve the joining of light metals for the production of aircraft, a new method of welding was born that used an electric arc to melt the material and a shield of inert gas around the electric arc to protect the molten metal from oxidation. Figures 1.1[1] and 1.2[2]) give an impression on some typical applications of plasma cutting.

In recent years, plasma cutting of different type of metals has increasingly attracted the attention of the industry. The use of oxygen as a cutting gas and development of finer nozzles have allowed plasma devices to offer a very high cutting quality. It is cheaper than the laser cutting and has an important advantage, namely, by choosing the appropriate plasma gas, one is able to use the plasma technique for cutting more inert metals. The cutting of a workpiece occurs as a result of melting/vaporizing the material by an extremely hot cylindrical plasma beam which burns and melts its way through the material, leaving a kerf in its wake.

The heat transfer from the plasma jet into the material accounts for most of the phenomena encountered subsequently: shrinkage, residual stresses, metallurgical changes, mechanical deformations, chemical modifications, etc.

One of the main problems occurring as a result of heat transfer from the plasma beam to

[1]Picture is taken from www.torchmate.com/automate/cncdemo.html
[2]Picture is taken from www.rtgstore.com/art

Figure 1.1: Plasma cutting process

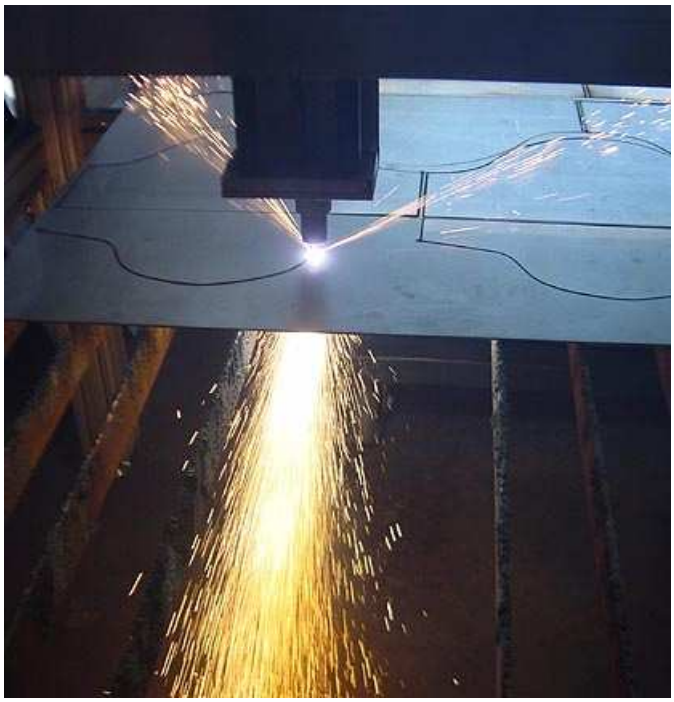

Figure 1.2: Another application of plasma cutting

the workpiece is the deformations of the cut edges after the material is cut and cooled down. Due to these deformations, the cut edges are not square any more which makes a lot of difficulties during the further applications of the metal. On the other hand, the speed of moving plasma beam can cause a formation of high or low speed drosses, which is another problem as the removal of the dross is an additional operation that increases the cost of the cutting. This issue leads to a problem of optimization of parameters entering the process and could be another aspect for mathematical modelling.

Investigations are needed for the prediction and control of the above mentioned phenomena concerning the plasma arc cutting process. To get a quantitative description of the process, one requires a mathematical model for it. Therefore a proper mathematical model has to be developed which must involve the different physical phenomena occurring in the workpiece during the cut, i.e. heat conduction, convection and radiation effects, mechanical deformations, phase transition, etc. The model has then to be numerically simulated, and the results of the simulations have to be verified by experiments.

1.2 Overview of the work

Our overall goal is to develop a general model including physical and mathematical modelling of thermal plasma cutting, which will serve as an important tool for understanding the observable problems.
In this work we are mainly involved in the development of a mathematical model describing the temperature distribution in the workpiece and the evolution of the geometry of the cutting front during the thermal cutting. This is a very important step towards the modelling of the whole process. The workpiece temperature plays a major role during the cutting as it later affects material deformations and is responsible for most problems arising in industry.
Let us outline the contents of the chapters. At the beginning of each chapter we have tried to give a brief introduction on the subject of the chapter in order to make the study more self-contained.
We start Chapter 2 by giving a brief description on thermal cutting of metals and stating some industrial problems arising during the cutting. The study then continues with the discussion of physical modelling of the process.
In Chapter 3 we are concerned with the mathematical modelling of the workpiece. There

we begin with a development of an one dimensional model. It may happen that the area of industrial applications for one dimensional models is limited, but this modelling is very useful to understand the main aspects of the problem description and apply them for the cases of higher dimensions. The main result in Chapter 3 is the establishment of a mathematical model for higher space-dimensions. At the end of the chapter we review some earlier results on the modelling of the heat flux density due to the plasma beam and describe a way to calculate the flux density on the absorbing surface.

In Chapter 4 we develop function spaces that are used in the weak formulation of the cutting model. Using the main concepts of Lebesgue functional spaces we define spaces commonly referred to as Soboloev spaces.

Variational formulation of the problem is the subject of Chapter 5. The cutting model belongs to the subclass of problems which are relatively easy to convert into variational inequality. We show how the nonlinear Signorini boundary conditions make it possible to rewrite the heat conduction equation in the form of variational inequality. As for the problem of determining the geometry of the cutting front, which is described by a Stefan boundary condition, we introduce the cutting front as a zero level set of a scalar function which takes care of all topological changes of the moving interface. At the end of the chapter we formulate the cutting model in its weak form as a coupled system consisting of a variational inequality (for calculating the temperature field) and a transport equation (for determining the cutting front).

Chapter 6 deals with the mathematical analysis of the weak model. Besides the nonlinear Signorini and Stefan boundary conditions occurring in the mathematical model, the time dependent domain of interest (the workpiece) makes essential difficulties for the mathematical treatment. Here also we begin with the analysis of one dimensional model. Main contribution of the chapter is the analysis of the coupled system using the principles of the theory of variational inequalities and analytical results from the study on general Hamilton-Jacobi equations.

One of the main difficulties to solve the cutting problem numerically is the time dependent domain. In Chapter 7 we specify a numerical method for the calculation of the numerical solution of the cutting model based on the modified Stefan-Signorini problem. In order to overcome the difficulties connected with the time dependent domain, we decouple the problem at each time step via defining the domain occupied by the workpiece explicitly

with the help of the level set function from previous time step. The space discretization for both heat conduction equation and level set equation is implemented by means of Finite Element Methods. For implementation purposes the software package *ALBERTA* is used, which is well suited for the problems in several space dimensions. It is flexible enough to switch between different dimensions easily, therefore the extension of simulations to the three dimensional case is relatively easy to implement.

In order to keep our work preferably self-contained, we include three appendicies in our work, which provide some introductory information on viscosity solution methods, finite element methods and ALBERTA.

Chapter 2

Problem statement and physical modelling

Plasma cutting is desirable for many metal cutting and welding applications. It can be performed on any type of conductive metal - mild steel, aluminium, stainless and carbon steel are some examples. Unlike other type of cuttings, plasma cutting can be used on any metal for applications such as stack cutting, bevelling, shape cutting, gouging and piercing. Plasma cutting can be successfully performed on a variety of material sizes as well; it can be used to cut anything from thin gauge aluminium to stainless and carbon steel up to several centimetres, depending upon the power of the cutting machine.

2.1 Device description

Before we start with the description of plasma cutting device, let us try to understand the meaning of the plasma itself. So, what is a plasma? When we are asked about the three states of the matter, we normally think of solid, liquid and gas. Consider, for example, water. The three states of this matter are ice, water and steam. If we add enough energy to an ice block, it will change from solid ice to liquid water. If we keep on adding more heat energy, the water vaporises resulting in steam (gas). When substantial heat is added to a water steam, it will change its phase one more time, namely from gas to *plasma*, which is usually called the fourth state of the matter. This last phase change is a result of ionisation, i.e. creation of free electrons and ions among the gas atoms. The presence of free electrons

as carriers of current makes the plasma electrically high conductive.

The main principles that apply to current conduction through metals also work in the case of plasma. For instance, we know that if we reduce the cross-section of a metal which carries the current, the resistance in the metal increases resulting in the heating of the metal. The same is true for a plasma gas: the more we reduce the cross-section of its flow,

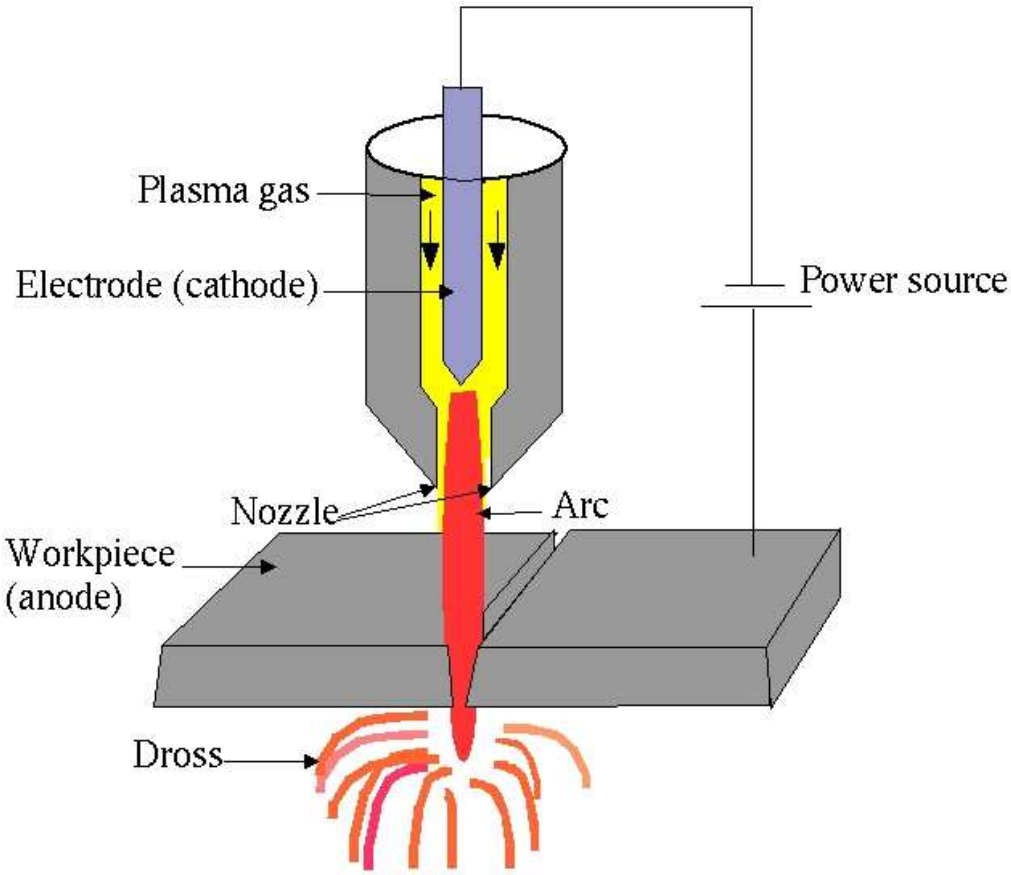

Figure 2.1: Schematic thermal plasma system

the hotter it gets. Thus, the heat source for plasma cutting is a high temperature and high velocity stream of partially ionized gas. The plasma stream appears as a result of a current which passes between a cathode and an anode. Due to the current, the plasma gas (mixture of nitrogen, hydrogen and argon) is heated to high temperatures and the Lorenz forces propel it down towards the anode in the form of high velocity jet. A schematic of the plasma cutting device is presented in Figure 2.1. It is mainly composed of a cathode, nozzle, plasma gas and current source. Here the role of the cathode is overtaken by the

electrode, while the workpiece acts as an anode. The hot plasma gas passing through the nozzle generates a high temperature jet, which is then used for cutting or welding purposes. Typical plasma temperatures are in the range of $10,000$K to $30,000$K and the velocity of the plasma jet can approach the speed of sound. The plasma forming gas is usually argon, argon-$H2$ or nitrogen. Depending on the type of the plasma gas used, material and thickness of the material, the speed of the cut can vary from 76.2cm/min to 750cm/min. The cutting gauge does not exceed 1.5cm.

2.2 Thermal cutting process and industrial problems

The essential idea of cutting is to focus a lot of power onto a small area of surface of the material producing intense surface heating. First the material on the surface melts and then evaporates. As the vapor is puffed away or the molten metal is removed by the high speed gas flow, so a hole develops in the material. The characteristics of the plasma jet highly depend on the used gas type, gas flow rate, arc current, arc voltage, nozzle size and speed of the torch. For example, if we sufficiently increase the gas flow rate, the velocity of the plasma jet will be so high that it will be able to remove the molten metal appeared by the heating, thus resulting in a development of a cut cavity through the workpiece. If we take a low gas flow rate, then the plasma jet becomes a highly concentrated heat source which can be effectively used for welding purposes.

As the plasma cutting advances by melting, a characteristic feature is the greater degree of melting towards the top of the workpiece resulting in top edge rounding and poor edge squareness. Top edge rounding is a slight rounding of the metal along the top edge of the cut and is mostly effected by material thickness. It is more apparent in thinner metals. The poor edge squareness causes additional difficulties on the next step in the manufacturing process. See Figure 2.2. If the cut piece has to be welded, a high quality cut with square edges is especially important for the integrity of the weld. One of the characteristics of the cut is the speed with which the plasma jet moves with respect to the workpiece. This speed is the main responsible for another problem in industry, namely, dross formation. If the cutting speed is slightly less than some maximum value (with a speed higher than this value no cut is possible), an undesirable phenomenon occurs. Some of the molten material does not leave the workpiece and sticks to the bottom forming the so called high-speed dross (see Figure 2.2). In some cases it is possible to get rid of the high-speed dross by reducing

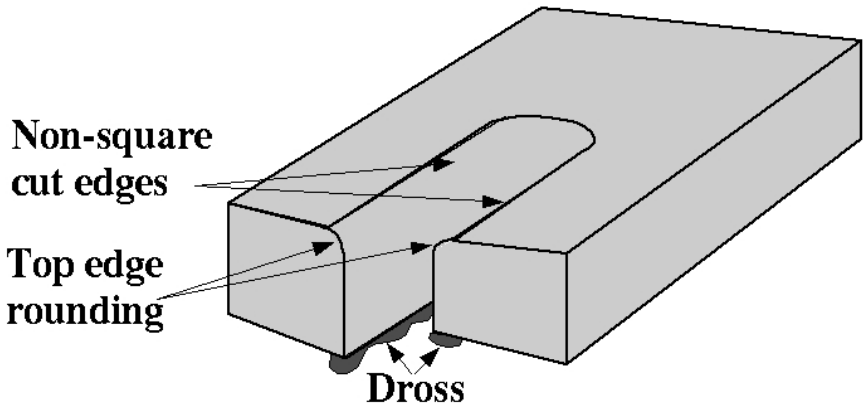

Figure 2.2: Some typical industrial problems

the speed of the cutting. However, if the cutting speed is too slow, the cutting kerf gets wider and it gets harder for the assisting gas to blow away the molten metal. So, further reduction in cutting speed below some limit once more leads to dross formation. This is the so-called low-speed dross. In both cases the removal of dross is an additional operation which increases the cost of cutting. The problem of dross formation is beyond the subject of present study. We refer to the work of Nemchinski [36] and references therein for more detailed discussions.

2.3 Physical modelling

Let us start with a small discussion on physical processes taking place during plasma cutting. Consider a high-power plasma beam striking a small area of metal surface. Shown in Figure 2.3 is a schematic illustration of the plasma cutting process. The figure shows the plasma beam penetrating through the workpiece, the advancing hole and different physical phenomena taking place in the material.

The first phenomenon we can observe is the absorption of the energy by the material. The absorption takes place within a thickness usually much less than a millimetre, so we can consider surface heating only. The temperature of the material surface does not rise infinitely. Part of the heat input from the plasma beam melts the metal resulting in solid-liquid phase change in the areas close to the source. When a material melts, latent heat is absorbed without any further rise in temperature. The second part of the heat is

transfered into the workpiece by conduction from hotter to colder metal resulting in rise of the temperature in the material.

Next physical process is due to the fact that the plasma beam pierces through the workpiece with some constant velocity, while the high velocity gas flow removes the molten material from the bottom of the cut, or the kerf.

An interesting phenomenon is the so-called solid-solid phase change. Actually, some parts of the material are heated up to very high temperatures (below the melting temperature though) forcing the formation of one solid phase (austenite, say), which can be later changed to another solid phase (pearlite, martensite, etc.) after we cool down the material to relatively low temperatures.

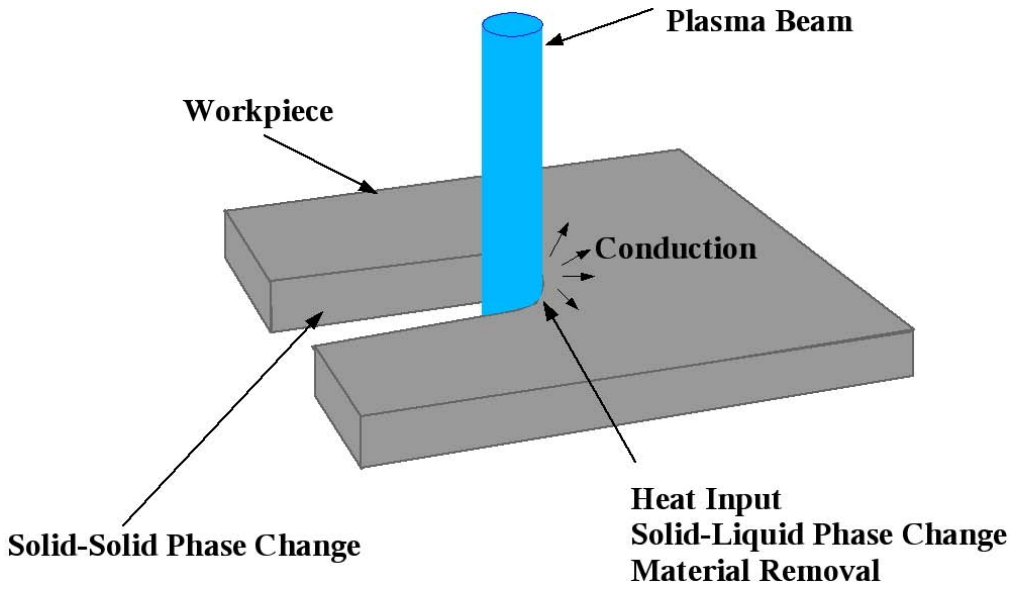

Figure 2.3: Picture of thermal cutting

In addition to high energy radiation generated by plasma, the intense heat of the beam creates substantial quantities of fumes and smoke from vaporizing metal in the kerf.

In this study we are mainly concerned with the problem of heat transfer and temperature distribution in the workpiece during the thermal plasma cutting. The problem is solved, if it is possible at any moment to identify the temperature of every point of the workpiece and the geometry of the workpiece. To be able to advance with our purposes, several modelling assumptions have to be made. The assumptions are imposed to overcome the mathematical

difficulties met from the analysis of the model. As we will see later, even with these kind of simplifications we are led to a relatively complicated mathematical model needing strong mathematical tools to analyse it and, finally, solve it by applying some numerical techniques. Assumptions are made as follows:

1. The workpiece is homogeneous and isotropic.
2. The material parameters (density, heat capacity, conductivity, etc.) of the workpiece are constant.
3. If the piece is large, then the heat exchange through the surface to surrounding can be neglected in regard to the heat flow in the material itself. This assumption makes sense because the heat conductivity of metals is much greater than the heat transmission through the surface.
4. The plasma beam has a cylindrical shape, and the heat flux from the plasma beam is emitted only in the normal direction to the surface of the cylinder.
5. The plasma device moves at a constant velocity with respect to the workpiece.
6. The heat flux density emitted by the plasma beam is constant and given;
7. The heat lost by radiation is negligible.
8. The effects of gravity and surface tension are negligible;
9. We neglect the thermal and mechanical effects caused by solid-solid phase changes.
10. We do not consider the side effects caused by the smoke of the vaporizing metal. By side effects we mean that, for example, the evaporated material does not interfere with incident plasma beam.

Chapter 3

Mathematical modelling

3.1 Introduction

As it was already mentioned in the previous chapter on physical modelling, the workpiece temperature plays an important role during the cutting process as it affects the material deformations. Thus, the effects of externally applied heat source on the temperature distribution of the workpiece become essential. Therefore, the ability to predict the temperature distribution in the workpiece is the first (and an important) step in the quantitative description of the cutting process. On the other hand, due to the fact that during the cutting material removal takes place (the molten material is immediately removed), the domain occupied by the workpiece changes in time. Therefore, the prediction of the geometry of the material, as the cutting advances, is another important issue to be investigated.
Having in mind the assumptions formulated in the previous chapter, the heat transfer in the workpiece and changes in the shape of the material during the plasma cutting can be modelled by non-stationary partial differential equations together with corresponding initial and boundary conditions.
The mathematical model should mainly include the

- temperature field analysis in the workpiece,
- effects of cutting on the geometry of the cut pieces,
- investigation of the properties of the material due to the solid-liquid phase change.

Although the present study is done for plasma cutting processes, the developed mathemati-

cal model is rather general and does not depend on the type of cutting. Any cutting process is a thermal process and involves diverse effects resulting from the heat input on the material surface. Important is the amount of energy absorbed by the workpiece which depends on the thermo-physical properties of the material as well as on the several parameters of the heat source (strength, moving speed, etc). Changing the appropriate parameters in the model makes it possible to consider *any type* of thermal cutting process.

3.2 Literature review

Before we start with the modelling of the workpiece, let us briefly summerize some earlier works concerning the subject. There is a vast number of scientific publications concerning different aspects of mathematical modelling of thermal cutting. Here is a short list of related works.

1. The work of Hafercamp et al. on numerical modelling of thermal plasma cutting, [19], has been the starting point of present work. A numerical model to calculate the heat input and temperature distribution into a workpiece due to a plasma arc cut process is described in the paper.

2. In his pioneering work [40] on mathematical theory of heat distribution during welding and cutting, Rosenthal outlines the fundamentals of the theory and derives solutions for linear two- and three-dimensional flow of heat in solids. He discussed point, linear and plane sources of heat. In the work the quasi-stationary state of the piece is described, i.e. the state where the temperature has no time dependence any more. This is reached via the transformation of coordinate system by taking $\xi := x - vs$ (v is the velocity of the moving source) and application of quasi-stationary assumption. It has been also shown that despite their apparent dissimilarity, both the welding and cutting processes may be traced to the same fundamental problem, namely, the problem of heat distribution due to the motion of heat source and the quasi-stationary state created thereby.

3. Schulz et al., [47], described the cutting process of the workpiece. The discussions have been done for a 3D free boundary problem for the motion of one phase boundary. In their work material is divided into three regions: cut edge, melting front and the rest of

the material. As a model, the heat conduction equation is written with the boundary conditions on these regions. The authors gave an ODE approximation for the PDE problem, which describes the dynamics of the process by means of the position of the moving boundary, heat content of the workpiece and the surface temperature. They also presented the variational formulation and solved the equation for the one dimensional case.

4. In his paper [29] Matsuyama deduced two basic equations; first to estimate the factors of area generation rate of cut surface, and second, to calculate the influence of the input heat characteristics on the kerf shapes and the relationship between the cutting speed and the cut thickness. The basis is the heat conduction equation applied in the quasi-stationary state.

5. The mathematical model, developed by Shen et al., [48], consists of two steps; before melting and after melting. The heat equation with corresponding boundary conditions is written for both steps. In the second step in addition to the conduction in the solid, the heat conduction in the already melted region is described. The analysis is done for one spatial dimension.

6. Kim, [27], considered an unsteady heat transfer model that deals with the metal-cutting process using a continuous Gaussian laser beam. Again the boundary was divided into three regions and the boundary conditions were written for each part. The numerical simulations were done using the time dependent boundary element method.

7. The article of Xi and Kar [56] deals with an one-dimensional heat conduction problem and investigates the melting rate during laser materials processing. The problem is solved approximately to obtain a correlation among melt depth, power density and laser irradiation time. A relationship between the melt depth, power density and an average melting velocity are expressed by simple analytic formulas.

8. Storti, [53], discussed a fixed domain numerical scheme for ablation problems based on the enthalpy formulation. He introduced the region where the material has been removed as a fictitious domain with appropriate material parameters (null specific

heat and arbitrary conductivity). The resulting model is then developed via two-phase Stefan problem.

9. In their paper Friedman and Jiang, [16], formulated the melting problem of an one dimensional slab as a Stefan problem with Signorini boundary conditions at the moving boundary. Thereby they established existence and uniqueness theorems as well as studied the regularity and some geometric features of the free boundary.

10. In [55] Bui An Ton considered a Stefan-Signorini problem with set-valued mappings in bounded domains where he imposed intersecting fixed and free boundary conditions. This problem arises in the study of heat conduction in melting solids. He proved the existence of a weak solution of Stefan-Signorini problem and showed the continuity of the moving interface.

3.3 Mathematical modelling – one dimensional case

We start the mathematical modelling of the cutting process with first considering the one-dimensional case. Let us imagine that we have a solid slab consisting of one material, extending from $x = 0$ to $x = L$, and having an initial temperature distribution θ_0 which is less than the melting temperature θ_m. Now we start to heat the slab by concentrating an amount of heat on the left face $x = 0$. Let the rate of heat flow per unit area be $j_{abs}(t)$. If $j_{abs}(t)$ is big enough and if heating continues long enough, then the temperature at $x = 0$ increases and reaches the melting temperature θ_m, thus starting the melting process of the solid slab. During the thermal cutting the molten material has to be immediately removed, say by being blown away. Therefore, it makes sense to assume here that the liquid material is removed immediately on formation. It is clear that after some period of time, say at time instant t, the face of the solid being initially at $x = 0$, will move forward, to a position $x = s(t)$. If the temperature is strictly less than θ_m at the left endpoint of the slab, the material stops melting; then due to the heat flow (e.g. plasma beam) $j_{abs}(t)$ melting will resume again, the resulting molten material is immediately removed, etc. The quantities of interest are the temperature of the solid $\theta(x, t)$ and the location of the advancing face $x = s(t)$ which we call the free boundary.

The mathematical model governing the melting problem described above looks as follows:

Problem 3.3.1. *Find the temperature distribution $\theta(x,t)$ in the solid region and the melted thickness $s(t)$ such that the one-dimensional heat equation is fulfilled*

$$\rho c_s \frac{\partial \theta}{\partial t} = \frac{\partial}{\partial x}\left(k\frac{\partial \theta}{\partial x}\right), \qquad s(t) < x < L, \quad 0 < t < T, \tag{3.1}$$

where ρ is the density of the slab, c_s is the specific heat and k is the heat conductivity of the material,
with boundary conditions on $x = s(t)$ in the form of inequalities

$$\begin{aligned} \theta &\leq \theta_m \\ -k\frac{\partial \theta}{\partial x} + j_{abs}(t) &\geq 0 \\ (\theta - \theta_m)\left(k\frac{\partial \theta}{\partial x} + j_{abs}(t)\right) &= 0 \end{aligned} \tag{3.2}$$

called the **Signorini** *boundary conditions, and*

$$-k\frac{\partial \theta}{\partial x} + \rho L_m s'(t) = j_{abs}(t) \qquad 0 < t < T \tag{3.3}$$

named the **Stefan** *boundary condition. Here L_m is the latent heat of melting, equal to the minimal portion of energy necessary for transforming the bulk of unitary mass of the substance from the solid state to liquid at the constant melting temperature θ_m.*
Further we assume that the right endpoint of the slab $x = L$ is insulated, i.e. no heat flux through that endpoint is possible

$$\frac{\partial \theta}{\partial x} = 0, \qquad x = L, \quad 0 < t < T. \tag{3.4}$$

As for initial conditions, we set

$$\theta(x,0) = \theta_0(x) < \theta_m \qquad 0 < x < L, \tag{3.5}$$

and

$$s(0) = 0. \tag{3.6}$$

To understand the background of the boundary conditions (3.2), we consider two different situations for the point on the boundary:
1. Select all points of the solid boundary, at which $\theta(x,t) < \theta_m$, i.e. the temperature on the left boundary is less than the melting temperature. This situation corresponds to the *heating phase*, namely, the end point of the material absorbs energy coming from the heat

source and completely conducts it into the slab. As a result, the boundary point heats up. The condition of complete conduction can be written as

$$-k\frac{\partial\theta}{\partial x} + j_{abs}(t) = 0,$$

meaning that the heat input from the external source is equal to the heat conducted into the material.

2. Select all points of the solid boundary such that $\theta(x,t) = \theta_m$, i.e. the temperature on the left boundary is equal to the melting temperature. This situation corresponds to the *melting phase*, namely, the end point of the material is melted and must be removed. The boundary condition for melting can be expressed as

$$-k\frac{\partial\theta}{\partial x} + j_{abs}(t) > 0,$$

meaning that the energy input from the heat source is greater than the amount of heat conducted. Indeed, this is clear, since part of the heat input is used for melting the material (latent heat is absorbed) and only a part of it is conducted.

Summing up both situations, we obtain the following conditions on the boundary of the slab

$$\theta(x,t) < \theta_m \;\Rightarrow\; -k\frac{\partial\theta}{\partial x} + j_{abs}(t) = 0,$$
$$\theta(x,t) = \theta_m \;\Rightarrow\; -k\frac{\partial\theta}{\partial x} + j_{abs}(t) > 0,$$

which is nothing else but the Signorini boundary conditions (3.2).

As for the Stefan boundary condition (3.3), it follows from the energy conservation law by its application to elementary volumes that contain both sides of the boundary at the same time. More precisely, let us assume that the interface point moves with velocity v, j_{abs} is the heat flux density absorbed by the slab boundary, and by q_c we denote the heat flux conducted in the solid phase. Latent heat is absorbed at a rate $-\rho L_m v$. The heat exchanged by the interface $x = s(t)$ itself through left endpoint is equal to $(j_{abs} - q_c)$. Applying the energy conservation law, we obtain

$$j_{abs} - q_c = -\rho L_m v.$$

This yields (using Fourier's law, $q_c = -k\frac{\partial\theta}{\partial x}$, and the identity $v = s'(t)$) the Stefan condition on the moving interface

$$-k\nabla\theta\cdot\nu + j_{abs} = \rho L_m v,$$

which is exactly the same as the condition (3.3).

3.4 Mathematical modelling – higher dimensional case

We first state the assumptions that are necessary to consider in order to give sense to our higher dimensional model.

Let Ω be an open and bounded domain in $\mathbb{R}^n$, $n = 2, 3$, occupied by the workpiece. The boundary $\partial\Omega$ of the domain is assumed to be piecewise smooth. Let $0 < T < +\infty$ be given, denote by $\theta(x,t)$ the temperature of the workpiece and I the time interval $(0,T)$. The initial temperature distribution of the workpiece is given by $\theta_0(x)$, which is less than the melting temperature at all points. For every $t \in I$ the domain Ω is assumed to consist of two non-intersecting parts, namely $\overline{\Omega} = \overline{\Omega_s(t)} \cup \overline{\Omega_c(t)}$, where $\Omega_s(t)$ and $\Omega_c(t)$ are the domains occupied by the solid part of the workpiece and cut cavity at a time instant t, respectively. Let $\partial\Omega_s(t)$ be the boundary of the time dependent domain $\Omega_s(t)$ at time t (free interface) and we assume that $\partial\Omega_s(t)$ is a Lipschitz curve. By ν we shall denote the unit outward normal vector of the domain $\Omega_s(t)$. Let j_{abs} be the heat flux density absorbed by the interface due to the plasma beam radiation. In addition to the terms defined above we will use the following notations (alike the one-dimensional case): ρ is the density of the workpiece, c_s is the specific heat, k is the heat conductivity of the material, L_m is the latent heat of melting, θ_m is the melting temperature, $v \geq 0$ is the velocity of the free interface. Finally, we denote

$$\Omega_T := \{(x,t) \mid x \in \Omega_s(t),\ t \in I\}.$$

With the above mentioned notations and assuming no heat exchange between the workpiece and the exterior through $\partial\Omega_s(t)$, the classical mathematical formulation of the problem can be formulated as follows:

Problem 3.4.1. *Find the function $\theta(x,t) \in \mathbb{C}_1^2(\Omega_T) \cap \mathbb{C}(\overline{\Omega_T})$, representing the temperature of the body, and the piecewise smooth surface $\partial\Omega_s(t)$ representing the free boundary of the solid domain $\Omega_s(t) = \{x;\ \theta(x,t) < \theta_m\}$ such that the heat conduction equation is fulfilled*

$$\rho c_s \frac{\partial\theta}{\partial t} = \nabla \cdot (k\nabla\theta) \qquad \text{in } \ \Omega_T, \tag{3.7}$$

with the following boundary conditions on $\partial\Omega_s(t)$:

$$\begin{aligned} \theta &\leq \theta_m \\ j_{abs} - k\nabla\theta \cdot \nu &\geq 0 \\ (\theta - \theta_m)(j_{abs} - k\nabla\theta \cdot \nu) &= 0 \end{aligned} \tag{3.8}$$

called the **Signorini** *boundary conditions and*

$$k\nabla\theta \cdot \nu - \rho L_m v \cdot \nu = j_{abs}, \tag{3.9}$$

named the **Stefan** *boundary condition.*
As for the initial conditions, we set

$$\theta(x,0) = \theta_0(x) < \theta_m, \qquad x \in \Omega, \tag{3.10}$$

$$\Omega_s(0) = \Omega. \tag{3.11}$$

Like in the one dimensional case, here also we try to interpret the boundary conditions (3.8) by considering two sets of points on the boundary $\partial\Omega_s(t)$:
1. All those points x on the boundary, at which

$$\theta(x,t) < \theta_m, \tag{3.12}$$

i.e. the temperature on some part of the boundary is less than the melting temperature. Cut edges behind the plasma jet or boundary surface, where no direct heat input takes place, are two sets of boundary points at which the strict inequality (3.12) is satisfied. At these points of the material the surface absorbs energy coming from the heat source and completely conducts it into the workpiece. As a result, surface heating takes place. The condition of complete conduction can be written as

$$j_{abs} - k\nabla\theta \cdot \nu = 0,$$

meaning that the heat input from the plasma jet is equal to the heat conducted into the material.
2. Select all points x on the solid boundary such that

$$\theta(x,t) = \theta_m, \tag{3.13}$$

i.e. the temperature at the points of boundary is equal to the melting temperature. The area of the cut edges very close to the plasma jet is a good candidate for being part of the boundary fulfilling (3.13). On this part of the boundary melting of the material takes place. The boundary condition for melting can be expressed as

$$j_{abs} - k\nabla\theta \cdot \nu > 0,$$

meaning that the energy input from the heat source is greater than the amount of heat conducted. Indeed, this is clear, since part of the heat input is used for melting the material (latent heat is absorbed) and only a part of it is conducted.
Summing up both cases, we obtain the following conditions on the boundary of the workpiece

$$\theta(x,t) < \theta_m \;\Rightarrow\; j_{abs} - k\nabla\theta\cdot\nu = 0,$$

$$\theta(x,t) = \theta_m \;\Rightarrow\; j_{abs} - k\nabla\theta\cdot\nu > 0,$$

which yields the Signorini boundary conditions (3.8).
The boundary condition (3.9) is referred to as the *Stefan condition* and follows from the energy conservation law by its application to elementary volumes that contain both sides of the boundary at the same time. More precisely, let us consider an element $d\gamma$ of interface that moves with velocity v, and denote by j_{abs} the heat flux (per unit surface) absorbed by the solid boundary and by q_c the heat flux conducted in the solid phase. Latent heat is absorbed at a rate $-\rho L_m v\cdot\nu d\gamma$. The heat exchanged by the interface $\partial\Omega_s(t)$ itself through $d\gamma$ is equal to $(j_{abs} - q_c\cdot\nu)d\gamma$. Applying the energy conservation law to the elementary surface $d\gamma$, we obtain

$$(j_{abs} - q_c\cdot\nu)\, d\gamma = -\rho L_m v\cdot\nu d\gamma.$$

This yields (dividing both sides by $d\gamma$ and using Fourier's law) the Stefan condition on the moving interface

$$k\nabla\theta\cdot\nu - \rho L_m v\cdot\nu \;=\; j_{abs}, \tag{3.14}$$

which is nothing else but the condition (3.9).

Remark 3.4.1. *The heat flux density j_{abs} and v are equal to zero on the part of boundary where no heat input takes place. Therefore, on that part of boundary we have homogeneous Neumann conditions.*

Remark 3.4.2. *The idea behind the Stefan boundary condition is relatively simple; the total heat flux absorbed by the interface is divided into two parts: one part is conducted and the other part is used to melt the material.*

Note, that both Signorini and Stefan boundary conditions are non linear. At each fixed instant t there exist two regions: in one region we have heating phase, on the other melting phase. Moreover, these regions are not prescribed, resulting in a "free boundary problem".

Remark 3.4.3. *The Problem 3.4.1 could be referred to as an one phase Stefan problem, although there are some important differences between them. The one-phase Stefan problem represents a special case of the classical two-phase formulation, with the temperature being constant in one of the phases, assuming the melting value. Here we have a different situation. First of all, we can not assume the value of the temperature in the cavity (where the melt is removed) equal to the melting temperature of the solid, because otherwise the cut edges will continue to melt and move forward, which does not correspond to the real situation of plasma cutting. Secondly, in our problem an additional heat source (plasma beam) is applied on the surface of the moving front and the heat flux at the interface enters the Stefan boundary condition which is not the case in classical one-phase Stefan problem.*

3.5 Heat flux due to the plasma beam

A feature common to most plasma and laser cutting processes is that they occur as a result of removing the material by melting and/or vaporization as intense laser light or a high-temperature, partially ionized plasma gas stream interacts with the material surface. The amount of heat generated by plasma arc or laser beam plays a very important role in the kinetics of thermal cutting processes. Let us first present some earlier studies on the matter. In relation to the measurable quantities (current voltage and power) Rosenthal [40] has made a study of the plasma arc and found that the energy delivered to the workpiece Q_w represents about 65% of the total energy Q_t supplied by the arc. We express it in formula by

$$Q_w = 0.65 Q_t = 0.65 \cdot constant \cdot V \cdot I_c \tag{3.15}$$

where V is the voltage drop in arc and I_c is the current intensity. Rosenthal discussed three types of moving heat sources: point source, line source and plane source. For each type of heat source he gave the relation between the temperature distribution and the heat Q_p delivered to the workpiece. For example, in the case of a point source the relation obtained is the following

$$\theta - \theta_0 = \frac{Q_p}{2\pi k} e^{-\lambda v \xi} \frac{e^{-\lambda v r}}{r}, \tag{3.16}$$

where $\xi = x - vt$, $\frac{1}{2\lambda} = \frac{k}{\rho c}$ and r is the radius of the plasma beam. Note, that this relation is valid only below $\theta = \theta_m$.

Arai et al. [2] described two categories of heat flux density measurements: i) indirect, measurements made by calculating heat transfer rates, using fundamental theories together with measurements of temperature and thermo physical properties, and ii) direct measurements using heat flux density sensors placed in the thermal field.
In the model of Schulz et al. [47] the heat flux density absorbed at the boundary is proportional to the laser beam intensity I via the absorption coefficient A_p:

$$j_{abs} = -A_p I e_z \cdot \nu, \tag{3.17}$$

where $e_z \cdot \nu$ is the angle of incidence of the laser beam and j_{abs} is, as usual, the heat flux density absorbed by the workpiece. The laser beam intensity I itself is characterized by the maximum intensity of the beam I_0 and the beam radius r:

$$I = -I_0(t) f\left(\frac{x - v_0 t}{r}\right) \tag{3.18}$$

where v_0 is the speed of feeding (the speed of the moving laser) and f is a given distribution $(0 \leq f \leq 1)$.
Bunting et al. [5] developed a relationship between the power density incident on a material and the cut speed in terms of the thermal properties of the material. They used the technique of Rosenthal on moving heat sources and got the relation

$$\frac{j_e}{h} = \frac{2k(\theta_m - \theta_0)}{r^2} \cdot \frac{1}{I(s)}, \tag{3.19}$$

where j_e is the heat flux density emitted from the surface of the heat source, h is the thickness of the material, $s = \frac{vr}{2\alpha}$ and $I(s)$ has been calculated by authors and could be expressed by

$$I(s) = \int_0^1 r' dr' \int_0^{2\pi} \exp(-sr' \cos\phi) K_0 s \left(r'^2 - 2r' \sin\phi + 1\right)^{1/2} d\phi, \tag{3.20}$$

where K_0 is the zeroth order modified Bessel function of the second kind, α is the heat diffusivity and the equation is written in cylindrical coordinates (r', ϕ) with dimensionless r'.
In studying the heat-affected zone during the laser cutting of stainless steel, Sheng et al. [49] expressed the beam energy $E_b(x, y)$ as a function of spatial coordinates via the beam intensity $I(x, y)$ of Gaussian type

$$E_b(x, y) = \int I(u, y) \frac{du}{v} = \int \frac{A(u, y) P}{\pi r^2 v} \exp\left(-\frac{u^2 + y^2}{r^2}\right) du, \tag{3.21}$$

where A is the absorptivity and P is the beam power.

In the following we describe a simple technique to calculate the heat flux density on the absorbing surface.

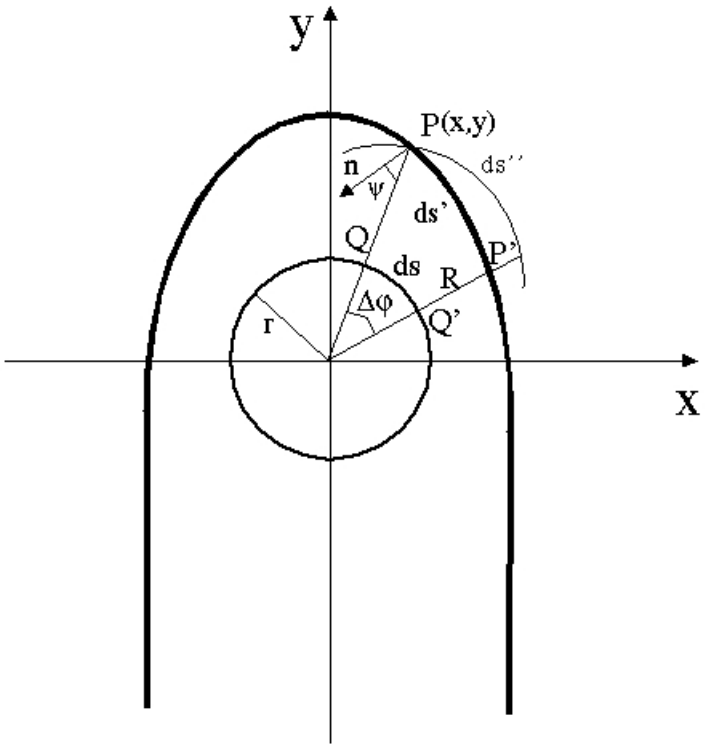

Figure 3.1: Emitted and absorbed heat flux density

For the calculations it is convenient to discuss the topic not in terms of point source, but in terms of incremental surface elements. Therefore consider, as illustrated in Figure 3.1, a small emitting surface of area (length) ds, where the point Q is located. Further, let us assume that the cylindrical surface of the plasma beam is emitting heat in the radial direction, i.e. the heat flux density vector at any point of the beam surface has the direction of the normal to the plasma surface at that point.[1]

We denote:

j_e – the heat flux density (the quantity of heat flowing across a unit area) emitted from the

[1]This assumption is made only for simplicity, the calculations can be also done for other flux density distributions.

arbitrary point Q of the surface of the plasma jet, j_{abs} – the heat flux density absorbed at the point P of the surface of the workpiece due to the emission from Q, r – the radius of the plasma beam.

Having at our disposal the heat flux density j_e at the point Q and the radius r of the beam, our aim is to calculate the heat flux density absorbed at the point P of the workpiece surface (see Figure 3.1).

Let dq be the rate at which the energy leaves the incremental area ds. Then the average flux j_e^{av} leaving ds is defined as

$$j_e^{av} = \frac{dq}{ds}, \tag{3.22}$$

and the flux due to the point Q on the beam surface is defined to be

$$j_e = \lim_{ds \to 0} \frac{dq}{ds}. \tag{3.23}$$

The flux emitted from ds is then completely absorbed (assume the material is a black body) by the surface of the material, more precisely, by the part of the surface which we denote by ds'. Then analogously to (3.22), the average heat flux density j_{abs}^{av} absorbed by ds' is

$$j_{abs}^{av} = \frac{dq}{ds'} \tag{3.24}$$

and owing to (3.23) we obtain

$$j_{abs} = \lim_{ds' \to 0} \frac{dq}{ds'} = \lim_{ds' \to 0} \frac{j_e ds}{ds'} \tag{3.25}$$

For cylindrical heat source we have

$$ds = r\Delta\varphi, \tag{3.26}$$

where $\Delta\varphi$ is the incremental angle between the lines connecting points P and P' with the center of the beam (see Figure 3.1).

Now let ds'' be an element of the spherical surface which we obtain by projecting ds' normal to the direction PQ (the direction that the point P makes with the emitting point Q). In terms of the drawings in Figure 3.1, the flux at the point P due to the energy leaving the point Q may be determined in terms of energy falling on the element ds'' of the circular surface (center at origin, radius R) which passes through P. We then obtain for the surface element ds''

$$ds'' = ds' \cos\psi \quad \text{as} \quad \Delta\varphi \to 0, \tag{3.27}$$

where ψ is the angle between the normal of the workpiece surface at point P and the line PQ.

Thus, we acquire

$$ds' = \frac{ds''}{\cos\psi} \tag{3.28}$$

If, for example, the interface is represented via a smooth graph, $y = f(x)$, then we can express $\cos\psi$ as

$$\cos\psi = -\frac{1}{\sqrt{x^2+f^2(x)}} \cdot \frac{1}{\sqrt{1+(f'(x))^2}} \cdot \begin{pmatrix} x \\ f(x) \end{pmatrix} \cdot \begin{pmatrix} f'(x) \\ -1 \end{pmatrix}, \tag{3.29}$$

where $\frac{1}{\sqrt{x^2+f^2(x)}} \begin{pmatrix} x \\ f(x) \end{pmatrix}$ represents the unit normal vector to the surface ds'' at point $P(x,y)$ and $\frac{1}{\sqrt{1+(f'(x))^2}} \begin{pmatrix} f'(x) \\ -1 \end{pmatrix}$ denotes the unit normal to the graph $y = f(x)$ at point $P(x,y)$. Inserting the expressions for ds' from (3.28) and $\cos\psi$ from (3.29) with $ds'' = R\Delta\varphi$ into (3.25), and taking into account that $ds' \to 0$ is in fact equivalent to $\Delta\varphi \to 0$, we obtain

$$\begin{aligned} j_{abs} &= -j_e \cdot \lim_{\Delta\varphi\to 0} \frac{r\Delta\varphi}{\frac{R\Delta\varphi}{\left(\sqrt{x^2+f^2(x)}\right)^{-1}\cdot\left(\sqrt{1+(f'(x))^2}\right)^{-1}\cdot(xf'(x)-f(x))}} \\ &= -j_e r \frac{xf'(x)-f(x)}{(x^2+f^2(x))\sqrt{1+(f'(x))^2}}. \end{aligned}$$

In general, the expression for $\cos\psi$ can be written in the form

$$\cos\psi = n \cdot \nu_r,$$

where ν_r is the unit vector at the point P pointing in the direction of the emitting point Q. Therefore, for general absorbing surfaces the heat flux on the moving front takes the form

$$j_{abs} = j_e \frac{r}{d_p} \cdot n \cdot \nu_r, \tag{3.30}$$

where d_p is the distance between the point P and the center of plasma beam.

Chapter 4

Definitions and functional analysis background

In this section we are going to introduce the function spaces that are used in the weak formulation of the cutting model. Using the main concepts of Lebesgue functional spaces we will define spaces commonly referred to as Sobolev spaces. The chapter includes only a small part of the known theory for Sobolev spaces – just enough to establish the weak formulation of the Stefan-Signorini problem.

4.1 Review of basic functional spaces

4.1.1 Banach spaces and Hilbert spaces

Let $(\mathbb{X}, d)$ be a metrical space.

Definition 4.1.1. *(Complete spaces)*
A sequence $(x_k)_{k\in\mathbb{N}}$ *in* $\mathbb{X}$ *is called a* Cauchy sequence *if and only if*

$$d(x_k, x_l) \to 0 \text{ for } k, l \to \infty.$$

We say that $(\mathbb{X}, d)$ *is a* complete *metrical space if every Cauchy sequence in* $\mathbb{X}$ *converges to a limit in* $\mathbb{X}$.

Definition 4.1.2. *(Banach Spaces)*
A normed space which is complete with respect to the induced metric is called a Banach space.

Definition 4.1.3. *(Partial derivatives)*
Let $u : \mathbb{R}^n \times \mathbb{R}^+ \to \mathbb{R}$ be a differentiable function for any $n \in \mathbb{N}$. Then we introduce the following definitions:

$$u_{x_i} = \frac{\partial u}{\partial x_i} := \text{ partial derivatives of } u,$$

$$\nabla u = (\dots \ u_{x_i} \ \dots) := \text{ the space gradient of } u,$$

$$u' = u_t = \frac{\partial u}{\partial t} := \text{ the time derivative of } u,$$

$$\frac{\partial u}{\partial \nu} = \nabla u \cdot \nu := \text{ partial derivative of } u \text{ in the direction of } \nu \in \mathbb{R}^n,$$

$$D^\alpha u = \frac{\partial^{|\alpha|} u}{\partial^{\alpha_1} x_1 \partial^{\alpha_2} x_2 \dots \partial^{\alpha_n} x_n} := \text{ mixed partial derivative of } u,$$

with a multi index $\alpha = (\alpha_1, ..., \alpha_n)$, $\alpha_i \in \mathbb{Z}$, $\alpha_i \geq 0$, $|\alpha| = \alpha_1 + \alpha_2 + ... + \alpha_n$.

For the rest of the chapter let $n \in \mathbb{N}$ and $\Omega \subset \mathbb{R}^n$ be a open and bounded set.

Definition 4.1.4. *(Spaces of Continuous Functions)*
For any nonnegative integer m we define the spaces of continuous functions

$$\mathbb{C}^m(\overline{\Omega}) := \{u : \Omega \to \mathbb{R}; \ u \text{ and all } D^\alpha u \text{ of orders } |\alpha| \leq m \text{ are continuous on } \Omega\}.$$

We abbreviate $\mathbb{C}^0(\Omega) := \mathbb{C}(\Omega)$ and set

$$\mathbb{C}^\infty(\Omega) := \bigcap_{m=0}^{\infty} \mathbb{C}^m(\Omega).$$

The norm of a continuous function u is defined as

$$\|u\|_{\mathbb{C}^m(\overline{\Omega})} := \sum_{|\alpha| \leq m} \|D^\alpha u\|_{\mathbb{C}^0(\overline{\Omega})},$$

where

$$\|u\|_{\mathbb{C}^0(\Omega)} := \sup_{x \in \Omega} |u(x)|.$$

Definition 4.1.5. *(Spaces of continuous functions with compact support)*
We denote by $\mathbb{C}_0(\Omega)$ *and* $\mathbb{C}_0^\infty(\Omega)$ *the subsets of* $\mathbb{C}(\Omega)$ *and* $\mathbb{C}^\infty(\Omega)$*, respectively, elements of which are functions with compact support in* Ω*. By support of the function* u *we mean*

$$supp\ u := \overline{\{x \in \Omega\ :\ u(x) \neq 0\}},$$

and if supp $u \subset\subset \Omega$ *then we say that* u *has a compact support in* Ω*.*

Definition 4.1.6. *(Spaces of Hölder Continuous Functions)*
For $0 < \lambda \leq 1$ *we define* $\mathbb{C}^{m,\lambda}(\overline{\Omega})$ *to be the subspace of* $\mathbb{C}^m(\overline{\Omega})$ *consisting of those functions* u *for which there exists a constant* h *such that*

$$|D^\alpha u(x) - D^\alpha u(y)| \leq h|x-y|^\lambda,\ x, y \in \Omega,$$

for $0 \leq \alpha \leq m$*. The functions from the space* $\mathbb{C}^{m,\lambda}(\overline{\Omega})$ *are called Hölder continuous and Lipschitz continuous for the case* $\lambda = 1$ *and* $m = 0$*.*

The constant h is called the Hölder constant. The space $\mathbb{C}^{m,\lambda}(\overline{\Omega})$ is then a Banach space with norm given by

$$\|u\|_{C^{m,\lambda}(\overline{\Omega})} = \|u\|_{C^m(\overline{\Omega})} + \max_{0\leq|\alpha|\leq m} \sup_{x,y\in\Omega, x\neq y} \frac{|D^\alpha u(x) - D^\alpha u(y)|}{|x-y|^\lambda}.$$

Definition 4.1.7. *(Inner Product Spaces and Hilbert Spaces)*
Let $\mathbb{X}$ *be vector space and* $(\cdot,\cdot)$ *the inner product defined on* $\mathbb{X} \times \mathbb{X}$*. Then* $\mathbb{X}$ *is called an* inner product space *and the norm on this space may be defined as*

$$\|x\|_{\mathbb{X}} = \sqrt{(x,x)_{\mathbb{X}}},\ x \in \mathbb{X}.$$

If $\mathbb{X}$ *is complete under this norm, then it is called a* Hilbert space*.*

Denote by $\mathbb{X}'$ the normed dual of the space $\mathbb{X}$ with the norm

$$\|x'\|_{\mathbb{X}'} = \sup\left\{|x'(x)| :\ \|x\|_{\mathbb{X}} \leq 1\right\}.$$

The following theorem shows that there exists an isometry between a Hilbert space $\mathbb{X}$ and its dual $\mathbb{X}'$.

Theorem 4.1.1. *(Riesz Representation Theorem)*
Let $\mathbb{X}$ *be a Hilbert space. Then any continuous linear functional* x' *from the space* $\mathbb{X}'$ *can be uniquely represented as*

$$x'(x) = (y,x) \text{ for some } y \in \mathbb{X}.$$

In this case

$$\|x'\|_{\mathbb{X}'} = \|x\|_{\mathbb{X}}$$

According to the Riesz Representation Theorem, we can identify any Hilbert space with its normed dual.

4.1.2 Basic concepts of Lebesgue spaces

Let Ω be a Lebesgue-measurable domain in $\mathbb{R}^n$ and let p be a positive real number. We denote by $\mathbb{L}^p(\Omega)$ the class of all measurable functions, defined on Ω:

$$\mathbb{L}^p(\Omega) := \left\{u : \|u\|_{\mathbb{L}^p(\Omega)} < \infty\right\}, \tag{4.1}$$

where the norm $\|u\|_{\mathbb{L}^p(\Omega)}$ is defined in the following way: for $1 \leq p < \infty$

$$\|u\|_{\mathbb{L}^p(\Omega)} := \left(\int\limits_{\Omega} |u(x)|^p dx\right)^{\frac{1}{p}}, \tag{4.2}$$

and for $p = \infty$ we set

$$\|u\|_{\mathbb{L}^\infty(\Omega)} := ess \sup_{x\in\Omega} \{|u(x)|\}. \tag{4.3}$$

The elements of $\mathbb{L}^p(\Omega)$ are actually equivalence classes of measurable functions satisfying (4.2) or (4.3), because we can identify all functions in $\mathbb{L}^p(\Omega)$ which are equal almost everywhere on Ω.
The following theorem gives some useful properties of $\mathbb{L}^p$-spaces over domains with finite volume. The proof of the theorem may be found in [1].

Theorem 4.1.2. *Assume $1 \leq p \leq q \leq \infty$. Then*

1. *$\mathbb{L}^p(\Omega)$ is a Banach space.*
2. *If $u \in \mathbb{L}^q(\Omega)$, then $u \in \mathbb{L}^p(\Omega)$ and*
$$\|u\|_{\mathbb{L}^p(\Omega)} \leq (vol(\Omega))^{\left(\frac{1}{p}-\frac{1}{q}\right)} \|u\|_{\mathbb{L}^q(\Omega)}. \tag{4.4}$$
3. *As a consequence of (4.4) we get a useful embedding result for $\mathbb{L}^p$-spaces, namely*
$$\mathbb{L}^q(\Omega) \hookrightarrow \mathbb{L}^p(\Omega). \tag{4.5}$$
4. *If $p < \infty$ then $\mathbb{L}^p(\Omega)$ is separable.*
5. *$\mathbb{L}^p(\Omega)$ is reflexive if and only if $1 < p < \infty$.*

4.2 Sobolev spaces

4.2.1 Weak (generalized) derivatives

The classical definition of derivative contains information about the function only near the given point. Of special importance is the notion of weak or distributional derivatives which does not care about point-wise values. Therefore, we will consider derivatives that can be interpreted as functions in the Lebesgue spaces. We know that point-wise values of functions in Lebesgue spaces are irrelevant and these functions are determined only by their global behaviour. The weak derivative will be used in the development of the variational formulation of the cutting model.

Definition 4.2.1. *A function u is said to be locally integrable on Ω, if it is defined on Ω almost everywhere and $u \in \mathbb{L}^1(K)$ for every compact K lying in the interior of Ω. The locally integrable function space is denoted by $\mathbb{L}^1_{loc}(\Omega)$.*

Now we are ready to define the notion of weak derivative.

Definition 4.2.2. *The function $u \in \mathbb{L}^1_{loc}(\Omega)$ possesses a weak derivative, if there exists a function $v \in \mathbb{L}^1_{loc}(\Omega)$ such that*
$$\int_\Omega v(x)\phi(x)dx = (-1)^{|\alpha|} \int_\Omega u(x)D^\alpha\phi(x)dx \qquad \text{for all} \quad \phi \in \mathbb{C}_0^\infty(\Omega).$$
We denote the weak derivative of u by $D^\alpha_w u$ and define $D^\alpha_w u = v$ (if such a v exists, of course).

4.2.2 Introduction to Sobolev spaces

The Sobolev spaces which play an important role in the variational formulation of partial differential equations are built on the function spaces $\mathbb{L}^p(\Omega)$ introduced in the previous section. The idea is to generalize the Lebesgue norms and spaces to include weak derivatives. Let again Ω be an open subset of $\mathbb{R}^n$.

Definition 4.2.3. *Let m be a non-negative integer and $1 \leq p \leq \infty$. We define the Sobolev norm $\|\cdot\|_{m,p}$ for any function $u \in \mathbb{L}^1_{loc}(\Omega)$ in the following form:*

$$\|u\|_{m,p} = \left(\sum_{0 \leq |\alpha| \leq m} \|D^\alpha_w u\|^p_{\mathbb{L}^p(\Omega)} \right)^{\frac{1}{p}} \text{ if } 1 \leq p < \infty, \tag{4.6}$$

$$\|u\|_{m,\infty} = \max_{0 \leq |\alpha| \leq m} \|D^\alpha_w u\|_{\mathbb{L}^\infty(\Omega)} \text{ if } p = \infty, \tag{4.7}$$

where we assume that the weak derivatives $D^\alpha_w u$ of u exist for all $|\alpha| \leq m$.
The Sobolev norm defines a norm on any vector space of functions provided we identify all functions in the case they are equal almost everywhere in Ω.

Definition 4.2.4. *For any positive integer m and $1 \leq p \leq \infty$ we define the Sobolev spaces*

$$\mathbb{W}^{m,p}(\Omega) := \left\{ u \in \mathbb{L}^1_{loc} : \ \|u\|_{m,p} < \infty \right\}.$$

Clearly $\mathbb{W}^{0,p}(\Omega) = \mathbb{L}^p(\Omega)$. For the finite element approximation of differential equations the following space is of great importance:

$$\mathbb{W}^{m,p}_0(\Omega) \equiv \text{ the closure of } \mathbb{C}^\infty_0(\Omega) \text{ in the space } \mathbb{W}^{m,p}(\Omega).$$

For an arbitrary integer m we get the following obvious chain of embeddings:

$$\mathbb{W}^{m,p}_0(\Omega) \hookrightarrow \mathbb{W}^{m,p}(\Omega) \hookrightarrow \mathbb{L}^p(\Omega).$$

The spaces $\mathbb{W}^{m,p}(\Omega)$ were first introduced by Sobolev [50], [51].

4.2.3 Some useful properties of Sobolev spaces

In this section we will present, mainly without proofs, some useful properties (useful for our further considerations) enjoyed by functions from Sobolev spaces. We will provide results in their general formulations. The special cases used in finite element formulations can be easily obtained with very simple calculations.
Let again $\Omega \subset \mathbb{R}^n$ be an open, bounded domain with $\partial\Omega \in \mathbb{C}^{0,1}$.

Theorem 4.2.1. *The Sobolev space $\mathbb{W}^{m,p}(\Omega)$ is a Banach space.*

Proof. For the proof we refer to [1]. □

Theorem 4.2.2. *(Sobolev Embedding Theorem)*
Assume $m, l \in \mathbb{N}$ and $p, q \in [1, \infty]$. Then the following statements hold:

1. *If $m \geq l$ and $m - \frac{d}{p} > l - \frac{d}{q}$, then $\mathbb{W}^{m,p}(\Omega)$ is continuously embedded in $\mathbb{W}^{l,q}(\Omega)$, i.e. there exists a constant c, such that for all $u \in \mathbb{W}^{m,p}(\Omega)$*

$$\|u\|_{l,q} \leq c \cdot \|u\|_{m,p}.$$

   The number $m - \frac{d}{p}$ is called the Sobolev number.

2. *If $m > l$ and $m - \frac{d}{p} > l - \frac{d}{q}$, then the embedding is compact.*

3. *If $m - \frac{d}{p} > k + \alpha$, then*

$$\|u\|_{\mathbb{C}^{k,\alpha}(\overline{\Omega})} \leq c \cdot \|u\|_{m,p} \quad \forall u \in \mathbb{W}^{m,p}(\Omega)$$

   i.e. the space $W^{m,p}(\Omega)$ is continuously embedded in $\mathbb{C}^{k,\alpha}(\overline{\Omega})$.

Proof. For the proof we refer to [1]. □

Sobolev functions can not be in general evaluated over lower-dimensional subsets, i.e. subsets having measure equal zero.

Theorem 4.2.3. *(Trace Theorem)*
Using the notations of the previous theorem, we assume that $m > l$ *and* $m - \frac{d}{p} > l - \frac{d-r}{q}$. *Then there exists a continuous linear embedding* $\gamma : \mathbb{W}^{m,p}(\Omega) \to \mathbb{W}^{l,q}(S)$, *where* S *is a smooth* $(d-r)$ *dimensional sub-manifold of* Ω. *Thus the estimate*

$$\|\gamma(u)\|_{l,q,s} \leq c \cdot \|u\|_{m,p} \ \forall u \in \mathbb{W}^{m,p}(\Omega)$$

holds.

Proof. The details of the proof one can find in [1]. □

The embedding operator γ is then called the trace operator. For example, if $u \in \mathbb{C}^{\infty}(\overline{\Omega})$, then the trace operator γ is determined as $\gamma(u) = u$.
For our future discussions it is useful to introduce the notation of Sobolev semi-norms.

Definition 4.2.5. *Let* m *be a non-negative integer and* $u \in \mathbb{W}^{m,p}(\Omega)$. *We define the Sobolev semi-norm* $|\cdot|_{m,p}$

$$|u|_{m,p} = \left(\sum_{|\alpha|=m} \|D_w^{\alpha} u\|_{\mathbb{L}^p(\Omega)}^p \right)^{\frac{1}{p}} \text{ if } 1 \leq p < \infty, \tag{4.8}$$

$$|u|_{m,\infty} = \max_{|\alpha|=m} \|D_w^{\alpha} u\|_{\mathbb{L}^{\infty}(\Omega)} \text{ if } p = \infty. \tag{4.9}$$

4.3 Spaces of vector-valued functions

Let $\mathbb{X}$ be a Banach space, (a, b) an open interval in $\mathbb{R}$ and dt the Lebesgue measure over (a, b).

Definition 4.3.1. *A function* $u : [a, b] \to \mathbb{X}$ *is called Bochner measurable, if there exists a sequence of simple functions* $\{u_k\}_{k \in \mathbb{N}}$ *such that*

$$\lim_{k \to \infty} u_k(t) = u(t) \text{ for almost all } t \in [a, b].$$

Definition 4.3.2. *If additionally*

$$\lim_{k \to \infty} \int_a^b \|u(t) - u_k(t)\|_{\mathbb{X}} dt = 0$$

then the function u is called Bochner-integrable and the integral

$$\int_a^b u(t)dt = \lim_{k\to\infty} \int_a^b u_k(t)dt$$

is said to be the Bochner-integral of u.

Definition 4.3.3. *Assume that $-\infty < a < b < \infty$ and the function $u : [a,b] \to \mathbb{X}$ is Bochner-measurable.*

1. *Define the function space*

$$\mathbb{C}(a,b;\mathbb{X}) := \{u : [a,b] \to \mathbb{X} \quad \textit{continuous}\},$$

with the norm

$$\|u\|_{\mathbb{C}(a,b;\mathbb{X})} := \max_{t\in[a,b]} \|u(t)\|_{\mathbb{X}}$$

2. *For $1 \le p < \infty$ we define the space of (classes) functions*

$$\mathbb{L}^p(a,b;\mathbb{X}) := \left\{u : [a,b] \to \mathbb{X} \quad \textit{Bochner-measurable; } \|u\|_{\mathbb{L}^p(a,b;\mathbb{X})} < \infty\right\}$$

with

$$\|u\|_{\mathbb{L}^p(a,b;\mathbb{X})} := \left(\int_a^b \|u(t)\|_{\mathbb{X}}^p dt\right)^{\frac{1}{p}}.$$

3. *For $p = \infty$ the space of almost everywhere over (a,b) bounded functions (classes of functions) is defined*

$$\mathbb{L}^\infty(a,b;\mathbb{X}) := \left\{u : [a,b] \to \mathbb{X} \quad \textit{Bochner-measurable; } \|u\|_{\mathbb{L}^\infty(a,b;\mathbb{X})} < \infty\right\}$$

with

$$\|u\|_{L^\infty(a,b;\mathbb{X})} := \inf_{a.a.t} \|u(t)\|_{\mathbb{X}}.$$

Theorem 4.3.1. *Let $-\infty < a < b < \infty$ and $\mathbb{X}$ is a Banach space. Then the spaces $\left(\mathbb{L}^p(a,b;\mathbb{X}), \|\cdot\|_{\mathbb{L}^p(a,b;\mathbb{X})}\right)$ and $\left(\mathbb{C}(a,b;\mathbb{X}), \|\cdot\|_{\mathbb{C}(a,b;\mathbb{X})}\right)$ are Banach spaces.*

Proof. See details of the proof in [24]. □

Further we define the weak derivative of a Bochner-integrable function.

Definition 4.3.4. *Let $(\mathbb{X}, (\cdot,\cdot))$ be a separable Hilbert space, $0 < T < \infty$ and $u \in \mathbb{L}^1(0,T;\mathbb{X})$. A function $v \in \mathbb{L}^1(0,T;\mathbb{X})$ is called the weak derivative of u if*

$$\int_0^T u(t)\varphi'(t)dt = -\int_0^T v(t)\varphi(t)dt \quad \forall \varphi \in \mathbb{C}_0^\infty(0,T).$$

Then we write $u' = v$ (if such a v exists, of course).

Definition 4.3.5. *We call every continuous linear mapping of $D((a,b))$ (space of distributions over (a,b)) into $\mathbb{X}$ a vectorial distribution over (a,b) with values in a Banach space $\mathbb{X}$.*

Coming back to our problem, we define by $\theta(t)$ the function $x \to \theta(x,t)$ and let us consider a bilinear form $\theta, \varphi \to a(\theta,\varphi)$ defined via

$$a(\theta,\varphi) = \int_{\Omega_s(t)} \nabla\theta \cdot \nabla\varphi dx,$$

which is a continuous, symmetric and coercive form on $\mathbb{H}^1(\Omega_s(t)) \times \mathbb{H}^1(\Omega_s(t))$, where $\mathbb{H}^1(\Omega) \equiv \mathbb{W}^{1,2}(\Omega)$.

Next, we would like to define the spaces of admissible functions for the Stefan-Signorini problem. Let $\mathbb{V}$ be the functional space defined as follows:

$$\mathbb{V} = \left\{ \theta \;\mid\; \theta \in \mathbb{L}^2\left(0,T;\mathbb{H}^1(\Omega_s(t))\right),\ \theta' = \frac{\partial\theta}{\partial t} \in \mathbb{L}^2\left(0,T;\left(\mathbb{H}^1(\Omega_s(t))\right)'\right) \right\}. \tag{4.10}$$

Provided with the scalar product

$$(\theta,\varphi)_{\mathbb{V}} := (\theta,\varphi)_{\mathbb{L}^2(0,T;\mathbb{H}^1(\Omega_s(t)))} + (\theta',\varphi')_{\mathbb{L}^2\left(0,T;(\mathbb{H}^1(\Omega_s(t))'\right)}, \tag{4.11}$$

$\mathbb{V}$ is a Hilbert space. Here we employed the result of Theorem 3 from [23] pp.166-167, which states that the spaces $\mathbb{L}^2\left(0,T;\mathbb{H}^1(\Omega_s(t))\right)$ and $\mathbb{L}^2\left(0,T;\mathbb{L}^2(\Omega_s(t))\right)$ endowed with the scalar products

$$(\theta,\varphi)_{\mathbb{L}^2(0,T;\mathbb{H}^1(\Omega_s(t)))} := \int_0^T (\theta(t),\varphi(t))_{\mathbb{H}^1(\Omega_s(t)}dt$$

and

$$(\theta,\varphi)_{\mathbb{L}^2(0,T;\mathbb{L}^2(\Omega_s(t)))} := \int_0^T (\theta(t),\varphi(t))_{\mathbb{L}^2(\Omega_s(t)}dt$$

have a Hilbert space structure. The appropriate norm is then defined as

$$\|u\|_{\mathbb{V}} := \left(\int_0^T \|u(t)\|^2_{\mathbb{H}^1(\Omega_s(t)}dt + \int_0^T \|u'(t)\|^2_{(\mathbb{H}^1(\Omega_s(t))'}dt \right)^{\frac{1}{2}}$$

$$= \left(\int_0^T \int_{\Omega_s(t)} |\nabla u|^2 dx dt + \int_0^T \left(\sup_{v \in \mathbb{H}^1(\Omega_s(t))} \frac{< u'(t), v >}{\|v\|_{\mathbb{H}^1(\Omega_s(t))}} \right)^2 dt \right)^{\frac{1}{2}}.$$

Next we define a closed subspace $\mathbb{V}_0$ of $\mathbb{V}$ in the following form:

$$\mathbb{V}_0 = \left\{ \theta \mid \theta \in \mathbb{V},\ \theta(0) = \theta_0,\ \text{where } \theta_0 \text{ is a given function in } \mathbb{L}^2(\Omega) \right\}. \tag{4.12}$$

Recalling that Sobolev functions can not be in general evaluated over lower-dimensional subsets, i.e. subsets having measure zero, it might look like the condition "$\theta(0) = \theta_0$" makes no sense. Fortunately, the following important embedding result makes the definition of the space $\mathbb{V}_0$ meaningful.

Theorem 4.3.2. *Any function $\theta \in \mathbb{V}$ is almost everywhere equal to a continuous function from $[0,T]$ to $\mathbb{L}^2(\Omega_s(t))$. Moreover,*

$$\mathbb{L}^2\left(0,T;\mathbb{H}^1(\Omega_s(t))\right) \cap \mathbb{H}^1\left(0,T;\left(\mathbb{H}^1(\Omega_s(t))\right)'\right) \subset \mathbb{C}\left(0,T;\mathbb{L}^2(\Omega_s(t))\right), \tag{4.13}$$

the space $\mathbb{C}\left(0,T;\mathbb{L}^2(\Omega_s(t))\right)$ being equipped with the norm of uniform convergence.

Proof. The theorem has been proved by Dautrey and Lions in [24]. □

Chapter 5

Weak formulation of the problem

5.1 Variational inequalities

In the theory of partial differential equations, the study of *variational inequalities* occupies a significant position, because of the importance which it assumes for various questions in mathematical modelling and numerical simulations of several real world problems. Variational inequalities arise, among other places, in the areas of elasticity, control and optimization, heat transfer, diffusion, etc.

The first source for the establishment of the theory of variational inequalities was the paper by Fichera (1964) on the analysis of Signorini problem in the theory of elasticity, [14]. Later the theory of variational inequalities was successfully developed by J.-L.Lions, G.Stampacchia and their students, [24],[25], etc. In a series of boundary value problems the solution has to satisfy some additional physical conditions ordered by the model. A good representative of such kind of problems is the *obstacle problem*. In addition to governing equation and standard boundary conditions, an obstacle constraint is imposed on the boundary of the domain of interest. Obstacle constraint says that, in addition, the boundary of the domain must lie above some given obstacle. This leads us to the concept of *variational inequalities*.

Mathematically speaking, let X be a Hilbert space, X' be the dual of X and let the pairing between X and X' be denoted by $\langle \cdot, \cdot \rangle$. Suppose that a closed and convex set K in X is given and let $a(u, v)$ be a bilinear continuous form on X. Finally, let the function f be an element of X'. We consider

Problem 5.1.1. *(Variational Inequality)*
Find $u \in K$ such that

$$a(u, v-u) \geq \langle f, v-u \rangle, \quad \forall v \in K. \tag{5.1}$$

It is worth to mention that when $K \equiv X$, the inequality (5.1) turns to be

$$a(u, v-u) = \langle f, v-u \rangle, \quad \forall v \in K,$$

which is a variational problem well investigated by Lax and Milgram.
We list some important results concerning the solvability of the variational inequality (5.1):

1. If K is a closed, convex set of X and $a(u, v)$ is coercive, then the Problem 5.1.1 has a unique solution, [25] and [28].

2. If instead of coercivity we assume that $a(u, v) \geq 0$ for $v \in X$, then the set of all solutions of Problem 5.1.1 is a (possibly empty) closed convex set, [25].

3. If the condition $a(u, v) \geq 0$ still holds and K is bounded, then there exists a solution to the Problem 5.1.1, [25].

4. If K is not bounded, then a necessary and sufficient condition that the solution of Problem 5.1.1 exists is that there is a constant $R > 0$ such that a function $u_R \in K_R$, where $K_R = K \cap B_R$ and B_R is the closed ball of radius R and center $0 \in \mathbb{R}^n$, satisfies

   $$|u_R| < R,$$

   where u_R is the solution of (5.1) with a small modification, i.e. in the inequality (5.1) we just replace K with K_R and u with u_R. This result is taken from [28].

5.1.1 Signorini problem and variational inequalities

There is a very close connection between variational inequalities and free boundary problems. Of course, not every free boundary problem allows us to reduce it to variational inequality. However, a large variety of real world problems dealing with heat transfer, or almost all obstacle problems can be reformulated into variational inequalities.
Our cutting model belongs to the subclass of problems which are relatively easy to convert into variational inequality. For our convenience, in the rest of the work we will abbreviate

the notation for the time dependent solid domain $\Omega_s(t)$ by writing just Ω_t instead and denoting its boundary by $\partial\Omega_t$.

Now we are going to show how the nonlinear Signorini boundary conditions (3.8) make it possible to rewrite the system (3.7)-(3.11) in the form of variational inequality[1]. For this purpose we introduce the set $\mathbb{K} \subset \mathbb{H}^1(\Omega_t)$ as follows

$$\mathbb{K} = \left\{\varphi \mid \varphi \in \mathbb{H}^1(\Omega_t),\ \varphi \leq 0 \text{ on } \partial\Omega_t\right\}, \tag{5.2}$$

where by writing '$\varphi \leq 0$ on $\partial\Omega_t$' we actually mean $\gamma\varphi \leq 0$ a.e. on $\partial\Omega_t$ with $\gamma\varphi$ denoting the trace of the function φ on $\partial\Omega_t$.

Lemma 5.1.1. *The introduced set $\mathbb{K}$ is a closed convex nonempty subset of $\mathbb{H}^1(\Omega_t)$.*

Proof. The proof of the convexity of $\mathbb{K}$ is trivial. If we take a sequence $\{\phi_n\} \subset \mathbb{K}$ such that $\phi_n \to \phi$ in $\mathbb{H}^1(\Omega_t)$, then

$$\|\gamma\phi_n - \gamma\phi\|_{\mathbb{L}^2(\partial\Omega_t)} \leq c \cdot \|\phi_n - \phi\|_{\mathbb{H}^1(\Omega_t)} \to 0,$$

where we used the statement of trace theorem 4.2.3 from Chapter 3 on continuous embedding of $\mathbb{H}^1(\Omega_t)$ into $\mathbb{L}^2(\partial\Omega_t)$. From $\phi_n \in \mathbb{K}$ follows $\gamma\phi_n \leq 0$ a.e. on $\partial\Omega_t$. Thus, $\gamma\phi \leq 0$ a.e. on $\partial\Omega_t$ which means that $\phi \in \mathbb{K}$ and therefore, we obtain that the set $\mathbb{K}$ is closed.

From the definition of $\mathbb{K}$ it follows immediately that $0 \in \mathbb{K}$ (more precisely, $\mathbb{H}^1_0(\Omega_t) \subset \mathbb{K}$), which shows that $\mathbb{K}$ is not empty. □

For the functions $\theta \in \mathbb{V}$ we can define their trace on the lateral boundary $\Gamma_t := \partial\Omega_t \times I$ of $Q_t := \Omega_t \times I$. For every fixed domain Ω_t it is known (see [25]) that $\theta|_{\Gamma_t} \in \mathbb{L}^2(0,T;\mathbb{H}^{\frac{1}{2}}(\partial\Omega_t))$. The latter allows us to define closed convex subsets $\mathbb{B}$ and $\mathbb{B}_0$ in the following way

$$\mathbb{B} = \{\theta \mid \theta \in \mathbb{V},\ \theta(t) \in \mathbb{K} \text{ a.e. in } [0,T]\} \tag{5.3}$$

$$\mathbb{B}_0 = \{\theta \mid \theta \in \mathbb{V}_0,\ \theta(t) \in \mathbb{K} \text{ a.e. in } [0,T]\} \tag{5.4}$$

Let us consider the following variational problem.

Problem 5.1.2. *Find $\theta \in \mathbb{B}_0$ such that*

$$\int_0^T \int_{\Omega_t} \theta'(\varphi - \theta)dxdt + \int_0^T \int_{\Omega_t} \nabla\theta \cdot \nabla(\varphi - \theta)dxdt \geq \int_0^T \int_{\partial\Omega_t} j_{abs}(\varphi - \theta)d\gamma dt \tag{5.5}$$

for all $\varphi \in \mathbb{B}$, $j_{abs} \in \mathbb{H}^1(\mathbb{R}^n) \cap \mathbb{L}^\infty(\mathbb{R}^n)$.

[1]For convenience we consider all material parameters to be equal to one and the melting temperature $\theta_m = 0$.

Lemma 5.1.2. *The Problem 5.1.2 is equivalent to the problem (3.7)-(3.8)+(3.10)-(3.11), i.e heat conduction equation with Signorini boundary conditions.*

Proof. First we show that the Problem 5.1.2 implies the Signorini problem (3.7)-(3.8)+(3.10)-(3.11). Indeed, since $\theta \in \mathbb{B}_0$, it satisfies by definition of $\mathbb{B}_0$

$$\theta(x,0) = \theta_0(x), \tag{5.6}$$

and

$$\theta \leq 0 \quad \text{on } \partial\Omega_t. \tag{5.7}$$

Now let $\phi \in D(\Omega_t \times (0,\infty))$. In (5.5) we "formally" take $\varphi = \theta + \phi$

$$\int_0^T \int_{\Omega_t} \theta' \phi dx dt + \int_0^T \int_{\Omega_t} \nabla\theta \cdot \nabla\phi dx dt \geq \int_0^T \int_{\partial\Omega_t} j_{abs} \phi d\gamma dt. \tag{5.8}$$

Taking $\varphi = \theta - \phi$ yields

$$-\int_0^T \int_{\Omega_t} \theta' \phi dx dt - \int_0^T \int_{\Omega_t} \nabla\theta \cdot \nabla\phi dx dt \geq -\int_0^T \int_{\partial\Omega_t} j_{abs} \phi d\gamma dt. \tag{5.9}$$

Combining inequalities (5.8) and (5.9) and taking into account that due to the compact support of ϕ in Ω_t the right hand sides of both equations vanish, we obtain

$$\int_0^T \int_{\Omega_t} \theta' \phi dx dt + \int_0^T \int_{\Omega_t} \nabla\theta \cdot \nabla\phi dx dt = 0, \tag{5.10}$$

which, after integration by parts, reduces to

$$\int_0^T \int_{\Omega_t} \left(\theta' - \Delta\theta\right) \phi dx dt = 0. \tag{5.11}$$

Therefore, in the sense of "distributions on Ω_t", θ satisfies the heat equation

$$\frac{\partial\theta}{\partial t} - \Delta\theta = 0 \quad \text{in } \Omega_t \times (0,T). \tag{5.12}$$

Applying Green's formula to the left hand side of (5.5), we obtain

$$\int_0^T \int_{\Omega_t} (\theta' - \Delta\theta)(\varphi - \theta) dx dt + \int_0^T \int_{\partial\Omega_t} \nabla\theta \cdot \nu(\varphi - \theta) d\gamma dt \geq \int_0^T \int_{\partial\Omega_t} j_{abs}(\varphi - \theta) d\gamma dt \tag{5.13}$$

Together with (5.12), the inequality (5.13) yields

$$\int_0^T \int_{\partial\Omega_t} (j_{abs} - \nabla\theta \cdot \nu)(\varphi - \theta) d\gamma dt \leq 0. \tag{5.14}$$

Now, let ϕ be an arbitrary function in $\mathbb{K}$. Then the function $\varphi = \theta + s\phi \in \mathbb{K}$ for any positive s and we are allowed to substitute it into (5.14):

$$\int_0^T \int_{\partial\Omega_t} (j_{abs} - \nabla\theta \cdot \nu)\, \phi d\gamma dt \leq 0, \quad \forall \phi \in \mathbb{K}. \tag{5.15}$$

Since the convex cone $\mathbb{K}$ is dense in $\mathbb{L}^2_-(\partial\Omega_t) := \left\{ v \in \mathbb{L}^2(\partial\Omega_t), v \leq 0 \ a.e. \text{ on } \partial\Omega_t \right\}$, the last inequality leads to

$$j_{abs} - \nabla\theta \cdot \nu \geq 0 \ \ a.e. \text{ on } \partial\Omega_t. \tag{5.16}$$

If we now "formally" take in (5.5) $\varphi = 0$ and $\varphi = 2\theta$, we obtain

$$\varphi = 0: \quad -\int_0^T \int_{\Omega_t} \theta' \theta dx dt - \int_0^T \int_{\Omega_t} \nabla\theta \cdot \nabla\theta dx dt \leq -\int_0^T \int_{\partial\Omega_t} j_{abs} \theta d\gamma dt, \tag{5.17}$$

or equivalently

$$\int_0^T \int_{\Omega_t} \theta' \theta dx dt + \int_0^T \int_{\Omega_t} \nabla\theta \cdot \nabla\theta dx dt \geq \int_0^T \int_{\partial\Omega_t} j_{abs} \theta d\gamma dt. \tag{5.18}$$

Analogously

$$\varphi = 2\theta: \quad \int_0^T \int_{\Omega_t} \theta' \theta dx dt + \int_0^T \int_{\Omega_t} \nabla\theta \cdot \nabla\theta dx dt \leq \int_0^T \int_{\partial\Omega_t} j_{abs} \theta d\gamma dt. \tag{5.19}$$

From (5.18) and (5.19) it follows that

$$\int_0^T \int_{\Omega_t} \theta' \theta dx dt + \int_0^T \int_{\Omega_t} \nabla\theta \cdot \nabla\theta dx dt = \int_0^T \int_{\partial\Omega_t} j_{abs} \theta d\gamma dt. \tag{5.20}$$

Assuming enough regularity on θ, we can perform integration by parts in (5.20) again and obtain

$$\int_0^T \int_{\Omega_t} \left(\theta' - \Delta\theta\right) \theta dx dt = \int_0^T \int_{\partial\Omega_t} (j_{abs} - \nabla\theta \cdot \nu)\, \theta d\gamma dt. \tag{5.21}$$

The heat equation (3.7) should be fulfilled, thus from (5.21) we deduce

$$\int_0^T \int_{\partial\Omega_t} (j_{abs} - \nabla\theta \cdot \nu)\, \theta d\gamma dt = 0. \tag{5.22}$$

Since $\theta \leq 0$ on the boundary $\partial\Omega_t$ and the condition (5.16) is fulfilled, we can state that

$$\theta\, (j_{abs} - \nabla\theta \cdot \nu) = 0 \ \text{ on } \partial\Omega_t, \tag{5.23}$$

which shows that under some regularity conditions on θ the Problem 5.1.2 implies the Signorini problem, i.e. heat equation plus Signorini boundary conditions.

To complete the proof of the lemma, it remains to show that the inequality (5.5) is a consequence of heat equation together with Signorini boundary constraints. Indeed, we multiply both sides of the homogeneous heat equation by $\varphi - \theta$ and integrate over the time-space domain $(0,T) \times \Omega_t$:

$$\int_0^T \int_{\Omega_t} \theta'(\varphi - \theta) dxdt + \int_0^T \int_{\Omega_t} \Delta\theta(\varphi - \theta) dxdt = 0.$$

An integration by parts in the second integral yields

$$\int_0^T \int_{\Omega_t} \theta'(\varphi - \theta) dxdt + \int_0^T \int_{\Omega_t} \nabla\theta \cdot \nabla(\varphi - \theta) dxdt - \int_0^T \int_{\partial\Omega_t} \nabla\theta \cdot \nu(\varphi - \theta) d\gamma dt = 0.$$

Now we make use of the Signorini constraint

$$j_{abs} - \nabla\theta \cdot \nu \geq 0$$

and substitute it in above integral equation. We get

$$\int_0^T \int_{\Omega_t} \theta'(\varphi - \theta) dxdt + \int_0^T \int_{\Omega_t} \nabla\theta \cdot \nabla(\varphi - \theta) dxdt \geq \int_0^T \int_{\partial\Omega_t} j_{abs}(\varphi - \theta) d\gamma dt,$$

which is the desired variational inequality of Problem 5.1.2. The proof of lemma is complete. □

Another equivalent formulation of the problem can be written in the following way:

Problem 5.1.3. *Find $\theta(t) \in \mathbb{K}$ for $t \in I$ such that*

$$\int_{\Omega_t} \theta'(\varphi - \theta) dxdt + \int_{\Omega_t} \nabla\theta \cdot \nabla(\varphi - \theta) dx \geq \int_{\partial\Omega_t} j_{abs}(\varphi - \theta) d\gamma \tag{5.24}$$

for all $\varphi \in \mathbb{K}$, $\theta(0) = \theta_0$.

Remark 5.1.1. *The condition on θ' forcing it to belong to the space $\mathbb{L}^2\left((0,T;\left(\mathbb{H}^1(\Omega_t)\right)\right)$ seems to be too restrictive. It will be useful to consider a more general weak formulation. We observe that if θ is a solution of (5.3),(5.4),(5.5) and $\varphi \in \mathbb{B}$, then*

$$\begin{aligned} \int_0^T \int_{\Omega_t} \theta'(\varphi - \theta) dxdt \quad &+ \quad \int_0^T \int_{\Omega_t} \nabla\theta \cdot \nabla(\varphi - \theta) dxdt \\ &= \int_0^T \int_{\Omega_t} (\varphi + \theta - \varphi)'(\varphi - \theta) dxdt + \int_0^T \int_{\Omega_t} \nabla\theta \cdot \nabla(\varphi - \theta) dxdt \end{aligned}$$

It follows

$$\begin{aligned} \int_0^T \int_{\Omega_t} \varphi'(\varphi-\theta)dxdt &+ \int_0^T \int_{\Omega_t} \nabla\theta\cdot\nabla(\varphi-\theta)dxdt \\ \geq \int_0^T (\varphi'-\theta')(\varphi-\theta)dt &+ \int_0^T \int_{\partial\Omega_t} j_{abs}(\varphi-\theta)d\gamma dt \\ = \frac{1}{2}\|\varphi(T)-\theta(T)\|^2 &- \frac{1}{2}\|\varphi(0)-\theta_0\|^2 + \int_0^T \int_{\partial\Omega_t} j_{abs}(\varphi-\theta)d\gamma dt \end{aligned} \tag{5.25}$$

Here we used the fact that if a function v belongs to $\mathbb{V}$, then the relation $\langle v', v\rangle = \frac{1}{2}\frac{d}{dt}\|v\|^2$ holds, [24]. If we now choose the function φ from the space $\mathbb{B}_0$, then the term $-\frac{1}{2}\|\varphi(0)-\theta_0\|^2$ can be also avoided. Note that in the Problem (5.25) we require only that $\theta \in \mathbb{L}^2(0,T;\mathbb{H}^1(\Omega_t))$, nothing is said about θ'.

5.2 Level set formulation

The technique we are going to apply for the investigation of the condition (5.30) is the level-set theory first introduced by Sethian and Osher [38]. Below we present some background material on the level set approach.

The main idea of level-set method is to embed the evolving front $\partial\Omega_t$ into a surface, *the level-set surface*, which has the property that its zero-level set always yields the desired moving interface. Thus, in order to find the unknown interface at any time t, we only need to locate the set for which the level-set surface vanishes (see Figure 5.1). The idea of Osher and Sethian is that instead of moving the initial front (circular curve left in the figure), which can do all sorts of weird things, one tries and instead moves the level set surface (right in the figure). In other words, the level set function expands, rises, falls, and does all the work. To find out where the front is, one should find the zero level set of the surface only.

Let Γ_0 be an initial interface bounding some open domain Ω_0. We wish to investigate and compute its motion under some velocity field which depends on several quantities. In other words, at any time instant t we aim to find a closed moving interface Γ_t in $\mathbb{R}^n$ with co-dimension one, which encloses our domain of interest Ω_t. The idea of level-set approach is to introduce a scalar function (level-set function) $\phi(x,t)$, $x\in\mathbb{R}^n$, $t\in\mathbb{R}^+$, such that at any

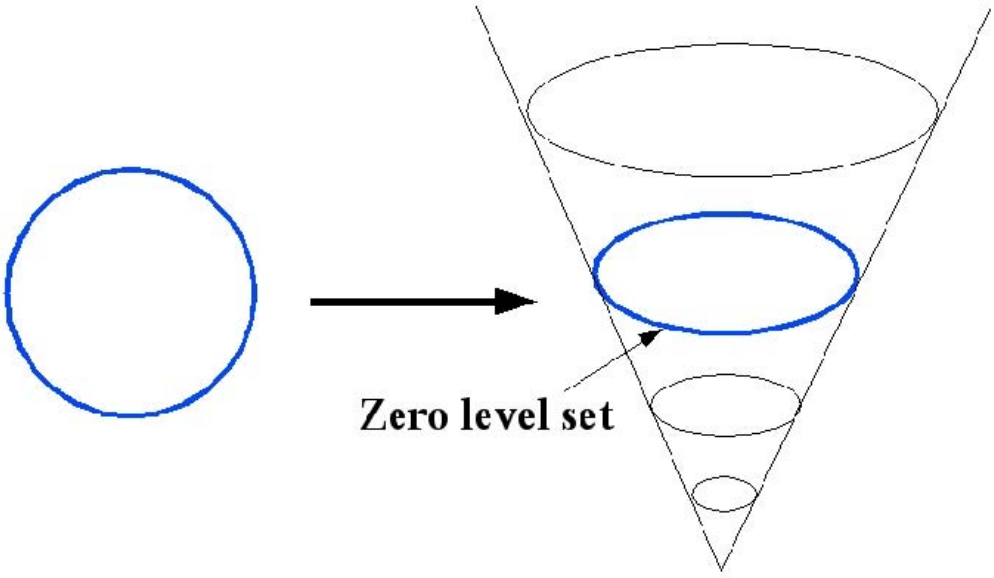

Figure 5.1: Initial curve (left) is embedded into a level-set surface (right).

arbitrary time instant t the zero-level set of $\phi(x,t)$ is the desired curve Γ_t, i.e.

$$\Gamma_t = \{x : \phi(x,t) = 0\}.$$

Conversely, we can associate with Ω_t an auxiliary function $\phi(x,t)$, which is Lipschitz continuous and satisfies the following conditions:

$$\begin{cases} \phi(x,t) > 0 & \text{in} \quad \Omega_t \\ \phi(x,t) = 0 & \text{on} \quad \Gamma_t \\ \phi(x,t) < 0 & \text{in} \quad \mathbb{R}^n - \bar{\Omega}_t. \end{cases}$$

It is clear that moving the interface is equivalent to updating the level set function ϕ.
What remains is to introduce an equation which will describe the motion of the level-set surface. For the derivation of this equation we follow the steps given in [34].
To obtain the equation for the level-set function we consider some level-set $\phi(x,t) = C$. The trajectory $x(t)$ of a particle located on this level-set should satisfy the equation

$$\phi(x(t),t) = C. \tag{5.26}$$

After differentiating the equation (5.26) we get

$$\phi_t + x'(t)\nabla\phi = 0. \tag{5.27}$$

Finally, denoting by $w := x'(t)$ the particle velocity, we arrive at the level-set equation

$$\phi_t + w \cdot \nabla\phi = 0. \tag{5.28}$$

Usually, the moving interface Γ_t has a prescribed velocity w, which might be a function of space variable x, time variable t, mean curvature, normal direction, etc. In our case this velocity also depends on the gradient of the temperature of the material, but we will address this issue a bit later.

There are certain advantages why we employ level set theory for our goal to capture the propagating interface (cutting front). The advantages are:

- Topological changes in the propagating front are handled properly. The position of the cutting front at time instant t is given by the zero level set of ϕ. With level set approach we avoid forcing this set to be a single curve. The curve is allowed to break (during cutting) or merge (during welding) as the time advances. In both cases the level set function remains single valued.

- The level set equation is a hyperbolic equation of first order. Therefore, we can apply all techniques of the theory of conservation laws in order to analyse the equation on solvability. For obtaining results on existence of unique weak solution, one is free to employ the concepts of viscosity solutions and method of characteristics. In addition, the level set equation can be accurately approximated by computational schemes borrowed from the numerical analysis of hyperbolic equations. For example, level set method is well adapted to applications of adaptive strategies, which lead to Narrow band level set methods and Fast marching methods [41].

- Main quantities such as domain, velocity, normal, etc. are easily expressible by level set function. This is a very important advantage as we will see later in Section 5.2.2.

5.2.1 Distance function

In addition to the level-set equation (5.28) we need an initial condition for ϕ as well. Taking into account the fact that the level-set function $\phi(x,t)$ is positive for $x \in \Omega$, negative for $x \notin \overline{\Omega}$ and equal zero on the domain boundary Γ_0, it is natural to choose the signed distance function as a good candidate for the initial value $\phi(x, t = 0)$. Thus, the initial condition for

(5.28) takes the form

$$\phi(x,0) = \begin{cases} d(x) & \text{for} \quad x \in \Omega \\ 0 & \text{for} \quad x \in \Gamma_0 \\ -d(x) & \text{for} \quad x \notin \Omega \end{cases} \tag{5.29}$$

where $d(x)$ is the distance from the point x to the initial curve Γ_0. An example of a distance function for a circle in the square is illustrated in Figure 5.2.

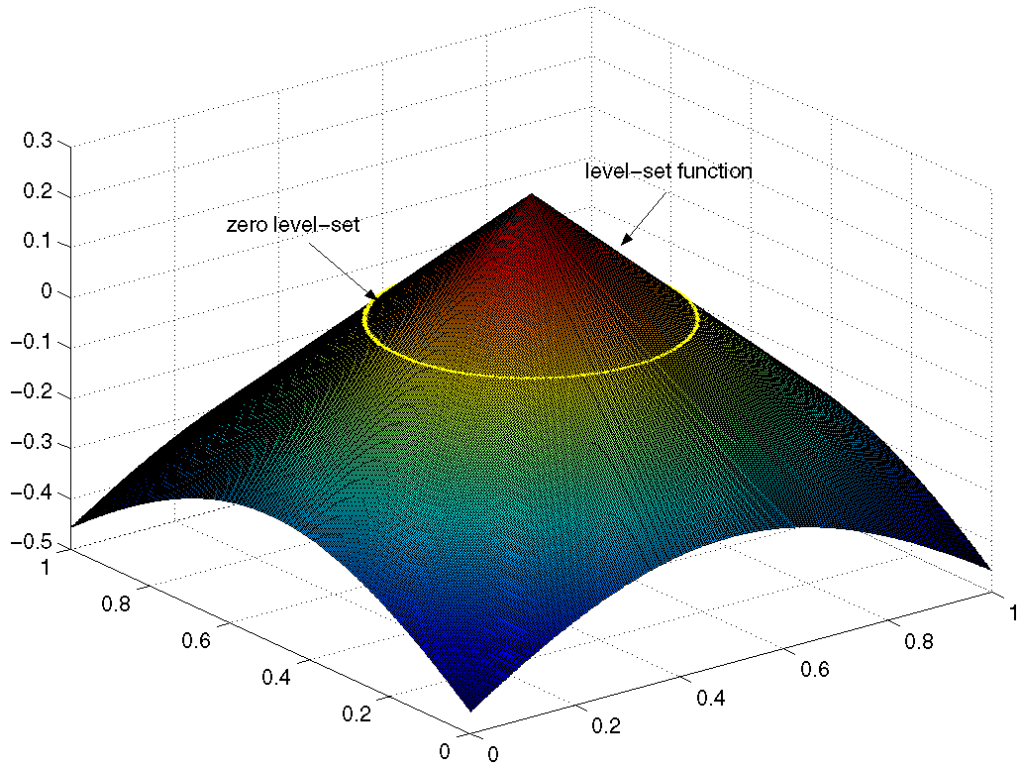

Figure 5.2: Distance Function for Circle

5.2.2 Stefan condition as level-set equation

Let assume at the moment that the temperature distribution θ in the workpiece is given. The problem of finding the second unknown of the cutting problem, namely the geometry of the cutting front, can be formulated as follows:

Problem 5.2.1. *Find a family of moving interfaces* $\{\partial\Omega_t\}_{t\in(0,T)}$ *such that*

$$k\nabla\theta\cdot\nu-\rho L_m v\cdot\nu = j_{abs} \text{ on } \partial\Omega_t \tag{5.30}$$

$$\partial\Omega_t|_{t=0} = \partial\Omega_0 \tag{5.31}$$

In order to apply the level-set theory shortly described in the previous section, we suppose that the moving interface $\Gamma_t := \partial\Omega_t$, which bounds the domain Ω_t occupied by the workpiece, is built into a level-set function $\phi(x,t)$. Now we redefine the terms occurring in the Stefan condition with the help of the level-set function ϕ.

The workpiece: the domain $\Omega_t := \Omega_s(t)$ is represented as

$$\Omega_t = \{x;\ \phi(x,t) > 0\}.$$

The cutting interface : the advancing cut front Γ_t is given by

$$\Gamma_t = \{x;\ \phi(x,t) = 0\}.$$

The unit normal: the unit outward normal ν to Γ_t has the following level-set representation

$$\nu = \frac{\nabla\phi}{|\nabla\phi|}.$$

The heat flux: for the absorbed heat flux j_{abs} we use its expression (3.30) derived in Section 3.5

$$j_{abs} = j_e r\cdot\nu\cdot\nu_r = j_e r\frac{\nabla\phi\cdot\nu_r}{|\nabla\phi|}.$$

The velocity of interface: the velocity of the moving interface in the normal direction can be represented as

$$v\cdot\nu = -\frac{\frac{\partial\phi}{\partial t}}{|\nabla\phi|}.$$

Indeed, for two dimensional domain (analogy works for any dimension) the interface is given by

$$\phi(x,y,t) = 0. \tag{5.32}$$

By chain rule,

$$\frac{d\phi}{dt} = \frac{\partial\phi}{\partial x}\cdot\frac{dx}{dt} + \frac{\partial\phi}{\partial y}\cdot\frac{dy}{dt} + \frac{\partial\phi}{\partial t} = 0. \tag{5.33}$$

Using the definitions $\nabla\phi = \left(\frac{\partial\phi}{\partial x}, \frac{\partial\phi}{\partial y}\right)$ and $v = \left(\frac{dx}{dt}, \frac{dy}{dt}\right)$ we arrive to

$$v\cdot\nabla\phi = -\frac{\partial\phi}{\partial t} \tag{5.34}$$

But

$$v \cdot \nabla\phi = v \cdot \frac{\nabla\phi}{|\nabla\phi|}|\nabla\phi| = v \cdot \nu|\nabla\phi|$$

Thus

$$v \cdot \nu = -\frac{\frac{\partial\phi}{\partial t}}{|\nabla\phi|}.$$

The terms in Stefan condition (5.30) are already defined by their level-set representation. All that remains is to substitute their expressions in (5.30).

$$k\nabla\theta \cdot \frac{\nabla\phi}{|\nabla\phi|} + \rho L_m \frac{\frac{\partial\phi}{\partial t}}{|\nabla\phi|} = j_e r \frac{\nabla\phi \cdot \nu_r}{|\nabla\phi|},$$

$$\frac{\partial\phi}{\partial t} + \frac{1}{\rho L_m}\left(k\nabla\theta - j_e r\nu_r\right) \cdot \nabla\phi = 0. \tag{5.35}$$

We can easily see that the last equation is simply the level-set equation with the velocity of convection equal to

$$w := \frac{1}{\rho L_m}\left(k\nabla\theta - j_e r\nu_r\right). \tag{5.36}$$

Note, that w is the velocity on the advancing front and is equal to something arbitrary elsewhere. The crucial point here is that not only the moving interface is embedded in a higher dimensional level set function, but also the velocity w itself is embedded in a level set function. Therefore, the velocity w has to be extended to other level sets in such a way that the new extension velocity matches the given velocity on the moving front itself. The important point here is that the extension should be done in a continuous manner in order to avoid a development of any discontinuity of the level set function. One way to construct an extension velocity is to extrapolate the velocity from the front to the entire domain, [41]. The idea is to define the velocity of every point on the mesh to be equal to the velocity of the closest point on the moving front (zero level set). For more details on the above mentioned method we refer to the work of [41] and references therein. In this study one can find various other approaches concerning the extension velocity as well.

Remark 5.2.1. *The velocity of propagating interface depends on the heat flux absorbed by the material at the cutting front (or emitted by the plasma beam), therefore, such parameters like the velocity with which the plasma beam advances in the cutting direction and the heat flux emitted by the beam are of central importance. On the other hand, since the molten material is removed immediately after it appears, the velocity of the front strongly depends on temperature distribution, more precisely, on the gradient of the temperature on the interface.*

In the expression of w one can see the dependence of velocity of the interface on several material parameters which one would naturally expect.

5.3 Weak formulation of Stefan-Signorini problem

Variational inequalities and the theory of level sets lead us to following weak formulation of the Stefan-Signorini problem (3.7)-(3.11):

Problem 5.3.1. *Find the pair $(\theta(x,t), \phi(x,t))$ representing the temperature and the moving interface, respectively, such that*

1. *$\theta \in \mathbb{B}_0$ and $\phi \in \mathbb{C}(Q)$ with $\phi(x,0) = \phi_0(x)$ in Ω,*

2. *$\theta \leq \theta_m$ on $\partial\Omega_t$,*

3. *θ satisfies the inequality*

$$\int_0^T \int_{\Omega_t} \varphi'(\varphi - \theta) dxdt + \int_0^T \int_{\Omega_t} \nabla\theta \cdot \nabla(\varphi - \theta) dxdt \tag{5.37}$$

$$\geq \int_0^T \int_{\partial\Omega_t} j_{abs}(\varphi - \theta) d\gamma dt + \frac{1}{2}\|\varphi(T) - \theta(T)\|^2 - \frac{1}{2}\|\varphi(0) - \theta_0\|^2,$$

   for all $\varphi \in \mathbb{B}$, $j_{abs} \in \mathbb{H}^1(R^n) \cap \mathbb{L}^\infty(R^n)$,

4. *ϕ is the solution of the equation*

$$-\int_Q \phi v' \; dxdt + \int_Q \phi v \nabla \cdot \omega \; dxdt - \int_Q \phi\omega \cdot \nabla v \; dxdt = \int_\Omega \phi_0 v(x,0) \; dx \tag{5.38}$$

   for all $v \in \mathbb{C}^1(0,T; C_0^1(\Omega_t))$ with $v(x,T) = 0$,

where ω is the velocity of the zero level-set of ϕ defined in (5.36) and $Q := \Omega \times I$.

Chapter 6

Analysis of the Model

6.1 Existence and uniqueness of classical solution – one dimensional case

We recall here the one-dimensional model already derived in Section 3.3. Our goal is to find the temperature distribution $\theta(x,t)$ of the solid region and the melted thickness $s(t)$ such that they satisfy the following conditions:

$$\rho c_s \frac{\partial \theta}{\partial t} = \frac{\partial}{\partial x}\left(k\frac{\partial \theta}{\partial x}\right), \qquad s(t) < x < L, \quad 0 < t < T, \tag{6.1}$$

$$\begin{aligned} \theta &\leq \theta_m \\ -k\frac{\partial \theta}{\partial x} + j_{abs}(t) &\geq 0 \\ (\theta - \theta_m)\left(k\frac{\partial \theta}{\partial x} + j_{abs}(t)\right) &= 0 \end{aligned} \tag{6.2}$$

$$-k\frac{\partial \theta}{\partial x} + \rho L_m s'(t) = j_{abs}, \qquad 0 < t < T, \tag{6.3}$$

$$\frac{\partial \theta}{\partial x} = 0, \qquad x = L, \quad 0 < t < T, \tag{6.4}$$

$$\theta(x,0) = \theta_0(x) < \theta_m, \qquad 0 < x < L, \tag{6.5}$$

$$s(0) = 0. \tag{6.6}$$

Below we state a result which delivers us a solution of above mentioned model. As usual all material parameters are set equal to one and the melting temperature is assumed to be zero.

Theorem 6.1.1. *There exists a unique solution of the one-dimensional cutting model (6.1)-(6.6).*

Proof. We provide here the outline of the proof only. The complete proof of this existence result is a simple consequence of the one done by Friedman and Jiang [16]. In their work they also studied the regularity and the geometrical features of the free boundary. Later, Jiang showed the uniqueness of the classical solution.
Step 1. Fix the free boundary $s(t)$ and consider the Signorini problem (6.1)+(6.2)+ (6.4) +(6.5)+(6.6). Then the following lemma is true:

Lemma 6.1.1. *Let $s \in \mathbb{C}^1[0,T]$ and $s(T) < L$. Then the problem (6.1)+(6.2)+(6.4)-(6.6) has a unique classical solution θ. Moreover the following estimates hold*

$$0 \leq \frac{\partial \theta}{\partial x}(s(t),t) + j_{abs} \leq C_0, \tag{6.7}$$

$$|\frac{\partial \theta}{\partial x}| \leq C_0, \tag{6.8}$$

$$|\frac{\partial^2 \theta}{\partial x^2}| + |\theta'| \leq C_1, \tag{6.9}$$

$$|\frac{\partial \theta}{\partial x}(x,t_1) - \frac{\partial \theta}{\partial x}(x,t_2)| \leq C_1 |t_1 - t_2|^{\frac{1}{2}}, \tag{6.10}$$

where C_0, C_1 are constants depending on the data of the problem.

Proof. The proof is illustrated in [16]. □

Step 2. We denote

$$X_A := \left\{ s \in \mathbb{C}^1[0,T]; s(0) = 0,\ 0 \leq s'(t) \leq A\ \forall t \in (0,T) \right\}$$

where A is a positive constant and T is small enough such that

$$s(T) \leq AT < L$$

After integration of the equation (3.1) and taking into account that θ solves the Signorini problem, we obtain

$$\int_0^t \left(j_{abs} + \frac{\partial \theta}{\partial x}(s(t),t) \right) dt = \int_0^t j_{abs}(t) + \int_{s(t)}^L \theta(x,t)dx - \int_0^L \theta_0(x)dx + \int_0^t \theta(s(t),t)s'(t)dt. \tag{6.11}$$

Now we take any $s \in X_A$ and solve the Signorini problem. The existence of the unique solution follows from Lemma 6.1.1. Set

$$Hs = \tilde{s}$$

where

$$\tilde{s}(t) = \int_0^t j_{abs}(t) + \int_{s(t)}^L \theta(x,t)dx - \int_0^L \theta_0(x)dx + \int_0^t \theta(s(t),t)s'(t)dt. \tag{6.12}$$

Step 3. We can show that the mapping H has a fixed point in X_A, [16]. One starts by showing that H maps the set X_A into itself. Next, one shows that H is a continuous mapping. What remains is to use the Shauder's fixed point theorem and state that the mapping H has a fixed point in X_A.

Step 4. Having in mind the existence of the fixed point of H and using the equations (6.11) and (6.12) we arrive at

$$s(t) = \int_0^t \left(j_{abs} + \frac{\partial \theta}{\partial x}(s(t),t) \right) dt.$$

Finally, the derivation of the last equation with respect to t leads us to

$$s'(t) = j_{abs} + \frac{\partial \theta}{\partial x}(s(t),t),$$

which is nothing else, but the Stefan condition (3.3). Thus the pair (θ, s) is the solution of one-dimensional Stefan-Signorini problem (3.1)-(3.6). □

6.1.1 Regularity of the free boundary

Another important issue is, of course, the regularity of the free boundary $s(t)$. From Stefan condition (3.3) and the estimate (6.10) of Lemma 6.1.1 it follows that

$$s(t) \in \mathbb{C}^{\frac{3}{2}}[0,T].$$

It can be shown that this regularity of the free boundary is optimal. Indeed, one can prove that, in general, the following holds:

$$s(t) \notin \mathbb{C}^{1+\alpha} \qquad \text{for all} \qquad \alpha > \frac{1}{2}.$$

For the complete proof of this statement we refer to [16].

6.2 Existence and uniqueness of the weak solution – higher dimensional case

6.2.1 Higher dimensional model

Let Ω be again a bounded open subset of $\mathbb{R}^n$, $n = 2, 3$, occupying the workpiece with a smooth boundary $\partial\Omega$. Let us consider again the mathematical model of the workpiece derived in Section 3.4.

Problem 6.2.1.

$$\rho c_s \frac{\partial \theta}{\partial t} = \nabla \cdot (k \nabla \theta) \qquad in\ \Omega_T, \tag{6.13}$$

$$\begin{aligned} \theta &\leq \theta_m \\ j_{abs} - k\nabla\theta \cdot \nu &\geq 0 \\ (\theta - \theta_m)(j_{abs} - k\nabla\theta \cdot \nu) &= 0 \end{aligned} \tag{6.14}$$

$$k\nabla\theta \cdot \nu - \rho L_m v \cdot \nu = j_{abs}, \tag{6.15}$$

$$\theta(x, 0) = \theta_0(x) < \theta_m \qquad x \in \Omega \tag{6.16}$$

$$\Omega_s(0) = \Omega \tag{6.17}$$

Our goal in the following sections is to analyse this cutting model using the theory of variational inequalities and level set method.

6.2.2 The abstract theory of penalty method

Let $\theta \in \mathbb{K}$ be the solution of the variational inequality

$$\int_\Omega \theta'(\varphi - \theta)dx + \int_\Omega \nabla\theta \cdot \nabla(\varphi - \theta)dx \geq \int_\Omega f(\varphi - \theta)dx \tag{6.18}$$

for all $\varphi \in \mathbb{K}$, some function f and $\theta(0) = \theta_0$.

The idea behind the penalty method is rather simple. We replace the inequality (6.18) with a sequence of approximating equations involving a *penalty term*. This term has the property that it increases if the solution "moves" far from the convex set $\mathbb{K}$. So, the role of the penalty term is to force the limit of the sequence of the approximate solutions to belong to $\mathbb{K}$. To formulate this in mathematical way, we follow the steps in [22].

Let $\mathbb{V}$ be a reflexive Banach space, $\mathbb{V}'$ its dual and assume that the norms in $\mathbb{V}$ and $\mathbb{V}'$ are strictly convex. Let $\mathbb{K}$ be a closed convex subset of $\mathbb{V}$.

Definition 6.2.1. *We call a mapping* $A : \mathbb{K} \to \mathbb{V}'$ monotone *if*

$$\langle A(x) - A(y), x - y\rangle \geq 0 \text{ for all } x, y \in \mathbb{K}.$$

The operator A *is called* strictly monotone *if the strict inequality holds, i.e. the equality holds only when* $x = y$.

Definition 6.2.2. *We say that the mapping* $A : \mathbb{K} \to \mathbb{V}'$ *is* coercive *if the following condition is satisfied:*

$$\frac{\langle A(x) - A(x_0), x - x_0\rangle}{|x - x_0|} \to +\infty \text{ as } |x| \to +\infty,\ x \in \mathbb{K}$$

for some element $x_0 \in \mathbb{K}$.

Definition 6.2.3. *Any operator* $\beta : \mathbb{V} \to \mathbb{V}'$ *is called the penalty operator, if it satisfies the following conditions:*

1. *operator* β *fulfils the Lipschitz condition (global or local),*
2. β *is a monotone operator,*
3. $\mathbb{K} = ker(\beta) := \{u \in \mathbb{V} \mid \beta(u) = 0\}$.

It is known, [22], that for a given convex set $\mathbb{K}$ there exists infinitely many penalty operators. For a parabolic variational inequality (6.18), the penalty operator β may be introduced via

$$\beta = J(I - P_K) \tag{6.19}$$

where J is the duality mapping from $\mathbb{V}$ to $\mathbb{V}'$, i.e. $J : \mathbb{V} \to \mathbb{V}'$ and

$$\langle J(v), v\rangle = \|J(v)\|_{\mathbb{V}'}\|v\|_{\mathbb{V}} \quad \forall v \in \mathbb{V}.$$

and the operator P_K is the projection operator onto the convex set $\mathbb{K}$, i.e. for any $v \in \mathbb{V}$ the projection $P_K v$ is the uniquely defined element from $\mathbb{K}$ such that

$$\|v - P_K v\| \leq \|v - u\| \quad \forall u \in \mathbb{K}.$$

It is up to verification that the operator defined in (6.19) is a penalty operator.
Now we approximate the variational inequality (6.18) by the following equation which we call the *equation with penalty* associated to the Problem (6.18):

$$\left(\theta'_\varepsilon, \varphi\right) + a\left(\theta_\varepsilon, \varphi\right) + \frac{1}{\varepsilon}\left(\beta(\theta_\varepsilon), \varphi\right) = (f, \varphi) \quad \forall \varphi \in \mathbb{V}. \tag{6.20}$$

The equation (6.20) is non-linear. The existence of the solution θ_ε is a result of the theory of monotone operators studied by several authors, [22],[32], etc. Important is that one can prove the following result, [24].

Lemma 6.2.1. *For $\varepsilon \to 0$ we have that*

$$\theta_\varepsilon \to \theta \text{ weak in } \mathbb{B},$$

where θ is the solution of the inequality (6.18).

The penalty method which we shortly described will serve as a main tool to prove the existence of the weak solution of cutting model.

6.2.3 Existence and uniqueness of the weak solution of Signorini problem

In the following we assume that the moving front $\partial\Omega_t$ and its normal velocity are given. It means that we fix the function $\phi(x,t)$ and consider the problem on a fixed domain Ω_t. We additionally assume that the zero level-set of the function $\phi(x,t)$ is a Lipschitz curve, i.e. the boundary of the domain occupied by the workpiece is a $\mathbb{C}^{0,1}$-boundary. Then the heat equation, together with the Signorini boundary conditions and initial condition, determines the temperature distribution θ. The problem can be formulated as follows.

Problem 6.2.2. *Solve the equation*

$$\frac{\partial\theta}{\partial t} = \Delta\theta \qquad \text{in } \Omega_T. \tag{6.21}$$

with boundary conditions on $\partial\Omega_t$

$$\begin{aligned} \theta &\leq 0 \\ j_{abs} - \nabla\theta\cdot\nu &\geq 0 \\ \theta(j_{abs} - \nabla\theta\cdot\nu) &= 0 \end{aligned} \tag{6.22}$$

and initial condition

$$\theta(x,0) = \theta_0(x) < 0, \qquad x \in \Omega. \tag{6.23}$$

We recall that the Problem 6.2.2 can be rewritten in a form of variational inequality, the weaker form of which is presented in Section 5.3. The proof of the existence and uniqueness

of this weak solution is presented below.

Having in disposal the relation

$$\mathbb{H}^1(\Omega_t) \subset \mathbb{L}^2(\Omega_t) \subset \left(\mathbb{H}^1(\Omega_t)\right)',$$

for a fixed t, let us state the following result.

Lemma 6.2.2. *Let $\theta_0 \in \mathbb{K}$ is given. Then there exists a unique function θ satisfying the following conditions:*

1. $\theta \in \mathbb{L}^2\left(0,T;\mathbb{H}^1(\Omega_t)\right) \cap \mathbb{C}\left(0,T;\mathbb{L}^2(\Omega_t)\right)$,
2. $\theta(t) \in \mathbb{K}$ *and* $\theta(t) \to \theta_0$ *in* $\mathbb{L}^2(\Omega_t)$ *as* $t \to 0$,
3. θ *satisfies the variational inequality*

$$\begin{aligned} &\int_0^s \int_{\Omega_t} \varphi'(\varphi-\theta)dxdt + \int_0^s \int_{\Omega_t} \nabla\theta\cdot\nabla(\varphi-\theta)dxdt \\ \geq\ &\int_0^s \int_{\partial\Omega_t} j_{abs}(\varphi-\theta)d\gamma dt + \frac{1}{2}\|\varphi(T)-\theta(T)\|^2 - \frac{1}{2}\|\varphi(0)-\theta_0\|^2, \end{aligned}$$

for all $\varphi \in \mathbb{B}$, $j_{abs} \in \mathbb{H}^1(\mathbb{R}^n) \cap \mathbb{L}^\infty(\mathbb{R}^n)$ and $\forall s \in [0,T]$.

Proof. For the proof we are going to apply the penalty method first introduced in [24], so let us first define the penalty operator like in (6.19), i.e.

$$\beta(\varphi) = J(\varphi - P_K\varphi),$$

where J in our particular case is the identity operator, and we set $P_K\varphi = \varphi^-$. Here we used the notations

$$\varphi^+(x) = \begin{cases} \varphi(x) & \text{if} \quad x \geq 0 \\ 0 & \text{if} \quad x < 0. \end{cases}$$

$$\varphi^-(x) = \begin{cases} 0 & \text{if} \quad x > 0 \\ -\varphi(x) & \text{if} \quad x \leq 0. \end{cases}$$

Using the fact that $\varphi = \varphi^+ - \varphi^-$, we can write the penalty operator in the form

$$(\beta(\varphi),\phi) = \int\limits_{\partial\Omega_t} \varphi^+\phi d\gamma, \quad \varphi,\phi \in \mathbb{H}^1(\Omega_t). \tag{6.24}$$

It is clear that the penalty operator defined in (6.24) is a monotone, bounded and semi-continuous operator and the equivalences

$$\beta(\varphi) = 0 \;\Leftrightarrow\; \varphi^+ = 0 \;\Leftrightarrow\; \varphi \in \mathbb{K}.$$

are satisfied. Let us first prove a basic result.

Lemma 6.2.3. *Assume that $j_{abs}(\cdot,t) \in \mathbb{L}^2(\partial\Omega_t)$ for all $t > 0$ and there exists a constant $C > 0$ such that*

$$\int_0^t \|j_{abs}\|_{\mathbb{L}^2(\partial\Omega_t)} dt \le C.$$

For $\varepsilon > 0$ let θ_ε be the penalty approximation to θ. Then

$$\frac{1}{\varepsilon}\theta_\varepsilon^+ \text{ are bounded in } \mathbb{L}^2(0,T;\mathbb{L}^2(\partial\Omega_t)). \tag{6.25}$$

Proof. The associated problem with penalty has the form

$$\begin{aligned}\int_0^t \int_{\Omega_t} \theta_\varepsilon' \varphi dx d\tau + \int_0^t \int_{\Omega_t} \nabla\theta_\varepsilon \cdot \nabla\varphi dx d\tau \;&+\; \frac{1}{\varepsilon}\int_0^t \int_{\partial\Omega_t} \theta_\varepsilon^+ \varphi d\gamma dt \\ &= \int_0^t \int_{\partial\Omega_t} j_{abs}\varphi d\gamma dt. \end{aligned}\tag{6.26}$$

Setting $\varphi = \theta_\varepsilon^+$ in (6.26), we obtain

$$\begin{aligned}\int_0^T \int_{\Omega_t} \theta_\varepsilon' \theta_\varepsilon^+ dx d\tau + \int_0^T \int_{\Omega_t} \nabla\theta_\varepsilon \cdot \nabla\theta_\varepsilon^+ dx d\tau \;&+\; \frac{1}{\varepsilon}\int_0^T \int_{\partial\Omega_t} \theta_\varepsilon^+ \theta_\varepsilon^+ d\gamma dt \\ &= \int_0^T \int_{\partial\Omega_t} j_{abs}\theta_\varepsilon^+ d\gamma dt. \end{aligned}\tag{6.27}$$

It is clear that

$$\int_0^T \int_{\Omega_t} \nabla\theta_\varepsilon \cdot \nabla\theta_\varepsilon^+ dx d\tau = \int_0^T \int_{\Omega_t} \nabla\theta_\varepsilon^+ \cdot \nabla\theta_\varepsilon^+ dx d\tau \ge 0.$$

Analogously we get

$$\int_0^T \int_{\Omega_t} \theta_\varepsilon' \theta_\varepsilon^+ dx d\tau \ge 0.$$

After dividing both sides of (6.27) by ε, we arrive at

$$\frac{1}{\varepsilon^2}\int_0^T \int_{\partial\Omega_t} (\theta_\varepsilon^+)^2 d\gamma dt \le \frac{1}{\varepsilon}\int_0^T \int_{\partial\Omega_t} j_{abs}\theta_\varepsilon^+ d\gamma dt$$

or, what is equivalent

$$\|\frac{1}{\varepsilon}\theta_\varepsilon^+\|^2_{\mathbb{L}^2(0,T;\mathbb{L}^2(\partial\Omega_t))} \le \|j_{abs}\| \|\frac{1}{\varepsilon}\theta_\varepsilon^+\|_{\mathbb{L}^2(0,T;\mathbb{L}^2(\partial\Omega_t))}. \tag{6.28}$$

Thus, by the assumption of the lemma

$$\|\theta_\varepsilon^+\|_{\mathbb{L}^2(0,T;\mathbb{L}^2(\partial\Omega_t))} \leq \varepsilon C.$$

□

Let us return to the equation (6.26). From the theory of evolution equations it is known that for every $\varepsilon > 0$ the equation (6.26) has a unique solution $\theta_\varepsilon \in \mathbb{B}$. The substitution $\varphi = \theta_\varepsilon$ in (6.26) yields

$$\frac{1}{2}\|\theta_\varepsilon(t)\|^2_{\mathbb{L}^2(\Omega_t)} - \frac{1}{2}\|\theta_0\|^2_{\mathbb{L}^2(\Omega_t)} + \int_0^t \int_{\Omega_t} \nabla\theta_\varepsilon \cdot \nabla\theta_\varepsilon dx d\tau \quad + \quad \frac{1}{\varepsilon}\int_0^t \int_{\partial\Omega_t} \theta_\varepsilon^+ \theta_\varepsilon d\gamma dt$$
$$= \int_0^t \int_{\partial\Omega_t} j_{abs}\theta_\varepsilon d\gamma dt. \quad (6.29)$$

It is clear that $0 \in \mathbb{K}$ and $\beta(0) = 0$. Then, because of the monotonicity of the penalty operator β, we get

$$(\beta(\theta), \theta) = (\beta(\theta) - \beta(0), \theta - 0) = \int_{\partial\Omega_t} \theta_\varepsilon^+ \theta_\varepsilon d\gamma dt \geq 0. \quad (6.30)$$

Using the inequality (6.30) and the fact that

$$\int_{\Omega_t} \nabla\theta_\varepsilon \cdot \nabla\theta_\varepsilon dx \geq C_1 \|\theta_\varepsilon\|^2_{\mathbb{H}^1(\Omega_t)}, \quad (6.31)$$

we conclude

$$\frac{1}{2}\|\theta_\varepsilon(t)\|^2_{\mathbb{L}^2(\Omega_t)} + C_1 \int_0^t \|\theta_\varepsilon\|^2_{\mathbb{H}^1(\Omega_t)} dt \leq \int_0^t \int_{\partial\Omega_t} j_{abs}\theta_\varepsilon d\gamma dt + \frac{1}{2}\|\theta_0\|^2_{\mathbb{L}^2(\Omega_t)},$$

or

$$\|\theta_\varepsilon\|_{\mathbb{L}^2(0,T;\mathbb{H}^1(\Omega_t))} + \|\theta_\varepsilon\|_{\mathbb{L}^\infty(0,T;\mathbb{L}^2(\Omega_t))} \leq C_2,$$

for every $\varepsilon > 0$, C_1 being some constant independent on ε. Thus, θ_ε are bounded in $\mathbb{L}^2(0,T;\mathbb{H}^1(\Omega_t)) \cap \mathbb{L}^\infty(0,T;\mathbb{L}^2(\Omega_t))$. Aubin's theorem implies that we can subtract a subsequence (again denote it by θ_ε) such that

$$\theta_\varepsilon \to \theta \quad \text{weak in } \mathbb{L}^2(0,T;\mathbb{H}^1(\Omega_t)),$$

$$\theta_\varepsilon \to \theta \quad \text{weak}^* \text{ in } \mathbb{L}^2(0,T;\mathbb{L}^2(\Omega_t)).$$

Hence, $\beta(\theta(t)) = 0$ almost everywhere which implies that $\theta(t) \in \mathbb{K}$ a.e.

Our next step is to prove that this limit θ fulfils the inequality (6.24). Consider any function $\varphi \in \mathbb{B}$, so $\varphi^+ = 0$. From equation (6.26) we obtain

$$\int_0^t \int_{\Omega_t} \varphi'(\varphi - \theta_\varepsilon) dx d\tau + \int_0^t \int_{\Omega_t} \nabla\theta_\varepsilon \cdot \nabla(\varphi - \theta_\varepsilon) dx d\tau + \frac{1}{\varepsilon} \int_0^t \int_{\partial\Omega_t} (\theta_\varepsilon^+ - \varphi^+)(\varphi - \theta_\varepsilon) d\gamma dt$$

$$= \int_0^t \int_{\partial\Omega_t} j_{abs}(\varphi - \theta_\varepsilon) d\gamma dt + \frac{1}{2}\|\varphi(T) - \theta(T)\|^2 - \frac{1}{2}\|\varphi(0) - \theta_0\|^2. \tag{6.32}$$

Again using the monotonicity of the penalty operator, we get

$$\begin{aligned} & \int_0^t \int_{\Omega_t} \varphi'(\varphi - \theta_\varepsilon) dx d\tau + \int_0^t \int_{\Omega_t} \nabla\theta_\varepsilon \cdot \nabla(\varphi - \theta_\varepsilon) dx d\tau \\ \geq & \int_0^t \int_{\partial\Omega_t} j_{abs}(\varphi - \theta_\varepsilon) d\gamma dt + \frac{1}{2}\|\varphi(T) - \theta(T)\|^2 - \frac{1}{2}\|\varphi(0) - \theta_0\|^2. \end{aligned}$$

Obviously, our goal now will be to take the limits of both sides of (6.33) as $\varepsilon \to 0$. Let ψ be any continuous function from $\mathbb{C}(0,T)$ such that $\psi(t) \geq 0$ for all $t \in [0,T]$. The inequality (6.33) then is equivalent to

$$\begin{aligned} & \int_0^T \psi(s) ds \Big[\int_0^t \int_{\Omega_t} \varphi' \varphi dx d\tau + \int_0^t \int_{\Omega_t} \nabla\theta_\varepsilon \cdot \nabla\varphi dx d\tau - \int_0^t \int_{\partial\Omega_t} j_{abs} \varphi d\gamma d\tau \\ & - \int_0^t \int_{\Omega_t} \varphi' \theta_\varepsilon dx d\tau + \int_0^t \int_{\partial\Omega_t} j_{abs} \theta_\varepsilon d\gamma d\tau \Big] \\ \geq & \int_0^T \psi(s) ds \left[\int_0^t \int_{\Omega_t} \nabla\theta_\varepsilon \cdot \nabla\theta_\varepsilon dx d\tau + \frac{1}{2}\|\varphi(T) - \theta_\varepsilon(T)\|^2 \right] - \int_0^T \psi(s) \frac{1}{2}\|\varphi(0) - \theta_0\|^2 ds. \end{aligned}$$

On the other hand

$$\begin{aligned} & \liminf \int_0^T \psi(s) ds \left[\int_0^t \int_{\Omega_t} \nabla\theta_\varepsilon \cdot \nabla\theta_\varepsilon dx d\tau + \frac{1}{2}\|\varphi(T) - \theta_\varepsilon(T)\|^2 \right] \\ & \geq \int_0^T \psi(s) ds \left[\int_0^t \int_{\Omega_t} \nabla\theta \cdot \nabla\theta dx d\tau + \frac{1}{2}\|\varphi(T) - \theta(T)\|^2 \right] \end{aligned}$$

Finally, taking the limit in (6.33) as $\varepsilon \to 0$, one arrives at the inequality

$$\begin{aligned} & \int_0^T \psi(s) ds \int_0^t \int_{\Omega_t} \varphi'(\varphi - \theta) dx d\tau + \int_0^t \int_{\Omega_t} \nabla\theta \cdot \nabla(\varphi - \theta) dx d\tau \\ \geq & \int_0^T \psi(s) \Big[\int_0^t \int_{\partial\Omega_t} j_{abs}(\varphi - \theta) d\gamma dt + \frac{1}{2}\|\varphi(T) - \theta(T)\|^2 - \frac{1}{2}\|\varphi(0) - \theta_0\|^2 \Big] ds. \end{aligned}$$

The last inequality is true for any $\psi \in \mathbb{C}(0,T)$, therefore the function θ satisfies the variational inequality (6.24) for almost all $t \in [0,T]$.

Uniqueness. For the proof of the uniqueness of the solution we will assume that there exist two different weak solutions of the Problem 6.2.2. The idea is to take the inequality (6.24), write it for θ_1 and test it with $\varphi = \theta_2$. Analogously we test the inequality (6.24) for θ_2 with $\varphi = \theta_1$ (see Remark 6.2.1). Adding both inequalities together, we obtain

$$-\int_0^t \int_{\Omega_t} (\theta_2-\theta_1)'(\theta_2-\theta_1)dxd\tau - \int_0^t \int_{\Omega_t} \nabla(\theta_2-\theta_1)\cdot\nabla(\theta_2-\theta_1)dxd\tau \geq \|\theta_2(T)-\theta_1(T)\|^2 \geq 0,$$

or equivalently

$$-\int_0^t \|\theta_2-\theta_1\|^2 d\tau - \int_0^t \int_{\Omega_t} (\nabla(\theta_2-\theta_1))^2 dxd\tau \geq 0.$$

The first term on the left hand side is always non-positive, so the inequality stays still valid if we throw it away:

$$\int_0^t \int_{\Omega_t} (\nabla(\theta_2-\theta_1))^2 dxd\tau \leq 0.$$

Thus, after applying the condition (6.31), we get $\theta_1 = \theta_2$.

Remark 6.2.1. *Let us note that the choice of the test function $\varphi = \theta_1$ (or the same for $\varphi = \theta_2$) is not "legal", because in general θ_1 and θ_2 will not belong to $\mathbb{B}$ where the test functions live. One can legalise this by taking φ "very" close to θ_1 (θ_2). For the complete procedure how to implement this we refer to [25].*

To prove that the solution θ belongs to the space $\mathbb{C}\left(0,T;\mathbb{L}^2(\Omega_t)\right)$, we define a function θ_δ as a solution of the ordinary differential equation

$$\delta\theta_\delta' + \theta_\delta = \theta,$$

$$\theta_\delta(0) = \theta_0, \quad \delta > 0.$$

Now we substitute $\varphi = \theta_\delta$ in (6.24):[1]

$$-\delta\int_0^t \|\theta_\delta\|^2 d\tau + \int_0^t \int_{\Omega_t} \nabla\theta\cdot\nabla(\theta_\delta-\theta)dxd\tau \geq \int_0^t \int_{\partial\Omega_t} j_{abs}(\theta_\delta-\theta)d\gamma dt + \frac{1}{2}\|\theta_\delta(T)-\theta(T)\|^2.$$

Thus

$$\|\theta_\delta(t)-\theta(t)\|^2 \leq 2\int_0^t \int_{\Omega_t} \nabla\theta\cdot\nabla(\theta_\delta-\theta)dxd\tau - \int_0^t \int_{\partial\Omega_t} j_{abs}(\theta_\delta-\theta)d\gamma dt.$$

For $\delta \to 0$ the expression on the right hand side tends to zero uniformly with respect to t, therefore, $\theta_\delta \to \theta$ in $\mathbb{L}^2(\Omega_t)$ uniformly with respect to $t \in [0,T]$. This is nothing else, but

[1] It is allowed since $\theta_\delta \in \mathbb{K}$.

the condition $\theta \in \mathbb{C}\left(0,T;\mathbb{L}^2(\Omega_t)\right)$.

To complete the proof of the Lemma 6.2.2, we show now that $\theta(t) \to \theta_0$ as $t \to 0$. Indeed, if we take in (6.24) any φ from the space $\mathbb{B}_0$, we obtain

$$\|\varphi(t)-\theta(t)\|^2 \leq \int_0^t \int_{\Omega_t} \varphi'(\varphi-\theta)dxd\tau + \int_0^t \int_{\Omega_t} \nabla\theta\cdot\nabla(\varphi-\theta)dxd\tau - \int_0^t \int_{\partial\Omega_t} j_{abs}(\varphi-\theta)d\gamma d\tau.$$

The right hand side tends to zero as $t \to 0$, so $\theta(t) \to \varphi(0) = \theta_0$ for $t \to 0$. □

Remark 6.2.2. *Using appropriate numerical schemes, one can show that the solution of the variational inequality (6.18) exists and is unique. Moreover,*

$$\theta, \theta' \in \mathbb{L}^2(0,T;\mathbb{H}^1(\Omega)) \cap \mathbb{L}^\infty(0,T;\mathbb{L}^2(\Omega)).$$

For the proof of this result we refer to [18].

6.2.4 Further regularity results

In the previous section we have shown that the solution θ of the evolutionary variational inequality is a continuous mapping from the time interval $[0,T]$ to the Sobolev space $\mathbb{L}^2(\Omega_t)$, i.e.

$$\theta \in \mathbb{L}^2\left(0,T;\mathbb{H}^1(\Omega_t)\right) \cap \mathbb{C}\left(0,T;\mathbb{L}^2(\Omega_t)\right).$$

In what follows we will present some further regularity results which are essential for the next section where we are going to analyse the level-set equation. The point is that for the proof of the existence and uniqueness of the weak solution of the level-set equation we need "enough" regularity for the velocity of the zero level-set. To be precise, the velocity w needs to be an $\mathbb{H}^1$-function in space. As one may remember, this velocity function contains also the gradient of the temperature, thus we require a $\mathbb{H}^2$-regularity for the temperature distribution in order to fulfil the condition on w to have an $\mathbb{H}^1$-property.

The regularity properties of the solution of variational inequalities have been studied by several authors. In their paper [17] Friedman and Kinderlehrer had studied a one phase Stefan problem by converting it to variational inequality,. A solution to this variational inequality is then interpreted as a generalized solution to the Stefan problem. Avoiding the complex discussions of time dependent convex sets $\mathbb{K}(t)$ (arising from time dependent

boundary conditions) by introducing an expedient penalty function, they were able to establish the existence, uniqueness and $\mathbb{L}^p$-estimates for the solution.

In his book Steinbach discussed the regularity of the solution of evolutionary variational inequality with respect to time and space. The study of the regularity of the solution with respect to time involves the approximation of the inequality problem by the Lewy-Stampacchia bounded penalization method. As for the regularity with respect to space, the author analysed the problem using the associated penalty problem and exploited a semi-discretization procedure in time together with the results from the elliptic regularity theory ($\mathbb{L}^p$-theory). For the complete discussions we refer to [52] and references therein.

Summarizing what has been said above, we include the results, needed for our further discussions, in the following theorem

Theorem 6.2.1. *Let the following assumption on the function j_{abs} be satisfied:*

$$j_{abs} \in \mathbb{L}^2\left(0,T;\mathbb{H}^{\frac{1}{2}}(\partial\Omega_t)\right).$$

Let the boundary of the workpiece $\partial\Omega_t$ be of the class $\mathbb{C}^{1,1}$ at every time instant t.
Then the solution θ of the variational inequality (6.24) will be such that

$$\theta \in \mathbb{H}^{1,\infty}\left(0,T;\mathbb{H}^1(\Omega_t)\right) \cap \mathbb{L}^2\left(0,T;\mathbb{H}^2(\Omega_t)\right).$$

If the function j_{abs} is such that

$$j_{abs} \in \mathbb{L}^\infty\left(0,T;\mathbb{H}^{\frac{1}{2}}(\partial\Omega_t)\right),$$

then the solution θ fulfils the regularity condition

$$\theta \in \mathbb{H}^{1,\infty}\left(0,T;\mathbb{H}^1(\Omega_t)\right) \cap \mathbb{L}^\infty\left(0,T;\mathbb{H}^2(\Omega_t)\right).$$

Proof. This theorem is a simple consequence of a more general result proved in [52]. □

6.2.5 Existence and uniqueness of the weak solution of level-set equation

In the previous section we discussed the existence and uniqueness result of the weak solution of Signorini problem assuming the level-set ϕ, or equivalently the boundary of the domain $\partial\Omega_t$, to be known. In this section we suppose that the temperature distribution $\theta(x,t)$ in

the workpiece is given meaning that the convection velocity $w = \nabla\theta - j_e r \nu_r$ of the level-set function $\phi(x,t)$ is known. We also assume that $\theta \in \mathbb{H}^{1,\infty}\big(0,T;\mathbb{H}^1(\Omega_t)\big) \cap \mathbb{L}^\infty\big(0,T;\mathbb{H}^2(\Omega_t)\big)$. The problem we are going to investigate below is the following

Problem 6.2.3. *Find the function $\phi(x,t) : \mathbb{R}^n \times (0,T) \to \mathbb{R}$, $n = 2,3$, such that*

$$\frac{\partial \phi}{\partial t} + w \cdot \nabla \phi = 0, \tag{6.33}$$

with initial condition

$$\phi(x,0) = \phi_0(x),$$

where ϕ_0 is some initial function satisfying

$$\partial\Omega_t|_{t=0} = \{x \in \mathbb{R}^n;\ \phi_0(x) = 0\}.$$

Remark 6.2.3. *We consider the Problem 6.2.3 on the whole space $\mathbb{R}^n$ for $n = 2,3$. However, it can occur that one needs to restrict himself to a bounded domain $\hat{\Omega}$. In this case appropriate boundary conditions must be prescribed on the outer domain boundary. Depending on the problem one can enforce Dirichlet or Neumann boundary conditions. The issue is that in some problems the moving boundary can grow up and finally touch the domain boundary $\partial\hat{\Omega}$ (independent of how we choose the initial surface). Specification of either boundary condition will provide an information on the location of intersection points (Dirichlet boundary condition) and the angle between the free boundary and $\partial\hat{\Omega}$ at those points (Neumann boundary condition).*

In the following section we will use the *method of characteristics* to obtain the existence and uniqueness result for the weak solution of the Problem 6.2.3.

6.2.6 Method of characteristics

We recall here the *method of characteristics*, which will solve the Problem 6.2.3 by converting the first order partial differential equation into an appropriate system of ordinary differential equations. Suppose that the characteristic curves corresponding to the given velocity field w are given by some curves $x(s)$. The family of these parametrized curves $x(s)$ is a solution of the initial value problem

$$\frac{dx(s)}{ds} = w(x(s),s) \text{ in } \mathbb{R}^n, \tag{6.34}$$

$$x(0) = \bar{x}. \tag{6.35}$$

We note that if $x(s)$ is a characteristic curve, then the level-set function $\phi(x,t)$ is constant along each characteristic. Indeed, if we differentiate $\phi(x,t)$ along one of these curves, we find that

$$\frac{d\phi(x(s),s)}{ds} = \frac{\partial\phi(x(s),s)}{\partial s} + \nabla\phi(x(s),s)\cdot x'(s) = \frac{\partial\phi}{\partial s} + w\cdot\nabla\phi = 0.$$

Therefore, the rate of change of ϕ along the characteristic is equal to zero confirming that ϕ is constant along these characteristics. Assuming that the velocity field w is Lipschitz continuous, it is known that exactly one characteristic $x(s)$ passes through $\bar{x}$, i.e. there exists a unique solution of the equation (6.34) with initial data (6.35).
Unfortunately, in our special problem we do not have enough regularity on temperature distribution θ in order to get a Lipschitz continuous velocity. Remember, that the velocity field w contains the gradient of the temperature which is a $\mathbb{H}^1$-function in space dimension. Thus, the situation tells us to analyse the problem in the contest of weak formulation.

Denote by Φ the closed bounded convex subset of $\mathbb{C}([0,T]\times\mathbb{R}^n)$ given by

$$\Phi = \big\{\phi;\phi\in\mathbb{C}([0,T]\times\mathbb{R}^n), |\phi|\le c\|\phi_0\|_{\mathbb{C}^1(\mathbb{R}^n)} \text{ and } \|\phi(x,t)-\phi(y,s)\|\le\delta\|\phi_0\|_{\mathbb{C}^1(\mathbb{R}^n)}$$
$$\text{for } |x-y|+|t-s|\le\delta\big\}$$

Lemma 6.2.4. *Let ϕ_0 be in $\mathbb{C}^1(\mathbb{R}^n)$ and $j_{abs}\in\mathbb{H}^1(\mathbb{R}^n)\cap\mathbb{L}^\infty(\mathbb{R}^n)$. Then there exists a unique solution $\phi\in\Phi$ of the equation*

$$-\int_Q \phi v'\ dxdt + \int_Q \phi v\nabla\cdot\omega\ dxdt - \int_Q \phi\omega\cdot\nabla v\ dxdt = \int_\Omega \phi_0 v(x,0)\ dx. \tag{6.36}$$

Proof. We set $\omega^\varepsilon = \eta_\varepsilon * \omega$, where η_ε is the Friedrich's mollifier in the variables (x,t). Thanks to the properties of a mollifier, we observe that the regularized velocity ω^ε belongs to the space $\mathbb{C}^\infty(\mathbb{R}^{n+1})$ and, particularly, is Lipschitz continuous.
Now let us consider the following auxiliary problem.

Problem 6.2.4. *Find the function $\phi_\varepsilon(x,t):\mathbb{R}^n\times(0,T)\to\mathbb{R}$, $n=2,3$, such that*

$$\frac{\partial\phi_\varepsilon}{\partial t} + \omega^\varepsilon\cdot\nabla\phi_\varepsilon = 0, \tag{6.37}$$

with initial condition

$$\phi_\varepsilon(x,0) = \phi_0(x). \tag{6.38}$$

Then the system of equations for characteristics is

$$\frac{dx(t)}{dt} = \omega^{\varepsilon}(x(t), t) \tag{6.39}$$

$$x(0) = \bar{x}. \tag{6.40}$$

From the theory of ordinary differential equations it is known that the initial value problem (6.39)-(6.40) has a unique solution $x(t) = X_{\varepsilon}(\bar{x}, t)$.
Set

$$\phi_{\varepsilon}(x, t) = \phi_0(X_{\varepsilon}^{-1}(x, t)),$$

then it is easy to verify that the function ϕ_{ε} solves (6.37). Further, using the regularity of ϕ_0 and for $|x - y| + |t - s| \leq \delta$, one gets

$$|\phi_{\varepsilon}(x, t) - \phi_{\varepsilon}(y, s)| = |\phi_0(\bar{x}) - \phi_0(\bar{y})| \leq |\bar{x} - \bar{y}| \|\phi_0\|_{\mathbb{C}^1(\mathbb{R}^n)}.$$

For $t = s = 0$ the condition $|x - y| + |t - s| \leq \delta$ becomes $|\bar{x} - \bar{y}| = |x(0) - y(0)| \leq \delta$, so we obtain the estimate

$$|\phi_{\varepsilon}(x, t) - \phi_{\varepsilon}(y, s)| \leq \delta \|\phi_0\|_{\mathbb{C}^1(\mathbb{R}^n)}.$$

Now multiplying the equation (6.37) with a smooth test function $v \in \mathbb{C}_0^{\infty}([0, T] \times \mathbb{R}^n)$ and doing some integration by parts, we get

$$-\int_Q \phi_{\varepsilon} v' \, dxdt + \int_Q \phi_{\varepsilon} v \nabla \cdot \omega^{\varepsilon} \, dxdt - \int_Q \phi_{\varepsilon} \omega^{\varepsilon} \cdot \nabla v \, dxdt = \int_{\Omega} \phi_0 v(x, 0) \, dx. \tag{6.41}$$

The function ϕ_{ε} being the classical solution of (6.37) obviously satisfies the integral equation (6.41).
Now we can take a subsequence of ϕ_{ε}, again denoting it by ϕ_{ε}, which converges uniformly to ϕ. Further, we have that $\omega^{\varepsilon} \to \omega$ weakly in $\mathbb{H}^1(Q)$, thus passing to the limit in (6.41) implies that ϕ solves the equation

$$-\int_Q \phi v' \, dxdt + \int_Q \phi v \nabla \cdot \omega \, dxdt - \int_Q \phi \omega \cdot \nabla v \, dxdt = \int_{\Omega} \phi_0 v(x, 0) \, dx, \tag{6.42}$$

which is obviously the weak formulation of the level-set equation

$$\frac{\partial \phi}{\partial t} + \omega \cdot \nabla \phi = 0, \tag{6.43}$$

with initial condition

$$\phi(x, 0) = \phi_0(x).$$

□

It is clear that $\phi_\varepsilon \in \Phi$ and the sequence ϕ_ε converges uniformly on compact subsets of $[0,T] \times \mathbb{R}^n$ with $\phi \in \Phi$.

6.2.7 The coupled system

In this section we are going to discuss on some issues concerning the existence and uniqueness of the weak solution of the Problem 6.2.1. The coupled system 6.2.1 consists of two sub-problems: heat equation with Signorini boundary conditions and level set equation. These two sub-problems are coupled through the temperature entering the expression of the interface velocity in the weak level set equation and integrals over the unknown interface which occur in the weak formulation of heat equation.

Let $(\bar{\phi}, \bar{\theta})$ be in $\Phi \times \mathbb{B}$ and let $\mathcal{L}$ be the mapping of $\Phi \times \mathbb{B}$ into the subsets of $\mathbb{L}^2(Q) \times \mathbb{L}^2(Q)$ defined by

$$(\phi, \theta) = \mathcal{L}(\bar{\phi}, \bar{\theta}), \tag{6.44}$$

where ϕ is the solution of level-set equation given by Lemma 6.2.4, θ is a solution of variational inequality given by Lemma 6.2.2. $\mathbb{B}$ and Φ are the solution sets for the variational inequality and level-set equation, respectively. If one would show that the mapping $\mathcal{L}$ is continuous, then, after application of Schauder's fixed point argument, it is possible to prove the existence and uniqueness of the solution of the coupled system. This issue is quite complicated (due to the time dependent domains entering the definition of solution set $\mathbb{B}$) and beyond the scope of this work. A good reference at this matter is a paper by Bui An Ton, who considered a similar problem with set-valued mappings in domains with fixed and free boundaries. In [55] he established the existence of a weak solution to Stefan-Signorini problem via fixed point technique.
In our study we are mainly interested in the existence of solutions of two above mentioned sub-problems. The point is that later we are going to treat the problem numerically and the idea of numerical approximation of the coupled system is to solve each sub-problem separately by taking the coupling quantities (known) from the previous time step.

Chapter 7

Numerical Results

7.1 Introduction

One of the main difficulties to solve the Stefan-Signorini Problem 5.3.1 numerically is the time dependent domain Ω_t, i.e. at each time instant t, due to the removal of the melt, we have to solve the equations in different domains. Such kind of problems are typically solved via two basic methods.

1. *Moving mesh approach*; in this method the mesh for the space discretization moves with the domain and has to be updated so that it conforms to the new interface.

2. *Fixed domain method*; in this approach there is no need to follow the moving boundary or to iterate it. The heat equation is solved over a fixed physical domain, which is rather easier than on a time dependent region. The position of the boundary (second unknown) can be deduced a posteriori as a feature of the solution. One way to use the fixed domain method is to introduce an enthalpy or total heat function which is responsible for the latent heat absorption or liberation at the interface. This function reformulates then the problem in such a way that the boundary conditions on the moving front are implicitly imbedded in a new form of the equation.

There are several drawbacks of the methods mentioned above. The moving mesh technique suffers mainly from difficulties of remeshing, i.e. if the domain changes drastically in time, we can move the nodes of the mesh together with the domain, but not infinitely long, at some instant t it is not possible to avoid remeshing, so we will need a new mesh for Ω_t generated by some mesh generator. But mesh generators are not always available, as

the difficulties of creating mesh generators increase with the dimension of the problem and complexity of the interfaces. On the other hand, for domains that do not change drastically, we may have to take care about the shape regularity of the moving grids by some smoothing techniques.
As for the enthalpy method, although it is rather easy to implement, because no remeshing is required, but this method does not model the cutting process accurately. Since the molten material is immediately removed after its appearance, we have no liquid phase anymore which is not the typical situation in most melting problems. This fact makes it difficult to define the correct enthalpy function.

7.2 Discretization of the cutting model

In this section we present a solution algorithm for the cutting model. For this purpose we decouple the problem by dividing the whole system into two sub-problems. In the first sub-problem we assume that the level function is given and solve the variational inequality on a *fixed* domain defined by the zero level set. As for the second sub-problem, we solve the weak level set equation assuming that the velocity of the cutting front (expressed via temperature field) is known. After we develop and test two separate algorithms, the next step is to consider the coupled system and establish a corresponding algorithm for the whole model. The coupled algorithm is then implemented using the Finite Element Toolbox ALBERTA developed by Schmidt and Siebert. We provide a very brief description of the software in Appendix C and refer to [46] for details.

7.2.1 Heat equation with Signorini boundary data on a time dependent domain

In the following section we provide a description of a numerical method for the calculation of the temperature field θ assuming that the cutting interface $\partial\Omega_t$ is given and sufficiently smooth. It means our object of investigation is the heat equation with Signorini boundary conditions.
We have already shown that the weak form of the heat conduction equation with Signorini boundary conditions is equivalent to a variational inequality, see Problem 5.1.3. A well known approach for solving the variational inequality (5.24) is the penalty method described

in Section 6.2.2. Recall that applying this method means that instead of Problem 5.1.3 one can consider a family of penalized problems: for $\varepsilon > 0$ find $\theta_\varepsilon \in \mathbb{V}_0$ such that

$$\int_{\Omega_t} \theta'_\varepsilon \varphi dx + \int_{\Omega_t} \nabla\theta_\varepsilon \cdot \nabla\varphi dx + \frac{1}{\varepsilon}\int_{\partial\Omega_t} \theta_\varepsilon^+ \varphi d\gamma = \int_{\partial\Omega_t} j_{abs}\varphi d\gamma, \quad \text{for all } \varphi \in \mathbb{V}. \tag{7.1}$$

Note that the set of test functions is the whole space $\mathbb{V}$ contrary to the space defined for the inequality (5.24).

Time discretization

To solve the penalty equation (7.1), we use a time discretization based on the ϑ-scheme. Let $0 = t_0 < t_1 < \cdots < t_N = T$ be a subdivision of $(0, T)$, denote $\tau_{n+1} = t_{n+1} - t_n$. For $0 \le \vartheta \le 1$, we are looking for a solution $\Theta^{n+1} \approx \theta(\cdot, t_{n+1})$[1] such that the semi-discrete equation

$$\begin{aligned}\int_{\Omega_{t_n}} \frac{(\Theta^{n+1} - \Theta^n)}{\tau_{n+1}}\varphi dx \quad &+ \quad \vartheta\int_{\Omega_{t_n}} \nabla\Theta^{n+1}\cdot\nabla\varphi dx + (1-\vartheta)\int_{\Omega_{t_n}} \nabla\Theta^n\cdot\nabla\varphi dx \\ &+ \quad \frac{1}{\varepsilon}\int_{\partial\Omega_{t_n}} \Theta^{+(n+1)}\varphi d\gamma = \int_{\partial\Omega_{t_n}} j^n_{abs}\varphi d\gamma \end{aligned} \tag{7.2}$$

is fulfilled.

Notice that integrations are done over the domain Ω_t and its boundary $\partial\Omega_t$ at a time instant t_n, i.e. at an old time step, therefore it is assumed that both the domain and its boundary are a priori known. This a priori known information on the boundary is provided by the solution of the level set equation, which is discussed in the next section.

Spatial discretization

For the calculation of the temperature distribution in the workpiece we turn to a finite element space discretization (triangulation) on the time dependent domain Ω_t.

Let

$$V(\Omega_t) = \{v \in \mathbb{H}^1(\Omega_t)\}$$

and

$$B(\Omega_t) = \{v \in V(\Omega_t) |\ v \le 0 \text{ on } \partial\Omega_t\}.$$

[1] In the following we skip the subscript ε

Now let $\{\mathcal{T}_h\}$ be a family of conforming triangulations of Ω.[2] As a finite approximation of the functional space V we set

$$V_h = \{\varphi_h \in \mathbb{C}(\bar{\Omega}_{h,t}) : \ \varphi_h|_T \in \mathbb{P}_n(T), \ \forall T \in \mathcal{T}_h\},$$

where $\mathbb{P}_n$ is the space of piecewise polynomials of order n and h is a parameter associated with the mesh size; with every mesh refinement this parameter is getting smaller and smaller. Denote by N the dimension of V_h. Further we approximate B by

$$B_h = \{\varphi_h \in V_h | \ \varphi_h(P) \leq 0 \text{ for all Lagrange nodes } P \in \Gamma_{h,t}\}.$$

The finite dimensional space B_h is a closed convex nonempty subset of V_h and $B_h \subset B$ for any parameter h.
As for the particular problem concerning the time dependent domain, we try to define the discrete domain Ω_{h,t_n} explicitly. This idea was implemented by Bänsch and Schmidt in [4], where they considered the Navier-Stokes flow in a time dependent liquid domain.

Definition 7.2.1. *An element T is called molten, iff T is completely melted, i.e. all $x \in T$ have reached the melting temperature and been removed. An element is called solid, iff it is not molten.*
Define the discrete domain

$$\Omega_{h,t_n} = \bigcup_T \{T, \ T \textit{ is solid}\}.$$

An example of a discrete domain is illustrated in Figure 7.1.

With this definition we can run over all mesh elements and mark them either solid or molten (removed). We formulate this by means of the following algorithm:

7.2.1 Algorithm. (Marking of solid domain)

1. Mark all triangles with positive level function values in all vertices as solid (triangles not intersected by the interface).

2. Continue by marking as solid all triangles with positive level function value in at least one vertex and negative level function value in at least one vertex (triangles that have intersection points with the moving front).

[2] We refer to Appendix B for the definition of a conforming triangulation.

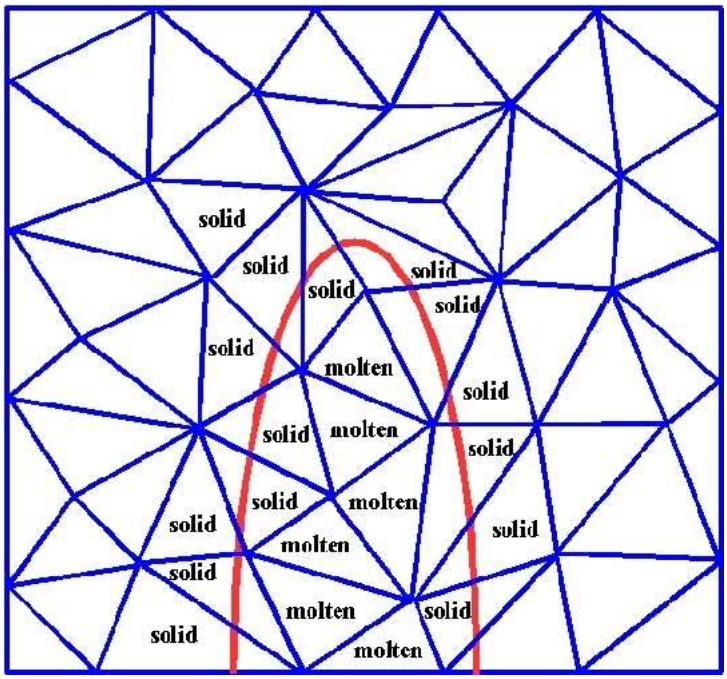

Figure 7.1: Solid and molten triangles

3. Mark all the other elements as molten.

This algorithm has a computational complexity that is linear in the number of triangles. Taking into account the above mentioned definitions, we are able now to formulate the full discretized problem.

Problem 7.2.1. *Take the "interpolant" of θ_0 as a discrete initial temperature. Given the temperature Θ_h^n (spatial approximation of Θ^n) and the domain Ω_{h,t_n} at time instant t_n, compute the updated temperature $\Theta_h^{n+1} \in V_h$ at time t_{n+1} according to*

$$\begin{aligned} & \frac{1}{\tau_{n+1}} \int_{\Omega_{h,tn}} \Theta_h^{n+1} \varphi_h dx + \vartheta \int_{\Omega_{h,tn}} \nabla \Theta_h^{n+1} \cdot \nabla \varphi_h dx + \frac{1}{\varepsilon} \int_{\partial\Omega_{h,tn}} I^{n+1}\big(\Theta_h^{+(n+1)} \varphi_h\big) d\gamma \\ = \; & \frac{1}{\tau_{n+1}} \int_{\Omega_{h,tn}} I^{n+1} \Theta_h^n \varphi_h dx - (1-\vartheta) \int_{\Omega_{h,tn}} \nabla I^{n+1} \Theta_h^n \cdot \nabla \varphi_h dx + \int_{\partial\Omega_{h,tn}} j_{abs}^n \varphi_h d\gamma, \end{aligned}$$

where $\varphi_h \in V_h$ and I^{n+1} is the Lagrange interpolation operator.

Applying the Galerkin approximation[3] with the Lagrange basis $\{\varphi_j\}_{j=1}^N$ to the equation (7.3) and rearranging the terms, we obtain a nonlinear system of algebraic equations. If we

[3]See Appendix B for an introduction to Galerkin's approach.

denote by

$$\Theta = (\theta_1, \theta_2, \ldots, \theta_N)^T$$

the vector of nodal values for θ_h, then the nonlinear equation for unknown coefficient vector Θ in matrix form reads

$$\frac{1}{\tau_{n+1}} M \left(\Theta^{n+1} - \Theta^n\right) + A\Theta^{n+1} + \frac{1}{\varepsilon} D(\Theta^{n+1}) = F^{(n+1)}, \tag{7.3}$$

where $M = (m_{ij})$ denotes the mass matrix, $A = (a_{ij})$ is the stiffness matrix, $F = (f_i)$ is the load vector and $D(\Theta^{n+1}) = (d_i(\Theta^{n+1}))$ is the nonlinear part. More precisely,

$$\begin{aligned}
m_{ij} &= \int_{\Omega_{h,t_n}} \varphi_i \varphi_j dx, \\
a_{ij} &= \int_{\Omega_{h,t_n}} \nabla\varphi_i \nabla\varphi_j dx, \\
f_i &= \int_{\partial\Omega_{h,t_n}} j^n_{abs} \varphi_i d\gamma, \\
d_i(\Theta^{n+1}) &= \begin{cases} \theta_i^{+(n+1)} & \text{if} \quad \text{the node } P_i \in \partial\Omega_{h,t_n}, \\ 0 & \text{otherwise.} \end{cases}
\end{aligned}$$

Nonlinear solver for the algebraic system

One way to solve the system (7.3) is the nonlinear Gauss-Seidel iteration for which we need to simplify the structure of mass matrix by employing a suitable numerical integration. A well known procedure is the so called *lumping the mass* method, which is equivalent to a quadrature formula using only the values in vertices. After such an approximation, the mass matrix M reduces to a diagonal matrix and the application of nonlinear solver is then easier. In other words, if $M = diag(m_i)$ is the lumped mass matrix, then the Gauss-Seidel equation for i-th coefficients θ_i^{n+1} reads

$$\frac{m_i}{\tau_{n+1}} \theta_i^{n+1} + a_{ii}\theta_i^{n+1} + \theta_i^{+(n+1)}) = \tilde{F}_i, \tag{7.4}$$

where

$$\tilde{F}_i = F_i^{n+1} + \frac{m_i}{\tau_{n+1}} \theta_i^n - \sum_{i \neq j} a_{ij}\theta_j^n.$$

We observe that for the prescribed sign of the i-th component $\tilde{F}_i$ the equation (7.4) turns to a linear equation, since depending on the sign of the right hand side of (7.4) the nonlinear term $\theta_i^{+(n+1)}$ is equal either to θ_i^{n+1} or zero. In both cases the equation is uniquely solvable.

Numerical example

Taking the domain of interest $\Omega \subset \mathbb{R}^2$ the unit circle and the time interval $[0, T] = [0, 0.5]$, we wish to compute the solution θ_h of the discretized equation (7.3) assuming that the evolution of the free boundary is a priori given. In order to introduce a level set function providing us with known free boundary, we define a new domain $\hat{\Omega} \subset \mathbb{R}^2$, which is much bigger than Ω itself and $\Omega \subset \hat{\Omega}$. Now we introduce a level set function defined on the new domain $\hat{\Omega}$ via

$$\phi(x, y, t) = 1 - \sqrt{x^2 + y^2 + 2t}, \quad (x, y) \in \hat{\Omega}, \ t \in [0, T]. \tag{7.5}$$

The zero level set of the function ϕ describes the evolution of a shrinking circle and will serve as a moving boundary for the penalty problem. At time $t = 0$ the level set function (7.5) is expressed via

$$\phi_0(x, y) := \phi(x, y, 0) = 1 - \sqrt{x^2 + y^2},$$

which is a function owning the unite circle as its zero level set. In this example we can specify an exact solution in order to investigate the order of convergence of our algorithm. We select an exact solution defined on $\hat{\Omega}$ and given by

$$\theta(x, y, t) = \begin{cases} -(1 - 2t - x^2 - y^2)^2 & \text{if} \quad x^2 + y^2 < 1 - 2t, \\ 0 & \text{if} \quad \text{otherwise.} \end{cases} \tag{7.6}$$

Introducing the new domain $\hat{\Omega}$ causes a small ambiguity for the solution of the discrete penalty Problem (7.3). This problem is defined on the discrete domain Ω_{h,t_n}, but not outside. What we can do is to add a new regularizing term to the penalty equation. The term takes the form

$$\varepsilon \int_{\hat{\Omega}} \nabla\theta \cdot \nabla\varphi dx,$$

where ε is a small parameter and can be selected to be the same as the parameter ε entering the penalty term. Taking $\hat{\Omega}_h$ to be the discrete counterpart of $\hat{\Omega}$, the modified

form of discrete equation (7.3) is then expressed via

$$\begin{aligned}
&\frac{1}{\tau_{n+1}}\int_{\Omega_h(t_n)}\Theta_h^{n+1}\varphi_h dx+\vartheta\int_{\Omega_h(t_n)}\nabla\Theta_h^{n+1}\cdot\nabla\varphi_h dx+\frac{1}{\varepsilon}\int_{\partial\Omega_h(t_n)}I^{n+1}\Theta_h^{+(n+1)}\varphi_h d\gamma\\
&+\vartheta\varepsilon\int_{\hat{\Omega}_h}\nabla\Theta_h^{n+1}\cdot\nabla\varphi_h dx\\
=\;&\frac{1}{\tau_{n+1}}\int_{\Omega_h(t_n)}I^{n+1}\Theta_h^{n}\varphi_h dx-(1-\vartheta)\int_{\Omega_h(t_n)}\nabla I^{n+1}\Theta_h^{n}\cdot\nabla\varphi_h dx+\int_{\partial\Omega_h(t_n)}j_{abs}^{n}\varphi_h d\gamma\\
&-(1-\vartheta)\varepsilon\int_{\hat{\Omega}_h}\nabla I^{n+1}\Theta_h^{n}\cdot\nabla\varphi_h dx. \qquad (7.7)
\end{aligned}$$

The initial data and boundary values are directly computed from (7.6). Dirichlet boundary conditions are employed for the outer boundary (boundary of $\hat{\Omega}$), since the moving interface does not touch the fixed boundary. An additional function f representing the right hand side of the heat equation must be calculated from the given exact solution

$$f(x,y,t)=\begin{cases}4(3x^2+3y^2+2t-1) & \text{if} \quad x^2+y^2<1-2t,\\ 0 & \text{if} \quad \text{otherwise.}\end{cases} \qquad (7.8)$$

The right hand side f does not appear in our model, but this is the price we have to pay for having a simple exact solution. As for the heat flux density j_{abs}, we use our model presented earlier in Section 3.

In the first instance, we implement our calculations non-adaptively on different time independent meshes with equally spaced time steps δt. Table 7.1 illustrates the observed evolution of the temperature error, where

l is the number of uniform refinements,

h is the length of the grid size, and

$Error(\theta_h)$ is the error between the exact and numerical solutions constructed by calculating the $\mathbb{L}^2$-norm $\|\theta-\theta_h\|$ and taking the maximum over all time steps, i.e.

$$Error(\theta_h)=\max_{1\le n\le N}\|\theta(\cdot,t_n)-\theta_h^n\|_{\mathbb{L}^2(\hat{\Omega}_h)}.$$

As a penalty parameter we take $\varepsilon=10^{-12}$. The log-log plot in Figure 7.2 shows the $\mathbb{L}^2$-norm of the error against the mesh size h. We see that the error is $O(h^{1.97})$ for linear elements and $O(h^{2.8})$ for quadratic elements, which is consistent with the optimal rate predicted by standard estimates for the linear heat equation. The relatively small difference in convergence rate can be probably explained by the non-linearity of our problem. It seems that the penalty operator and the new introduced regularizing term make their influence on the rate of convergence.

l	h	δt	$Error(\theta_h)$ *lin. elements*
2	3.0	$2.0 \cdot 10^{-2}$	1.4142
4	1.5	$5.0 \cdot 10^{-3}$	$4.09 \cdot 10^{-1}$
6	0.75	$1.25 \cdot 10^{-3}$	$1.76 \cdot 10^{-1}$
8	0.375	$3.125 \cdot 10^{-4}$	$6.15 \cdot 10^{-2}$
10	0.1875	$7.81 \cdot 10^{-5}$	$1.57 \cdot 10^{-2}$
12	0.0936	$1.95 \cdot 10^{-5}$	$4.1 \cdot 10^{-3}$
14	0.0469	$4.88 \cdot 10^{-6}$	$1.05 \cdot 10^{-3}$

l	h	δt	$Error(\theta_h)$ *quad. elements*
2	3.0	$2.0 \cdot 10^{-2}$	$4.91 \cdot 10^{-1}$
4	1.5	$2.5 \cdot 10^{-3}$	$2.52 \cdot 10^{-1}$
6	0.75	$3.125 \cdot 10^{-4}$	$4.07 \cdot 10^{-2}$
8	0.375	$3.91 \cdot 10^{-5}$	$7.81 \cdot 10^{-3}$
10	0.1875	$4.88 \cdot 10^{-6}$	$1.36 \cdot 10^{-3}$
12	0.0936	$6.1 \cdot 10^{-7}$	$2.21 \cdot 10^{-4}$
14	0.0469	$7.63 \cdot 10^{-8}$	$3.42 \cdot 10^{-5}$

Table 7.1: Error calculations for several uniform refinements: left for linear elements, right for quadratic elements

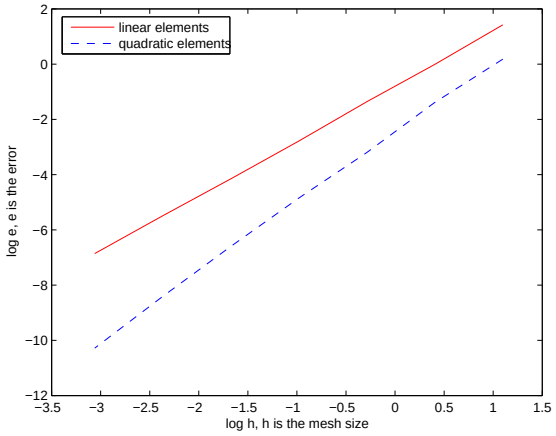

Figure 7.2: Rates of convergence of variational inequality with a given level set function.

7.2.2 Discretization of the level set equation

Numerical methods for the level-set theory has been extensively developed, especially using finite difference schemes, [38],[41], [42],[39], etc. Several studies on finite element solutions have been done by Barth and Sethian, [3]. In their work they described a finite element algorithm for the solution of the level set equation which involved remeshing. Chessa, Smolinski and Belytschko, [6], described the interface arising in solidification problems as a level set function and updated it by a stabilized finite element scheme. In the work of Ohmori, [37], the interface between two fluids is considered as the zero level set of pseudo-density function governed by the transport equation, which is then approximated by means of Lax-Wendroff finite element scheme.

Viscosity solution of the level set equation

In our considerations we will use the advantages of the theory of viscosity solutions which is well suited for numerical implementations. The idea, based on [10], is to add a small viscosity term to the level-set equation (6.33) and consider the approximate problem

Problem 7.2.2. *Find the function* $\phi_\varepsilon(x,t) : \mathbb{R}^n \times (0,T) \to \mathbb{R}$, $n = 2, 3$, *such that*

$$\frac{\partial \phi_\varepsilon}{\partial t} + w \cdot \nabla \phi_\varepsilon = \varepsilon \Delta \phi_\varepsilon, \tag{7.9}$$

$$\phi_\varepsilon(x,0) = \phi_0(x),$$

where ε *is a positive constant.*

The advantage of the method is that equation (7.9) is an initial-value parabolic equation, which can be shown to have a smooth solution. The viscosity term $\varepsilon\Delta\phi$ plays a role of a regularizer of the level-set equation (6.33). The limit of the smooth solution ϕ_ε as ε vanishes provides us with some sort of weak solution of (6.33). For a brief introduction to the method of vanishing viscosity we refer to Appendix A and references therein.
Now we are able to write down the variational form of (7.9) desired by finite element approximation. We skip the index ε and write the weak form of (7.9) as

$$\int_{\hat{\Omega}} \frac{\partial \phi}{\partial t} \varphi dx + \int_{\hat{\Omega}} w \cdot \nabla \phi \varphi dx + \varepsilon \int_{\hat{\Omega}} \nabla \phi \cdot \nabla \varphi dx = 0, \tag{7.10}$$

where φ is a continuous test function and $\hat{\Omega}$ is a bigger domain which contains the domain Ω occupied by the workpiece. For example, we can take $\hat{\Omega} = \mathbb{R}^n$.

Time discretization

For the level set field, we use the same mesh as for the temperature field.
Let again $0 = t_0 < t_1 < \cdots < t_N = T$ be a partition of $(0,T)$, $I_n = (t_{n-1}, t_n)$ and $\tau_n = t_n - t_{n-1}$. For $0 \le \vartheta \le 1$ a time discretization of the level-set equation (6.33) is performed using the ϑ-scheme. We are looking for a finite element solution $\Phi^{n+1} \approx \phi(\cdot, t_{n+1})$ such that

$$\int_{\hat{\Omega}} \frac{\Phi^{n+1} - \Phi^n}{\tau_{n+1}} \varphi dx + \vartheta \int_{\hat{\Omega}} w^{n+1} \cdot \nabla \Phi^{n+1} \varphi dx + (1-\vartheta) \int_{\hat{\Omega}} w^{n+1} \cdot \nabla \Phi^n \varphi dx +$$

$$+ \vartheta\varepsilon \int_{\hat{\Omega}} \nabla \Phi^{n+1} \cdot \nabla \varphi dx + (1-\vartheta)\varepsilon \int_{\hat{\Omega}} \nabla \Phi^n \cdot \nabla \varphi dx = 0. \tag{7.11}$$

Generally, this scheme is first order accurate except $\vartheta = \frac{1}{2}$, where it is second order accurate in time. Note that for $\vartheta = 1$, one gets the backward (implicit) Euler scheme, for $\vartheta = 0$ the forward (explicit) Euler scheme is obtained, while for $\vartheta = \frac{1}{2}$ one gets the Crank-Nicholson scheme.

Spatial discretization

We again use the method of finite elements on a conforming triangulation of $\hat{\Omega}$. Let $\{\mathcal{T}_h\}$ be a family of proper and shape regular triangulations of the domain $\hat{\Omega}$ and V_h a corresponding finite element space with piecewise polynomial functions of degree $n \geq 1$ on $\mathcal{T}_h$. Note that unlike the finite element space for the variational inequality from the previous chapter, here V_h is the approximation of the space $V(\hat{\Omega})$, i.e. the space is defined on a time independent domain $\hat{\Omega}$.
The full discretized problem for the calculation of the geometry of the workpiece is the following

Problem 7.2.3. *Take the "interpolant" of ϕ_0 as a discrete initial level function. Given the level Φ_h^n (spatial approximation of Φ^n) at time instant t_n. Compute the updated level function $\Phi_h^{n+1} \in V_h$ at time t_{n+1} according to*

$$\int_{\hat{\Omega}_h} \frac{\Phi_h^{n+1}}{\tau_{n+1}} \varphi_h dx + \vartheta \int_{\hat{\Omega}_h} w_h^{n+1} \cdot \nabla \Phi_h^{n+1} \varphi_h dx + \vartheta\varepsilon \int_{\hat{\Omega}_h} \nabla \Phi_h^{n+1} \cdot \nabla \varphi_h dx$$

$$= \int_{\hat{\Omega}_h} \frac{\Phi_h^n}{\tau_{n+1}} \varphi_h dx - (1-\vartheta) \int_{\hat{\Omega}_h} w_h^{n+1} \cdot \nabla \Phi_h^n \varphi_h dx - (1-\vartheta)\varepsilon \int_{\hat{\Omega}_h} \nabla \Phi_h^n \cdot \nabla \varphi_h dx. \tag{7.12}$$

Applying the Galerkin approximation to the equation (7.12), we obtain

$$\sum_j \int_{\hat{\Omega}} \Phi_j^{n+1} \varphi_i \varphi_j dx + \vartheta \sum_j \int_{\hat{\Omega}} \Phi_j^{n+1} w^{n+1} \cdot \nabla \varphi_j \varphi_i dx + (1-\vartheta) \sum_j \int_{\hat{\Omega}} \Phi_j^n w^{n+1} \cdot \nabla \varphi_j \varphi_i dx +$$

$$+ \vartheta\varepsilon \sum_j \int_{\hat{\Omega}} \Phi_j^{n+1} \nabla \varphi_j \cdot \nabla \varphi_i dx + (1-\vartheta)\varepsilon \sum_j \int_{\hat{\Omega}} \Phi_j^n \nabla \varphi_j \cdot \nabla \varphi_i dx = 0. \tag{7.13}$$

Equation (7.13) can be reorganized and put in the matrix form

$$\sum_j \left(\frac{1}{\tau_{n+1}} m_{ij} + \vartheta\varepsilon a_{ij} + \vartheta c_{ij} \right) \Phi_j^{n+1} = \sum_j \left(\frac{1}{\tau_{n+1}} m_{ij} - (1-\vartheta)\varepsilon a_{ij} - (1-\vartheta) c_{ij} \right) \Phi_j^n \tag{7.14}$$

where the matrices $M = (m_{ij})$, $A = (a_{ij})$ and $C = (c_{ij})$ are defined as

$$m_{ij} = \int_{\hat{\Omega}} \varphi_i \varphi_j dx,$$

$$a_{ij} = \int_{\hat{\Omega}} \nabla\varphi_i \nabla\varphi_j dx,$$

$$c_{ij} = \int_{\hat{\Omega}} w^{n+1} \cdot \nabla\varphi_j \varphi_i dx.$$

Note that the system matrix on the left hand side is not the same as the matrix applied on the solution from the previous time step standing on the right hand side. Galerkin method performs well, if the parameter ε is greater or equal to the mesh size h, but if $\varepsilon << h$ then the method can produce an oscillating solution which is not close to the exact solution. However, if the exact solution happens to be smooth, then the Galerkin approximation will produce good results even for $\varepsilon < h$ (see [21]). To handle the difficulties connected with $\varepsilon < h$, we either decrease the mesh size h until it is smaller than ε or simply solve a modified problem with diffusion term $h\Delta\phi$. The latter produces non-oscillating solutions, but has the drawback of introducing a great amount of extra diffusion. The most important disadvantage is that due to the viscosity term the method is at most first order accurate, i.e. the error is at best $O(h)$.

Solver for the algebraic system

The resulting system (7.14) of algebraic equations is obviously a linear system, therefore, high efficient linear solvers can be applied successfully. In our examples and applications we have used the generalized minimal residual (GMRES) method, which is very well suited to systems with non-symmetric matrices.

Numerical examples

Example 1.

Let us first demonstrate the numerical solution of a level set problem whose exact solution is known. Let the domain of interest be $\hat{\Omega} = [-4, 4]^2$ and suppose we are given a level set function

$$\phi(x, y, t) = \begin{cases} \cos(\frac{\pi}{4}(x^2 + y^2 + 2t)) - \cos\frac{\pi}{4} & \text{if} \quad x^2 + y^2 + 2t \leq 4, \\ -1 - \cos\frac{\pi}{4} & \text{if} \quad x^2 + y^2 + 2t > 4 \end{cases}.$$

For $t = 0$ we obtain

$$\phi_0(x,y) = \begin{cases} \cos(\frac{\pi}{4}(x^2+y^2)) - \cos\frac{\pi}{4} & \text{if} \quad x^2+y^2 \leq 4, \\ -1 - \cos\frac{\pi}{4} & \text{if} \quad x^2+y^2 > 4 \end{cases}.$$

It is easy to verify that the function $\phi(x,y,t)$ satisfies the level set equation

$$\phi' + w \cdot \nabla\phi = 0,$$

where the velocity vector w has the form

$$w(x,y) = \left(-\frac{x}{x^2+y^2}, -\frac{y}{x^2+y^2}\right), \tag{7.15}$$

with ϕ_0 serving as a starting function.

Taking into account the fact that

$$\begin{cases} \phi_0(x,y) > 0 & \text{if} \quad x^2+y^2 < 1, \\ \phi_0(x,y) = 0 & \text{if} \quad x^2+y^2 = 1, \\ \phi_0(x,y) < 0 & \text{if} \quad x^2+y^2 > 1. \end{cases}$$

we conclude that the initial function $\phi_0(x,y)$ is a level function with the circle of radius $r = 1$ being its zero level set. Now we are interested in the evolution of this zero level set which can be explicitly given via

$$\Gamma(t) = \{x \in \mathbb{R}^2 : \ |x| = \sqrt{1-2t}\}.$$

Obviously, $\Gamma(t)$ represents the evolution of a shrinking circle at time t.

We test our algorithm with the help of the given exact solution $\phi(x,y,t)$ and different regularizing parameters ε which depend on the grid size h. In Tables 7.2.2 and 7.2.2 we report the error behaviour after different uniform refinements, where

l is the number of uniform refinements,

h is the length of the grid size, and

$Error(\phi_h)$ is the error between the exact and numerical solutions constructed by calculating the $\mathbb{L}^2$-norm $\|\phi - \phi_h\|$ and taking the maximum over all time steps, i.e.

$$Error(\phi_h) = \max_{1 \leq n \leq N} \|\phi^n - \phi_h^n\|_{\mathbb{L}^2(\hat{\Omega}_h)},$$

$EOC :=$ experimental order of convergence defined by the formula:

$$EOC := \frac{\log(\frac{\|u^* - u_1\|}{\|u^* - u_2\|})}{\log(\frac{N_2}{N_1})},$$

where u^* is the exact solution (it can be also the solution on the finest grid), u_1 and u_2 are two approximate solutions of the problem, and N_1, N_2 are the numbers of elements in the mesh.

l	h	$Error$ $\varepsilon = h$	EOC $\varepsilon = h$	$Error$ $\varepsilon = h^2$	EOC $\varepsilon = h^2$	$Error$ $\varepsilon = h^3$	EOC $\varepsilon = h^3$	$Error$ $\varepsilon = 10^{-12}$	EOC $\varepsilon = 10^{-12}$
2	4.000	3.7712	–	3.7712	-	3.7712	-	3.7712	-
4	2.000	2.5086	0.5881	2.8727	0.3926	3.2257	0.2254	2.0286	0.8946
6	1.000	1.5613	0.6842	1.5613	0.8797	1.5613	1.0469	0.7210	1.4925
8	0.500	0.9023	0.7911	0.6149	1.3444	0.4318	1.8544	0.2023	1.8336
10	0.2500	0.5121	0.8172	0.1927	1.6741	0.0885	2.2868	0.0536	1.9163
12	0.1250	0.2826	0.8577	0.0532	1.8569	0.0184	2.2661	0.0137	1.9682
14	0.0625	0.1517	0.8976	0.0138	1.9467	0.0041	2.1661	0.0035	1.9689

Table 7.2: Convergence rates for $\varepsilon = h$, $\varepsilon = h^2$, $\varepsilon = h^3$, $\varepsilon = 10^{-12}$ and several uniform refinements (linear elements).

l	h	$Error$ $\varepsilon = h$	EOC $\varepsilon = h$	$Error$ $\varepsilon = h^2$	EOC $\varepsilon = h^2$	$Error$ $\varepsilon = h^3$	EOC $\varepsilon = h^3$	$Error$ $\varepsilon = 10^{-12}$	EOC $\varepsilon = 10^{-12}$
2	4.000	3.1929	–	3.9918	-	4.7206	-	2.5925	-
4	2.000	1.8126	0.8169	2.3412	0.7698	2.7873	0.7602	0.4684	2.4687
6	1.000	1.2286	0.5611	1.2286	0.9303	1.2073	1.2072	0.1181	1.9879
8	0.500	0.7925	0.6325	0.4802	1.3554	0.2769	2.1245	0.0271	2.1238
10	0.2500	0.4769	0.7328	0.1494	1.6846	0.0419	2.7245	0.0050	2.4384
12	0.1250	0.2723	0.8085	0.0411	1.8621	0.0056	2.9036	0.0018	2.1878
14	0.0625	0.1489	0.8709	0.0107	1.9416	0.0007	2.9742	0.0005	1.8481

Table 7.3: Convergence rates for $\varepsilon = h$, $\varepsilon = h^2$, $\varepsilon = h^3$, $\varepsilon = 10^{-12}$ and several uniform refinements (quadratic elements).

Example 2.

Next we test our algorithm in the case when the velocity of the transport of the level set function involves a given temperature field. As a known temperature distribution we take the one described in the numerical example of Section 7.2.1, i.e.

$$\theta(x,y,t) = \begin{cases} -(1-2t-x^2-y^2)^2 & \text{if} \quad x^2+y^2 < 1-2t, \\ 0 & \text{if} \quad \text{otherwise.} \end{cases} \tag{7.16}$$

As for the exact solution of level set equation, we take

$$\phi(x,y,t) = 1 - \sqrt{x^2+y^2+2t}. \tag{7.17}$$

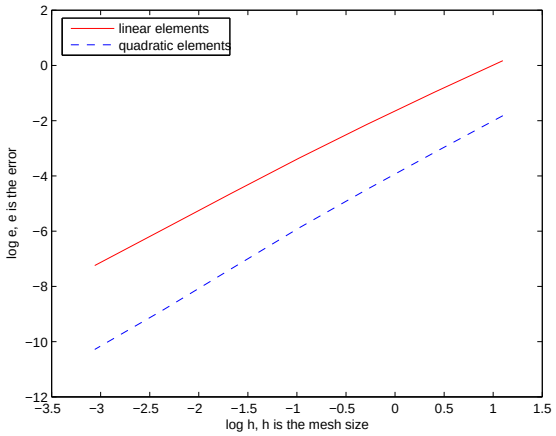

Figure 7.3: Rates of convergence of level set equation with a given temperature distribution.

Given the functions $\theta(x, y, t)$ and $\phi(x, y, t)$, we are able to calculate the initial data of the problem, boundary values, velocity of transport and right hand side of the level set equation. We do our calculations on $\hat{\Omega} = [-3, 3]^2$ and time interval $[0, 0.5]$. Uniform meshes with different grid sizes and time steps are employed. The computation results for linear and quadratic elements are summarized in Table 7.4. The numerical results for the convergence

l	h	δt	$Error(\phi_h)$ *lin. elements*
2	3.0	$2.0 \cdot 10^{-2}$	1.1880
4	1.5	$5.0 \cdot 10^{-3}$	$3.81 \cdot 10^{-1}$
6	0.75	$1.25 \cdot 10^{-3}$	$1.18 \cdot 10^{-1}$
8	0.375	$3.125 \cdot 10^{-4}$	$3.47 \cdot 10^{-2}$
10	0.1875	$7.81 \cdot 10^{-5}$	$9.63 \cdot 10^{-3}$
12	0.0936	$1.95 \cdot 10^{-5}$	$2.61 \cdot 10^{-3}$
14	0.0469	$4.88 \cdot 10^{-6}$	$7.13 \cdot 10^{-4}$

l	h	δt	$Error(\phi_h)$ *quad. elements*
2	3.0	$2.0 \cdot 10^{-2}$	$1.62 \cdot 10^{-1}$
4	1.5	$2.5 \cdot 10^{-3}$	$4.31 \cdot 10^{-2}$
6	0.75	$3.125 \cdot 10^{-4}$	$1.12 \cdot 10^{-2}$
8	0.375	$3.91 \cdot 10^{-5}$	$2.77 \cdot 10^{-3}$
10	0.1875	$4.88 \cdot 10^{-6}$	$6.26 \cdot 10^{-4}$
12	0.0936	$6.1 \cdot 10^{-7}$	$1.41 \cdot 10^{-4}$
14	0.0469	$7.63 \cdot 10^{-8}$	$3.42 \cdot 10^{-5}$

Table 7.4: Error calculations for several uniform refinements: left for linear elements, right for quadratic elements.

rates are demonstrated in Figure 7.3. The optimal rate of $O(h^2)$ is observed for quadratic elements. The numerical rate of convergence with linear elements is included in Figure 7.3 as well. In this case the convergence rate is around $O(h^{1.88})$ which is suboptimal.

7.2.3 Coupling of sub-problems

We recall that the weak coupled system consists of variational inequality and level set equation. The corresponding discrete problem is analogously coupled, on one hand, through the temperature Θ_h^n entering the expression of the interface velocity in the weak level set equation and, on the other hand, via integrals over the domain Ω_{h,t_n}, as well as interface $\partial\Omega_{h,t_n}$, which occur in the formulation of variational inequality. Assume, we have done a time discretization of the problem. In order to determine the temperature field Θ_h^{n+1} and the level set Φ_h^{n+1} at $n+1$-st time step, we calculate first the new temperature Θ_h^{n+1} having in disposal the old value Φ_h^n of the level set function. With the updated temperature distribution we are able to compute the interface velocity, plug it into the level set equation and evaluate the new free boundary $\partial\Omega_{h,t_{n+1}}$ as the zero level set of the new level function Φ_h^{n+1}.

As for the discrete spaces, we employ the same finite element space V_h and triangulation $\{\mathcal{T}_h\}$ for the calculation of both temperature Θ_h^n and level function Φ_h^n. This allows us to save all needed efforts for the administration and optimization of two different meshes. The disadvantage of solving two sub-problems on the same grid is the impossibility of having an optimal mesh for both sub-problems simultaneously.

Let us now demonstrate an algorithm, which we implement for the numerical treatment of the coupled problem.

7.2.2 Algorithm. Cutting Model
Take $\phi(x,0) = \phi_0(x)$ to be, say, the signed distance to the interface and $\theta(x,0) = \theta_0(x)$ the initial temperature distribution of the workpiece.

Step 1. Specify the discrete initial functions Θ_h^0 and Φ_h^0 as the Lagrange interpolation of θ_0 and ϕ_0, respectively.

Step 2. $n = n + 1$.

Step 3. Given the value Φ_h^n, calculate the discrete function Θ_h^{n+1} via

$$\begin{aligned}
&\frac{1}{\tau_{n+1}}\int_{\Omega_h(t_n)}\Theta_h^{n+1}\varphi_h dx+\vartheta\int_{\Omega_h(t_n)}\nabla\Theta_h^{n+1}\cdot\nabla\varphi_h dx+\frac{1}{\varepsilon}\int_{\partial\Omega_h(t_n)}I^{n+1}\Theta_h^{+(n+1)}\varphi_h d\gamma\\
&+\vartheta\varepsilon\int_{\hat{\Omega}_h}\nabla\Theta_h^{n+1}\cdot\nabla\varphi_h dx\\
=\;&\frac{1}{\tau_{n+1}}\int_{\Omega_h(t_n)}I^{n+1}\Theta_h^{n}\varphi_h dx-(1-\vartheta)\int_{\Omega_h(t_n)}\nabla I^{n+1}\Theta_h^{n}\cdot\nabla\varphi_h dx+\int_{\partial\Omega_h(t_n)}j_{abs}^{n}\varphi_h d\gamma\\
&-(1-\vartheta)\varepsilon\int_{\hat{\Omega}_h}\nabla I^{n+1}\Theta_h^{n}\cdot\nabla\varphi_h dx.
\end{aligned}$$

Step 4. Compute the new velocity ω_h^{n+1} of the cutting front with[4]

$$\omega_h^{n+1}:=\nabla\theta_h^{n+1}-j_e r\nu_r,$$

where ω_h^{n+1} is the extension velocity from the front $\partial\Omega_{h,t_n}$ to the entire domain $\hat{\Omega}_h$.

Step 5. Calculate the new level function Φ_h^{n+1} with

$$\begin{aligned}
&\int_{\hat{\Omega}_h}\frac{\Phi_h^{n+1}}{\tau_{n+1}}\varphi_h dx+\vartheta\int_{\hat{\Omega}_h}w_h^{n+1}\cdot\nabla\Phi_h^{n+1}\varphi_h dx+\vartheta\varepsilon\int_{\hat{\Omega}_h}\nabla\Phi_h^{n+1}\cdot\nabla\varphi_h dx\\
=&\int_{\hat{\Omega}_h}\frac{\Phi_h^{n}}{\tau_{n+1}}\varphi_h dx-(1-\vartheta)\int_{\hat{\Omega}_h}w_h^{n+1}\cdot\nabla\Phi_h^{n}\varphi_h dx-(1-\vartheta)\varepsilon\int_{\hat{\Omega}_h}\nabla\Phi_h^{n}\cdot\nabla\varphi_h dx.
\end{aligned}$$

Step 6. Set the new domain occupied by the workpiece and its boundary using the updated level function Φ_h^{n+1}:

$$\Omega_{h,t_{n+1}}=\left\{x;\ \Phi_h^{n+1}(x,t_{n+1})>0\right\},$$

$$\partial\Omega_{h,t_{n+1}}=\left\{x;\ \Phi_h^{n+1}(x,t_{n+1})=0\right\}.$$

Step 7. If $t_n<T$, then go to *Step 2.*

Step 8. Stop.

Now we make some important remarks on the steps of the algorithm. In Step 2 we solve the variational inequality on the fixed domain. Fixed, because we assume the interface or the zero level set known from the previous time step. The existence of the solution of variational inequality (5.37) on a fixed domain is proved in Lemma 6.2.2 which makes the implementation of Step 2 legal. In Step 3 we solve the level set equation with a given velocity field containing the gradient of the temperature. But the gradient of the temperature is known from Step 2, therefore, we can employ the Lemma 6.2.4 to ensure the existence and

[4]The material parameters are set equal to one.

uniqueness of the weak solution of level set equation. To conclude, our analytical results obtained earlier in Chapter 6 allow us to start the implementation of Algorithm 7.2.2, with an aim to show the convergence of numerical schemes.

Some remarks on distance function

For numerical accuracy the level set function must stay well behaved in the sense that, except for isolated points,

$$0 < c \leq \|\nabla\phi\| \leq C$$

for some constants c and C. In practice, it is desirable for many problems that $\phi(x,t)$ be a signed distance function, i.e.

$$\|\nabla\phi\| = 1.$$

However, the level set function ceases to be an exact distance function even after one time step. Why this is important? We expressed the quantities like the outer normal to Ω_t and velocity of the interface with the help of the gradient $\nabla\phi$. In order to keep the approximations to those quantities relatively accurate, we wish to avoid having steep or flat gradients develop in ϕ. We face the same problem when defining the discrete interface $\partial\Omega_h$. For the calculation of $\partial\Omega_h$ we need the values of the level set function Φ_h at the two vertices of edges of triangles bounding the discrete domain. Now, if the gradient $\nabla\Phi_h$ is steep, then values of the function at these two points have the same order of magnitude, which is not desirable.

This problem was first introduced by Chop in [7], where he showed enormous round-off errors arising from the flat gradients.

One way to avoid these numerical difficulties is to reinitialize the function Φ_h to be an exact distance function from the evolving front $\partial\Omega_t$ at each time step, [7]. The reinitialization is the construction of the distance function to the zero level set of a given level set function. To be more precise, assume a level set function $\hat{\phi}(x)$ is given, we want to construct a function $\phi(x)$ such that

$$\hat{\phi}^{-1}(0) = \phi^{-1}(0) \text{ and } \|\nabla\phi\| = 1.$$

There are several methods for reinitialization of Φ_h. In [54], Sussmann, Smereka and Osher presented an algorithm for reinitializing the level set function to be an exact signed distance function from the moving front. The idea behind this method is that given a function Φ_h^n

(level set function at time t_n) that is not a distance function, one can evolve it into a function Ψ that is an exact signed distance function and, therefore, has the same zero level as Φ_h^n. This is accomplished by iterating the equation

$$\Psi_t = S(\Psi_0)(1 - |\nabla\Psi|)$$

to steady state, where $\Psi_0 := \Phi_h^n$ and S denotes the sign function. As in [54], one can smooth the sign function S by the equation

$$S(\Psi_0) = \frac{\Psi_0}{\sqrt{\Psi_0^2 + \varepsilon^2}}.$$

By using this approach, one approximates the distance function to zero level set of Φ_h^n avoiding to explicitly find the zero level of Φ_h^n.

Another method for construction of signed distances is due to Sethian and Adalsteinsson, [42]. Again assuming that a function Φ_h^n is given and does not correspond to the signed distance function. The idea behind this method is to solve an Eikonal equation

$$|\nabla\Psi| = 1$$

on either side of the front, with $\Psi = 0$ on the zero level set of Φ_h^n.

We present a different approach, which can be implemented effectively avoiding any reinitialization of level set function. At every time step we can approximate the time dependent domain Ω_t by its discrete counterpart $\Omega_{h,t}$ using the Definition 7.2.1 and determine the exact distance function at every mesh point explicitly. Although this approach is expensive, we have to pay the price since we need the discrete interface for calculations of temperature field. The Algorithm 7.2.2 should be then modified as follows:

7.2.3 Algorithm. Modified Cutting Model

Take $\phi_0(x)$ and $\theta_0(x)$ as in Algorithm 7.2.2.

Step 1. Specify Θ_h^0 and Φ_h^0.

Step 2. $n = n + 1$.

Step 3. Calculate the discrete function Θ_h^{n+1}.

Step 4. Compute the velocity ω_h^{n+1}.

Step 5. Calculate the new level function Φ_h^{n+1}.

Step 6. Set the new domain using Φ_h^{n+1}.

Step 7. Compute the exact signed distance function Ψ to the zero level of Φ_h^{n+1}.

l	h	δt	$Error(\theta_h)$	$Error(\phi_h)$	$Total/Error$
2	3.0	$2.0 \cdot 10^{-2}$	1.4142	1.2278	2.6421
4	1.5	$5.0 \cdot 10^{-3}$	$4.09 \cdot 10^{-1}$	$3.79 \cdot 10^{-1}$	$7.88 \cdot 10^{-1}$
6	0.75	$1.25 \cdot 10^{-3}$	$1.76 \cdot 10^{-1}$	$1.24 \cdot 10^{-1}$	$3.01 \cdot 10^{-1}$
8	0.375	$3.125 \cdot 10^{-4}$	$6.15 \cdot 10^{-2}$	$3.69 \cdot 10^{-2}$	$9.85 \cdot 10^{-2}$
10	0.1875	$7.81 \cdot 10^{-5}$	$1.56 \cdot 10^{-2}$	$9.69 \cdot 10^{-3}$	$2.53 \cdot 10^{-2}$
12	0.0936	$1.95 \cdot 10^{-5}$	$4.12 \cdot 10^{-3}$	$2.63 \cdot 10^{-3}$	$6.76 \cdot 10^{-3}$
14	0.0469	$4.88 \cdot 10^{-6}$	$1.04 \cdot 10^{-3}$	$7.11 \cdot 10^{-4}$	$1.75 \cdot 10^{-3}$

Table 7.5: Error calculations for cutting model.

Step 8. Set $\Phi_h^{n+1} := \Psi$ **.**

Step 9. If $t_n < T$, then go to *Step 2.*

Step 10. Stop.

Numerical example for the coupled system

In this section we discuss the convergence rate for the Algorithm 7.2.2. We compute the discrete solution of cutting model (Θ_h, Φ_h) for several uniformly refined meshes and equally spaced time stepsize. Here we present the numerical results for linear elements only. As an exact solution (θ, ϕ) for the numerical test we employ the temperature distribution (7.16) and level set function (7.17), respectively. Like in the case of sub-problems, the corresponding initial data, boundary values and right hand sides are computed directly from the given exact solution.

After the implementation of the Algorithm 7.2.2, we again measure the $\mathbb{L}^2$-error between the exact and computed solutions. Some of the obtained numerical results are shown in Table 7.5. The log-log plot 7.4 demonstrates results concerning the rate of convergence of the cutting algorithm. A rate very close to an optimal of $O(h^2)$ is observed. Reminding that the calculations are done for linear finite elements, we can report a convergence rate $O(h^{1.96})$ for variational inequality, $O(h^{1.9})$ for level set equation and $O(h^{1.94})$ for total error (see Figure 7.4). An interesting question is how the rate of convergence changes when we compare the error we make by solving the sub-problems and the error contributions of each sub-problem in the coupled system. We refer to Figure 7.5 demonstrating this comparison. As one can see, for very coarse grids there is a small difference between the convergence rates of coupled problem and decoupled sub-problem for temperature calculation. This

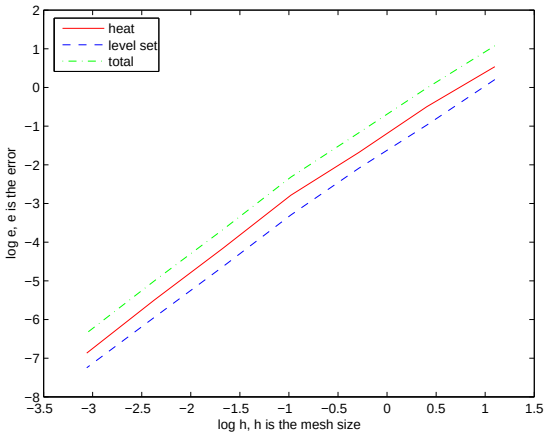

Figure 7.4: Computed convergence rates for the coupled problem.

problem disappears after a couple of uniform refinements (see Figure 7.5). The situation with level set equation is fine, the convergence rates for coupled and decoupled algorithms overlap which is illustrated in the right plot of the figure.

7.3 Adaptive methods

A global or uniform refinement of the mesh may lead to the best reduction of the error per refinement level, but the amount of new unknowns might be much larger than needed to reduce the error below the given tolerance. Using local mesh refinement, we hope to do much better.

The aim of an adaptive method is to compute a numerical solution in such a way that the error is of a prescribed accuracy and the number of degrees of freedom is as small as possible. Using adaptive discretization methods, numerical approximation within a prescribed accuracy can often be gained with only a small portion of work. To be more precise, the aim is the generation of a mesh which is adapted to the problem such that a given criterion is fulfilled by the finite element solution on this mesh. As a criterion we may require that for a given *tolerance* the estimated error between the exact and discrete solution satisfies the condition

$$\|\theta - \theta_h\| \leq tolerance,$$

where $\|\cdot\|$ is some appropriate norm. An optimal mesh resulting from such an adaption

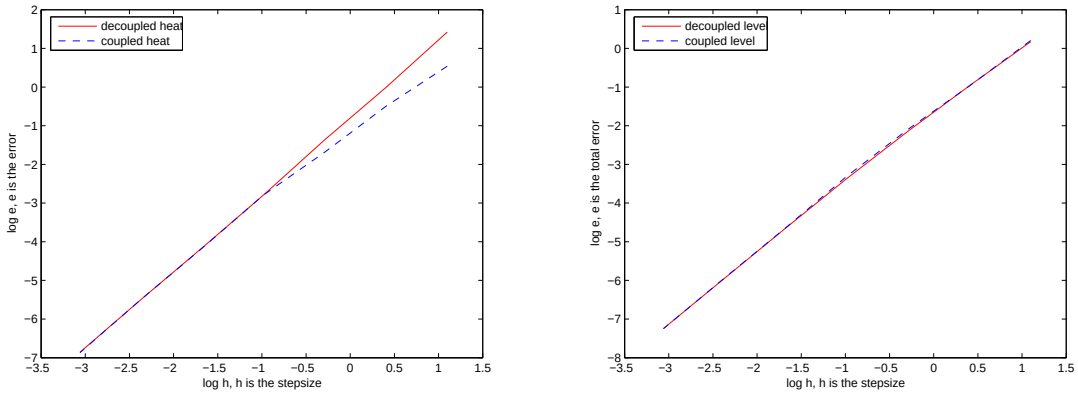

Figure 7.5: Comparison of convergence rates for coupled and decoupled problems, left: heat, right: level set.

should be as coarse as possible while meeting the above mentioned criterion. This can save a lot of computing time and memory requirements.

A standard implementation of adaptive finite element method consists of iterating the procedure

$$\ldots \text{ solve } \Rightarrow \text{ estimate } \Rightarrow \text{ mark } \Rightarrow \text{ refine/coarsen } \ldots$$

We briefly discuss each step of the procedure separately.

Solve: At this step we solve a system of equations, linear or non-linear depending on the model problem under consideration. Multi-grid or Krylov space methods and Newton method can be efficiently employed for obtaining a solution of the system.

Estimate: Adaptive control of the error between the exact and discrete solutions is built on local *error indicators* and global *error estimates*. The error indicator is a non-negative real number assigned to each triangle, which has its largest values in the triangles whose refinement would be most beneficial for reducing the discretization error. An error estimate can be defined only globally and should be a good approximation of the discretization error in an appropriate norm. An error indicator is used to guide adaptive remeshing, while an error estimate can be used as a stopping criterion for the program, or just to give the user some idea of how accurate is the solution.

Error estimates for discretization are of two forms:

- a priori error estimates;
- a posteriori error estimates.

An *a priori* error estimate relates the error between the exact and the approximate solution to the regularity of the exact solution, while an *a posteriori* error estimate is a computable estimate for the error in a suitable norm in terms of the actual numerical solution and data of the problem. Such an estimate allows to compute the solution with a prescribed error tolerance.

Mark: Using the information based on local error indicators, a set of triangular elements are marked for refinement or coarsening.

Refine/coarsen: In this step we implement a suitable refinement or coarsening procedure in order to refine/coarsen the marked triangles from the previous step. It is worth mentioning that the issues concerning the interpolation and restriction of degrees of freedom during mesh refinement and coarsening must be considered as well and appropriate methods should be used for fitting the finite element functions to a new generated finite element spaces.

7.3.1 Error estimates

For the control of mesh adaption we are going to use an a posteriori error estimate for the temperature, which can be deduced from appropriate a priori estimate of the error. Therefore, let us consider the heat conduction equation and state the results on error estimates obtained by Eriksson and Johnson in [12].

The heat equation is classically described by the following evolution equation plus initial and boundary conditions (for the sake of simplicity we set all material parameters equal to one):

$$\theta_t - \Delta\theta = f \text{ in } \Omega \times (0,T), \tag{7.18}$$

where $\theta = \theta(x,t)$ represents the temperature, t is the time variable, $T > 0$ is a fixed number, $\Omega \subset \mathbb{R}^n$ is as usual a bounded domain with a Lipschitz boundary $\partial\Omega$ and $f = f(x,t)$ describes the volume heat sources.

As for the boundary conditions, we impose Dirichlet boundary conditions on the whole boundary $\partial\Omega \times (0,T)$:

$$\theta = 0 \text{ on } \partial\Omega \times (0,T). \tag{7.19}$$

The cases of other type of boundaries (Neumann, Robin) are treated analogously.

Finally, we assume that the temperature distribution at $t = 0$ is given via

$$\theta(x,0) = \theta_0(x) \quad x \in \Omega. \tag{7.20}$$

A priori error estimates

A priori estimates for the error between continuous and discrete solution can be derived by i) first proving an approximation result for the solution of the semi-discrete problem (discretization is done only in space), and ii) then using more or less the standard estimates for time discretization of systems of ordinary differential equations.
For example, for the backward Euler time discretization and piecewise linear finite element space over a triangulation $\mathcal{T}$ in space, the error estimate reads:
Assuming that θ is smooth enough, we have

$$\begin{aligned}\max_{0\le k\le N}\|\theta(t_k)-\theta_h^k\|_{\mathbb{L}^2(\Omega)} \;\le\; c\Bigg(&\|\theta_0-\theta_h^0\|_{\mathbb{L}^2(\Omega)}+\Bigg(h(\mathcal{T})^4\|\theta_0\|^2_{\mathbb{H}^2(\Omega)}\\ &+h(\mathcal{T})^4\int_0^{t_N}\|\theta'\|^2_{\mathbb{H}^2(\Omega)}dt+(\Delta t)^2\int_0^{t_N}\|\theta''\|^2_{\mathbb{L}^2(\Omega)}dt\Bigg)^{\frac{1}{2}}\Bigg).\end{aligned}$$

We observe that the error converges to zero quadratically in $h(\mathcal{T})$ and linearly in Δt. For the Crank-Nicholson scheme, one can get quadratic convergence in Δt as well, but under higher regularity assumptions on θ.

A posteriori error estimates

A posteriori error estimates for parabolic problems usually consist of four different types of terms:

- terms estimating the initial error;
- terms estimating the error from discretization in space;
- terms estimating the error from mesh coarsening between time steps;
- terms estimating the error from discretization in time.

Thus, the total estimate can be split into parts

$$\eta_0,\ \eta_h,\ \eta_c,\ \text{and}\ \eta_\tau$$

estimating these four different error parts.
Eriksson and Johnson [12] proved an a posteriori error estimate for the discontinuous

Galerkin time discretization of the heat equation. The error estimate for piecewise constant time discretization and piecewise linear discretization in space is given by

$$\begin{aligned}\|\theta(t_N)-\Theta_N\|_{\mathbb{L}^2(\Omega)} \;\leq\; & \|\theta_0-\Theta_0\|_{\mathbb{L}^2(\Omega)} \\ & + \max_{1\leq n\leq N}\Bigg(\Big(\sum_{T\in\mathcal{T}_n} C_1 h_T^4 \|f\|^2_{\mathbb{L}^\infty(I_n,L^2(T))} \\ & + C_2 h_T^3 \|[n\cdot\nabla\Theta_n]\|^2_{\mathbb{L}^\infty(I_n,L^2(\partial T\setminus\partial\Omega))}\Big)^{\frac{1}{2}} \\ & + C_3\|\Theta_n-\Theta_{n-1}\|_{\mathbb{L}^2(\Omega)} + C_4\Big\|h_T^2\frac{[\Theta_{n-1}]}{\tau_n}\Big\|^*_{\mathbb{L}^2(\Omega)}\Bigg),\end{aligned}$$

where Θ_n is the discrete solution on $I_n := (t_{n-1}, t_n)$, $\tau_n = t_n - t_{n-1}$ is the n^{th} time step size, $[\cdot]$ denotes jumps over edges or between time intervals. The last term $C_4\|\dots\|^*$ is present only in case of mesh coarsening. The constants C_i depend on the time t_N and the size of the last time step: $C_i = C_i(\log(\frac{t_N}{\tau_N}))$.
This leads to the following error estimator parts:

$$\begin{aligned}\eta_0 &= \Big(\sum_{T\in\mathcal{T}_0}\|\theta_0-\Theta_0\|_{\mathbb{L}^2(T)}\Big)^{\frac{1}{2}},\\ \eta_h &= \Big(\sum_{T\in\mathcal{T}_n} C_1 h_T^4\|f\|_{L^\infty(I_n,L^2(T))} + C_2 h_T^3\|[n\cdot\nabla\Theta_n]\|^2_{\mathbb{L}^\infty(I_n,L^2(\partial T\setminus\partial\Omega))}\Big)^{\frac{1}{2}},\\ \eta_c &= \Big(\sum_{T\in\mathcal{T}_n} C_4\Big\|h_T^2\frac{[\Theta_{n-1}]}{\tau_n}\Big\|_{L^2(T)}\Big)^{\frac{1}{2}},\\ \eta_\tau &= C_3\|\Theta_n-\Theta_{n-1}\|_{\mathbb{L}^2(\Omega)}.\end{aligned}$$

When a bound *tol* is given for the total error produced in each time step, the widely used strategy is to allow one fixed portion $\Gamma_h\, tol$ to be produced by the spatial discretization, and another portion $\Gamma_\tau\, tol$ of the error to be produced by the time discretization, with $\Gamma_h + \Gamma_\tau \leq 1.0$. The adaptive procedure now tries to adjust time step sizes and meshes such that in every time step

$$\eta_\tau \approx \Gamma_\tau\, tol \quad \text{and} \quad \eta_h + \eta_c \approx \Gamma_h\, tol\,.$$

7.3.2 Adaptive refinement strategies. Equidistribution strategy

Mesh refinement is especially important, being one of the major reasons for using an unstructured mesh. The philosophy for the implementation should be the changing of meshes

successively by local refinement or coarsening, based on error estimators or error indicators which are computed a posteriori from the discrete solution and given data on the current mesh.
Several adaptive strategies are proposed in the literature that provide us with a criteria which elements should be marked for refinement. The procedure of any adaptive refinement strategy is simple: elements where the error estimate is large will be marked for refinement, while elements with a small estimated error are left unchanged.

Adaptive refinement for elliptic problems

The general outline of an adaptive algorithm for a stationary problem is as follows, [46]. Starting from an initial triangulation $\mathcal{T}_0$, we produce a sequence of triangulations $\mathcal{T}_k$, $k = 1, 2, \ldots$, until the estimated error is below the given tolerance:

7.3.1 Algorithm. General adaptive refinement strategy for stationary problems

```
Start with T_0 and error tolerance ε
k := 0
do forever
   solve the discrete problem on T_k
   compute local error estimate η and local indicators η_T, T ∈ T_k
   if η ≤ ε then
      stop
   else mark elements for refinement or coarsening, according to a marking
   strategy
   refine mesh T_k, producing T_{k+1}
   k := k + 1
enddo
```

Since a discrete problem has to be solved in every iteration of this algorithm, the number of iterations should be as small as possible. Thus, the marking strategy should select not too few mesh elements for refinement in each cycle. On the other hand, not much more elements should be selected than is needed to reduce the error below the given tolerance.
In the sequel, we describe only one of the marking strategies which we are going to use for solving the cutting problem. The strategy is called the *equidistribution strategy* [12]. Let

N_k be the number of mesh elements in $\mathcal{T}_k$. If we assume that the error is equidistributed over all elements, i. e. $\eta_T = \eta_{T'}$ for all $T, T' \in \mathcal{T}_k$, then

$$\eta \;=\; \left(\sum_{T \in \mathcal{T}_h} \eta_T^2 \right)^{1/2} \;=\; \sqrt{N_k}\, \eta_T \;\stackrel{!}{=}\; \varepsilon \qquad \text{and} \qquad \eta_T \;=\; \frac{\varepsilon}{\sqrt{N_k}}\,.$$

We can try to reach this equidistribution by refining all elements, where it is disturbed because the estimated error is larger than $\varepsilon/\sqrt{N_k}$. To make the procedure more robust, a parameter $\theta \in (0,1)$, $\theta \approx 1$, is included in the method.

7.3.2 Algorithm. Equidistribution strategy [12].

```
Start with parameter θ ∈ (0,1), θ ≈ 1

for all T in T_k do
   if η_T > θε/√N_k then mark T for refinement
enddo
```

If the error η is already near ε, then the choice $\theta = 1$ leads to the selection of only very few elements for refinement, which results in more iterations of the adaptive process. Thus, θ should be chosen smaller than 1, for example $\theta = 0.9$.

Although the above mentioned equidistribution strategy is described for refinement purposes, it can also be used to mark mesh elements for coarsening. Actually, elements will only be coarsened if all neighbour elements which are affected by the coarsening process are marked for coarsening, too. This makes sure that only elements where the error is small enough are coarsened. Let us show how strategy works both for refinement and coarsening. Equidistribution of the tolerated error ε leads to

$$\eta_T \;\approx\; \frac{\varepsilon}{\sqrt{N_k}} \qquad \text{for all } T \in \mathcal{T}.$$

If the local error at an element is considerably smaller than this mean value, we may coarsen the element without producing an error that is too large. If we are able to estimate the error after coarsening, for example by assuming an asymptotic behaviour like

$$\eta_T \;\approx\; c\, h_T^{\lambda}\,, \quad \lambda > 0\,,$$

we can calculate a threshold $\theta_c \in (0, \theta)$ such that the local error after coarsening is still below $\theta\,\varepsilon/\sqrt{N_k}$ if it was smaller than $\theta_c\,\varepsilon/\sqrt{N_k}$ before. If the error after coarsening gets larger than this value, the elements would directly be refined again in the next iteration.

7.3.3 Algorithm. Equidistribution refinement/coarsening strategy

`Start with parameters` $\theta \in (0,1)$, $\theta \approx 1$, `and` $\theta_c \in (0,\theta)$

`for all` T `in` $\mathcal{T}_k$ `do`

`if` $\eta_T > \theta\,\varepsilon/\sqrt{N_k}$ `then mark` T `for refinement`

`if` $\eta_T + \eta_{c,T} < \theta_c\,\varepsilon/\sqrt{N_k}$ `then mark` T `for coarsening`

`enddo`

Adaptive refinement for parabolic problems

The adaptive refinement procedures described so far can be extended to time dependent problems. In time dependent problems the mesh is adapted to the solution in every time step using a posteriori error estimators. An additional work may be invested to control the time step sizes adaptively as well. Schmidt and Siebert in [46] suggest an algorithm for the adaptive control of time step size in parabolic problems.

7.3.4 Algorithm. Time step size control

Take parameters $\delta_1 \in (0,1)$, $\delta_2 > 1$, time step size τ_{old}, tolerances tol_τ and TOL_τ of error produced by the time discretization.

Step 1. Start with time step size $\tau := \tau_{old}$.

Step 2. Solve one time step according to Algorithm 7.2.3.

Step 3. Compute η_τ.

Step 4. If $\eta_\tau > TOL_\tau$, then set $\tau := \delta_1\tau$ and go to Step 2.

Step 5. If $\eta_\tau < tol_\tau$, then set $\tau := \delta_2\tau$.

Step 6. End.

For Euler time discretization of the non-homogeneous heat equation with piecewise linear finite elements, an estimate η_τ looks like

$$\eta_\tau := c\left(\|\theta_h^{n+1} - \theta_h^n\| + \|f\|\right).$$

For the cutting problem we define

$$\eta_\tau := \tau\left(c_1\|\theta_h^{n+1} - \theta_h^n\|_{\mathbb{L}^2(\hat{\Omega})} + c_2\|\Phi_h^{n+1} - \Phi_h^n\|_{\mathbb{L}^2(\hat{\Omega})}\right),$$

where c_1, c_2 are given positive parameters. With the help of defined η_τ we compute the change in temperature and level set function in one timestep and use this value for adaptive

control of time step size.
The above algorithm controls the time step size only, nothing is done for mesh adaption. There are several possibilities to combine both controls. One possible way would be to do the step size control with the old mesh, then adapt the mesh and then check the time error again. We refer to [46] for a time and space adaptive algorithm.

A recursive approach to mesh refinement and coarsening

The crucial problem in the local mesh refinement is the maintenance of the mesh conformity. One way to solve the problem is nonrecursive. At first an element is divided, what in general breaks conformity and then conformity is recovered dividing some other elements. Another, recursive, approach maintains conformity during the whole refinement process carefully controlling the order in which elements are divided. This approach requires certain preprocessing to provide for termination of the recursion.
To calculate the numerical solutions, we use the recursive approach, implemented in ALBERTA. Moreover, to divide the triangles, the bisection of elements is used. For every element (triangle), one of its edges is marked as the refinement edge and the element is refined into two children triangles by cutting its edge at its midpoint.

Definition 7.3.1. *A triangle is called compatibly divisible, if its marked edge is also the marked edge of the triangle that shares that edge.*

We start the refinement with some triangle of the mesh. We call this triangle a "calling triangle". Now if we bisect the calling triangle, in most cases we will get nonconformity. To keep the mesh conforming, we say that the bisection of a triangle is only allowed, when it is compatibly divisible or it is a boundary triangle, i.e. its marked edge lies on the boundary of the domain (see Figure 7.6). So, starting with the calling triangle, we check whether

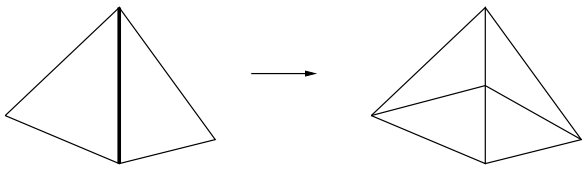

Figure 7.6: Recursive bisection operation. The common edge is the refinement edge for both triangles.

it is compatibly divisible. If yes, then we bisect it and the neighbour that has the same

marked edge simultaneously. If the calling triangle is not compatibly divisible, we go to the neighbouring triangle and proceed as above till we find a compatibly divisible triangle or we come to a boundary triangle.

Two cases are possible:

Case 1: If on our recursive path we meet a triangle which is compatibly divisible, then after dividing it by bisection, the corresponding calling triangle of this refined triangle will, for sure, become compatibly divisible. So we can now bisect it and obtain a new compatibly divisible calling triangle from the previous step.

Case 2: If during the recursion we come to a boundary triangle, and the edge to be bisected lies on the boundary, then after a simple bisection of the edge which lies on the boundary will make the corresponding calling triangle compatibly divisible. It means after a single bisection of a boundary triangle we are in the Case 1.

Theorem 7.3.1. *The described recursive bisection algorithm terminates after a finite time and the shape regularity for all elements at all levels is preserved.*

Proof. See [33] for the proof. □

Another simple choice (nonrecursive) of bisection of an element is the direct method. As in the recursive case, here also, if a triangle is compatibly divisible, then we bisect the triangle and the neighbour simultaneously as a pair. But if a triangle (calling triangle) is not compatibly divisible, then we do the following: we immediately bisect the neighbour triangle, after which the calling triangle will become compatibly divisible, and then bisect the pair. Applying this procedure to all triangular elements of the mesh, we will avoid the nonconformity of simplicies. For an illustration we refer to Figure 7.7. In the first step we

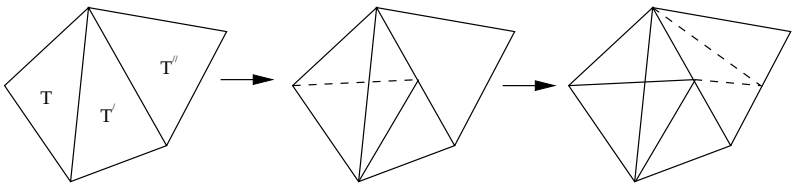

Figure 7.7: Nonrecursive bisection of the triangle T. T' is the neighbour opposite the first vertex of T, T'' is the neighbour opposite the first vertex of T'.

bisect the triangle T'. The triangle T now is compatibly divisible and we bisect it (dashed line) together with its new neighbour. In the second step we apply the same procedure to T''.

7.3.5 Algorithm. Nonrecursive algorithm

```
for all triangles T ∈ T_k do
  if T is compatibly divisible then
    bisect T together with its neighbour
  else bisect the neighbour of T lying on its refinement edge
  bisect T and its new neighbour
enddo
```

The coarsening algorithm is somehow the converse operation of the refinement algorithm. Here also we are allowed to coarsen triangles only in pairs by removing the vertex which is located on the common edge. For illustration look at Figure 7.6 in direction from right to left. Nevertheless, there is a difference between refinement and coarsening algorithms. During refinement, the bisection of an element can enforce the refinement of the neighbouring element, which need not to be refined. During coarsening, an element is allowed to be coarsened only if all elements involved in the operation are marked for coarsening.

7.4 Adaptive method for cutting model

There are several possible adaptive procedures that can be applied to cutting model, here are three of them:

- temperature controlled adaptive refinement;
- level set based adaptive refinement;
- combined adaptivity

In the following we discuss the advantages and drawbacks of each procedure in detail.

Temperature controlled adaptive refinement

The idea of using the *temperature controlled adaption* is that one adapts the mesh paying attention *only* to the discrete temperature θ_h. At the areas close to the plasma beam big temperature variations take place, therefore, we expect that the error between the exact and discrete solutions at these places is relatively big. Consequently, the mesh near the heat source has to be refined in order to reduce the error.

The main advantage of such a method is that the number of degrees of freedom are very small. There is an important drawback of temperature controlled refinement though. The refinement of cutting interface near the plasma beam leaves the mesh around the moving front far from the heat source unchanged. For example, the boundary of the workpiece, where no heat input takes place can not be refined because of the absence of big temperature variations there. This results in a coarser mesh around the zero level set, which may allow an increase of the error in the solution of level set equation. We will come back to this issue in the next section and illustrate the calculation results.

Level set based adaptive refinement

A second way to refine our mesh adaptively, is the *level set based adaption*. In the algorithms described in previous sections we have used the approach to solve the initial value partial differential equation for the level set function ϕ in the entire computational domain. In this approach not only the zero level set but also all other level sets are updated. In problems such as those encountered in image processing (see [41]) this approach is desirable. In the settings of our problem the behaviour of non-zero level sets is not interesting, since the only desirable curve for the calculation of the cutting front is the zero level set of ϕ.
It is intuitively clear (also known from the physical experiments) that the temperature has big variations when we are close to the cutting front and varies very little far from the interface. The interface velocity depends on the gradient of the temperature, therefore, the speed function changes rapidly near the moving front. Thus, adaptive refinement of the mesh may be desired in the regions close to the zero level curve. As we are highly interested in the evolution of the zero level set of ϕ identified with the cutting front, the mesh can be adaptively refined around its location and coarsened far from the zero level set.
Thus, for a good approximation of the solution we aim to refine only near the front of interest. We consider elements close to the interface at each time step. A way to implement it is to choose elements that lie less than some given distance away from the moving front. There are several advantages of this approach. Refining the mesh only in a neighbourhood of the zero level set instead of doing the work on the entire computational domain is one of the main advantages. A fine mesh near the moving interface may be also a proper one for the variational inequality as big temperature variations take place near the cutting front only. Therefore, we hope to do better with this approach compared with the temperature

controlled refinement.

The approach is similar to the *Narrow band approach*, first introduced by Chop in [7] and extensively analysed by Adalsteinsson and Sethian, [42]. The difference is that they perform the computations only near the zero level set, which may require additional attention to the conditions enforced on the boundaries of the narrow band.

The idea is illustrated in Figures 7.8. We again start with a circle of radius one (black circle in the middle of each left column picture) and let it shrink according to velocity given by (7.15). The exact solution shows that the curve vanishes at $t = 0.5$. The figures present the computed solution and corresponding adaptively refined mesh at three times $t = 0.05$, $t = 0.2$ and $t = 0.35$.

Combined adaptivity

Under the term *combined adaptivity* we understand a method which combines two adaptive refinement approaches discussed in the previous sections. More precisely, in this method we

- adaptively refine the mesh inside the solid domain using appropriate a posteriori error estimates for heat equation, and

- use the level set based adaptive refinement method to create an adaptive mesh near the moving boundary (zero level set).

It is worth mentioning that the best way to generate an optimal mesh for the cutting problem is an adaptive method, which uses a posteriori error estimates for both variational inequality and level set equation. The method can provide a practical criteria to control the adaptive mesh refinement and construct a stopping condition for the solver. A proper implementation of this approach requires as well, that instead of solving the problem on the same mesh, we construct two different meshes for each sub-problem and solve the coupled system by computing each unknown on its own triangulation with its own error estimator. The toolbox ALBERTA is able to easily handle the employment of several meshes simultaneously, but we leave this work for our future studies.

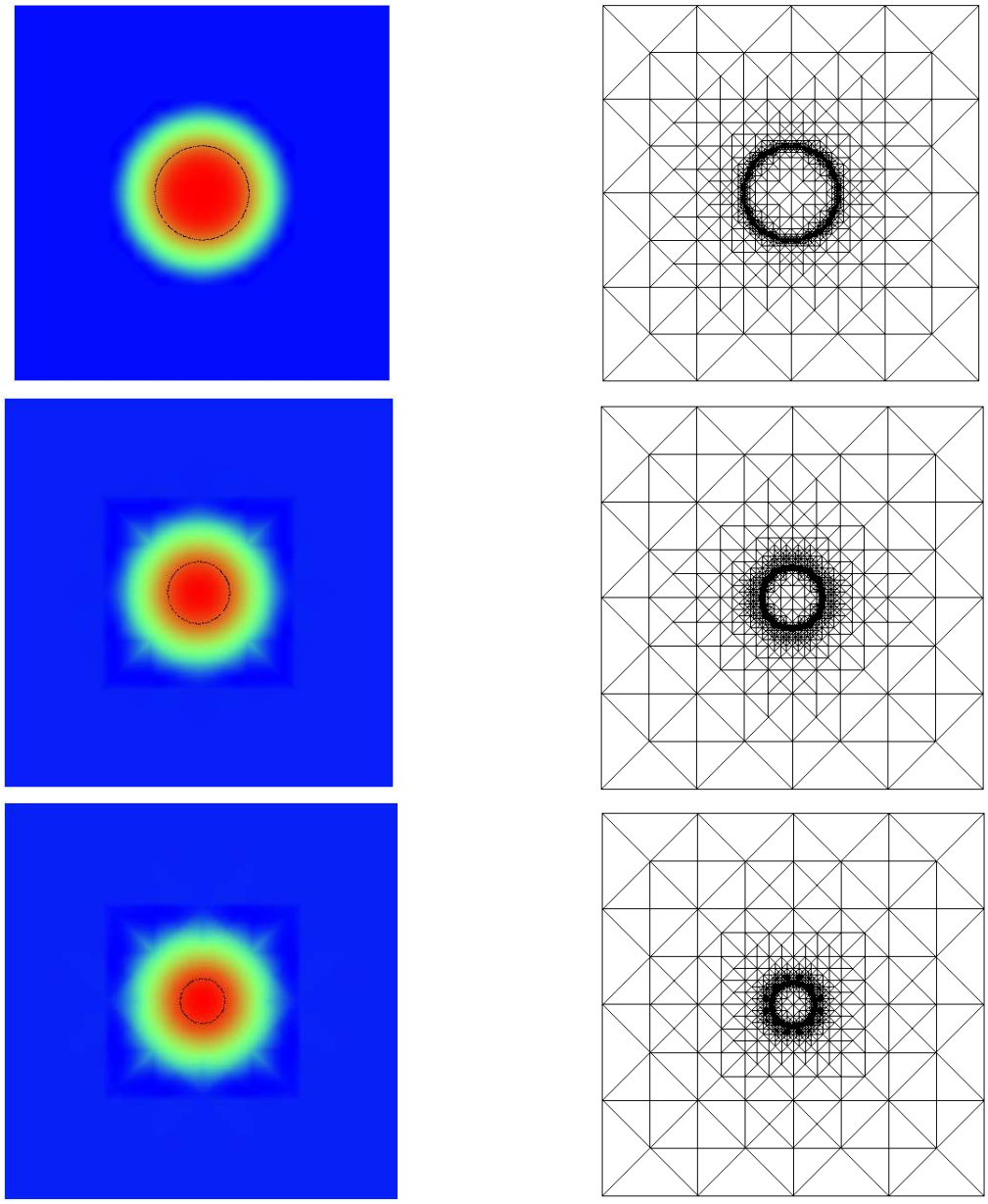

Figure 7.8: Level sets (left) and corresponding adaptively refined meshes (right)

7.5 Numerical experiments

7.5.1 Thermal cutting of a workpiece

Finally, let us apply the cutting algorithm on a problem, the exact solution of which is a priori unknown. As a domain of interest (workpiece to be cut) we take $\Omega = [-1, 1]^2$ and the final time is taken to be $T = 1$. Let initial temperature $\theta_0(x)$ be constant equal to the ambient temperature and as an initial level set function we select the distance function. The plasma beam is represented via a circle, the center of which is initially located on the left side of the workpiece at point $(-1.3, 0)$. When the cutting process starts, the plasma source moves along the x-axis, and the center changes its position at each time step with a given velocity v. Therefore, we can describe the plasma beam as a circle of constant radius r centered at $(\alpha(t), 0)$ with $\alpha(t) = -1.3 + vt$. The heat flux density is calculated with the help of the model developed in Section 3 resulting in appearance of another parameter j_e which is responsible for the amount of heat emitted by the plasma source. The non-homogeneous Dirichlet boundary conditions on the outer boundary are handled in the standard fashion since the interface does not touch the fixed boundary.

We start our simulations with the following parameter set: $j_e = 4.8$, $r = 0.2$, $v = 160$, penalty parameter $\varepsilon = 10^{-12}$ and viscosity parameter being equal to the mesh size. The parameter set is selected such that we may be able to show a qualitative behaviour of the system. For quantitative behaviour one should select a material to be cut, corresponding material parameters and an appropriate plasma gas which will have an influence on the plasma parameter j_e. In this case a space and time scaling of the problem should be done as well.

The initial temperature distribution, domain configuration and mesh are plotted in Figure 7.9. As a refinement technique let us select the different refinement approaches described in Section 7.4.

We start with temperature controlled adaptive refinement. In Figure 7.10 we only show the changing mesh. As one can easily see, the elements located near the zero level set and far from the beam are not refined resulting in error increase in the solution of level set equation.

Now we recompute the solution employing the level set based adaptive refinement. Figure 7.11 illustrates the computation results for different time steps. Left column shows the temperature development in the workpiece. As one can see, the temperature variations are high

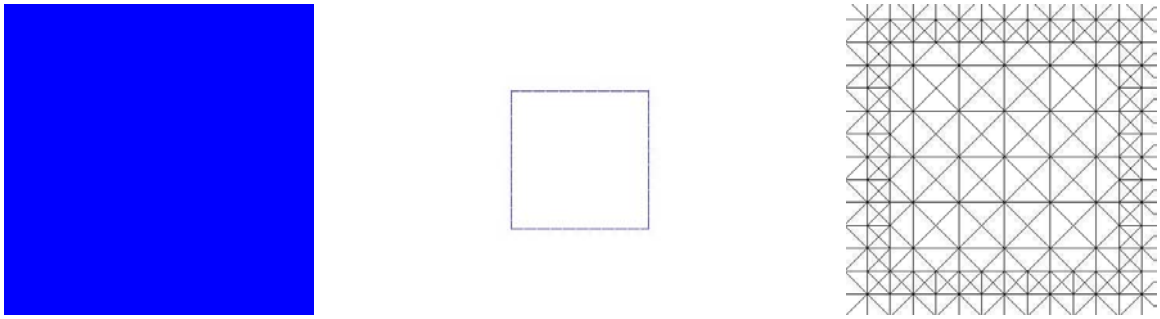

Figure 7.9: Initial temperature, workpiece geometry and computing mesh.

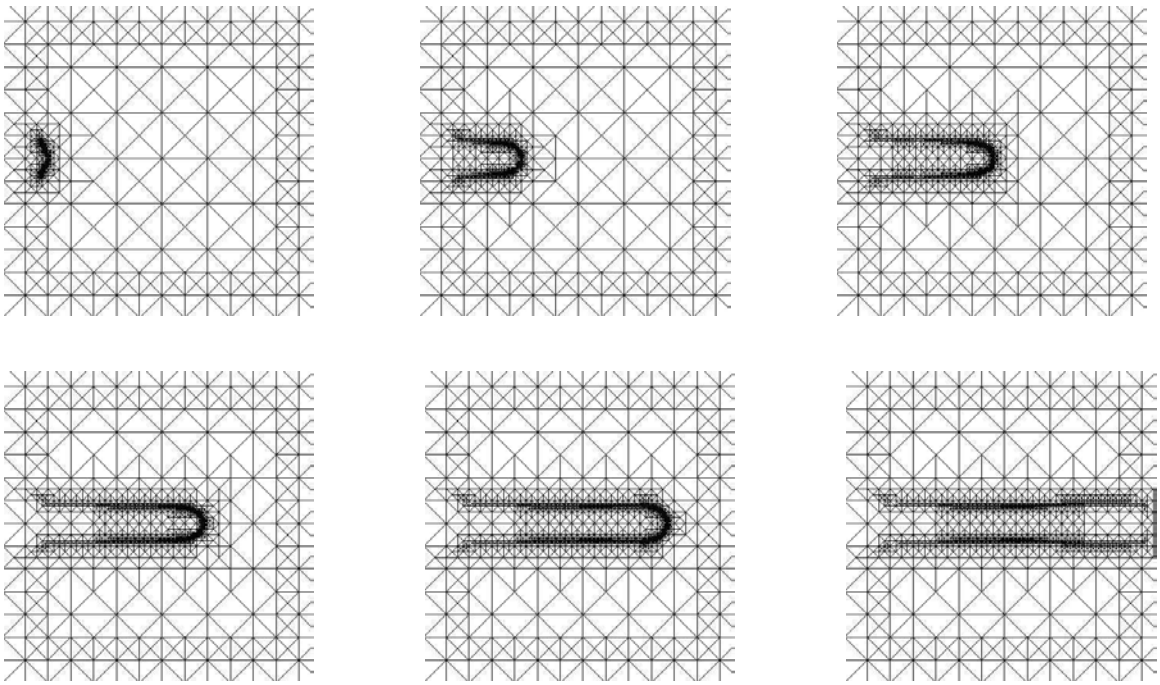

Figure 7.10: Adaptively refined mesh using the temperature controlled refinement. The important refinement around the zero level set is missing.

close to the cutting front with almost negligible temperature changes far from the melting interface. This result verifies one of our modelling assumption, where we consider the heat input by the plasma beam to have a surface effects only. Pictures in the middle column demonstrate the evolution of the zero level set representing the workpiece geometry. A very small rounding of sharp corners of the square workpiece is observed during the simulations, which appears as a result of the regularization of level set equation via vanishing viscosity term. The right column of Figure 7.11 illustrates the corresponding mesh generated by adaptive procedure. Finally, let us solve the problem selecting the combined adaptivity as a refinement method. Recall that in this case we adapt the mesh inside the solid domain using the a posteriori error estimates for heat equation described in Section 7.3 and implement the level set based adaptive refinement close to the zero level set. Figure 7.12 illustrates the computation results. We only plot the adaptively refined mesh, as it is the most interesting issue in this case.

7.5.2 Flattening effects

In Section 7.2.3 we have mentioned that in some cases it is impossible to maintain the numerical accuracy for the level set function ϕ, because flat and/or steep regions may develop as the interface moves. This leads to flattening of the level set function: $\nabla\phi$ may become very small near the moving front, rendering the computation and contour plotting at those places inaccurate. With our approach we do not face any flattening problems. In order to show this, we just take a look at the behaviour of non-zero level sets as well. Let us start with the test problem considered in Section 7.2.2. There we have a unit circle acting as a zero level set. Figure 7.13 shows the evolution of the zero level set (red circle) together with several other level sets (blue circles). As one can see, all of them are behaving well during the time steps and no flattening effect is observable.
Now let us follow the situation with cutting problem. We repeat the calculations and, like above, investigate the behaviour of several non-zero level sets of ϕ_h. Figure 7.14 shows the results, which comes to demonstrate the absence of any flattening effect.

7.5.3 Sensitivity to numerical parameters

In the numerical study of cutting problem, determination of the sensitivity of calculated results to variations or uncertainties in input numerical parameters is crucial to understand-

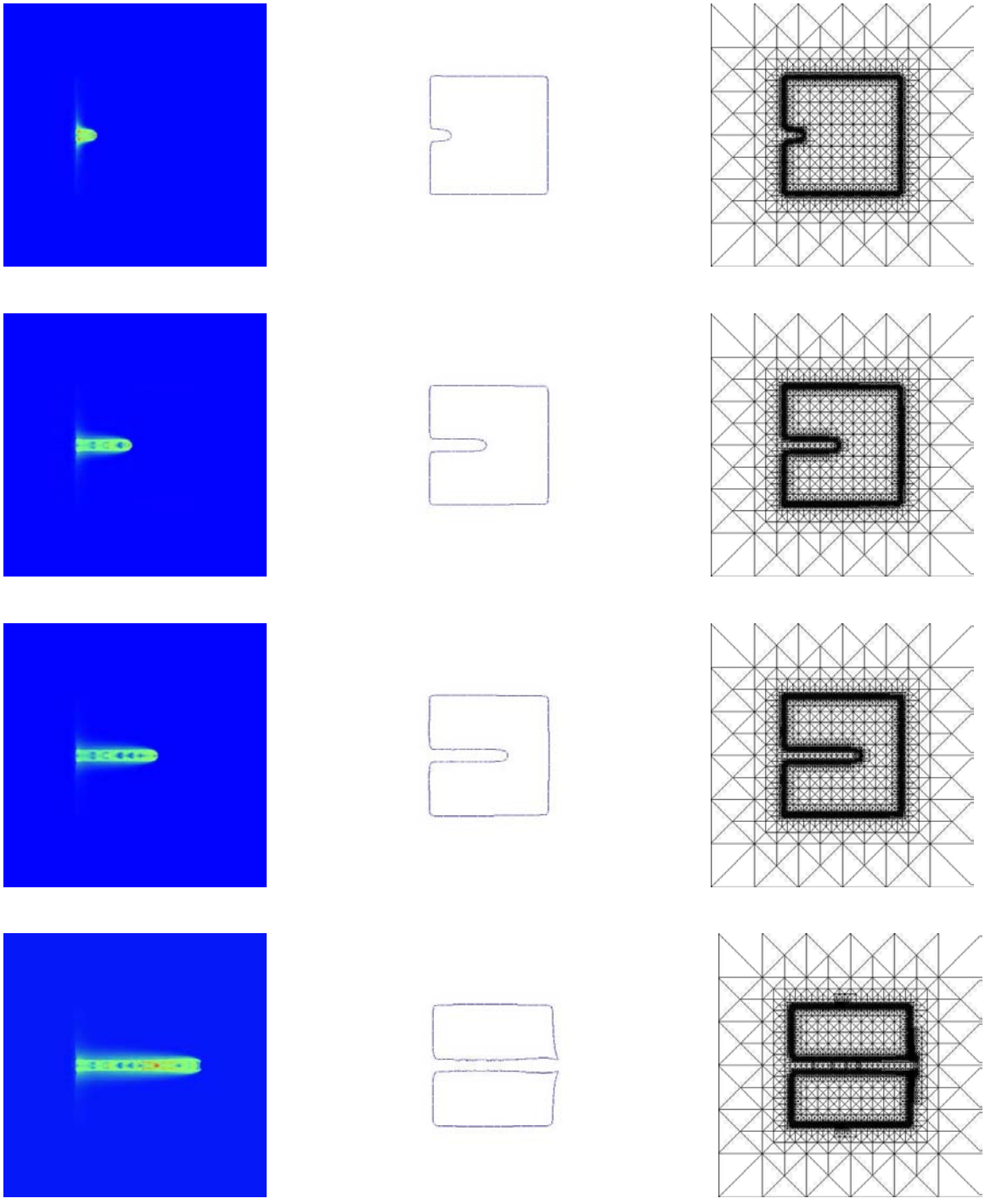

Figure 7.11: Cutting of the workpiece. Left: temperature, middle: level set, right: mesh. As a refinement method, the level set based adaptivity is used.

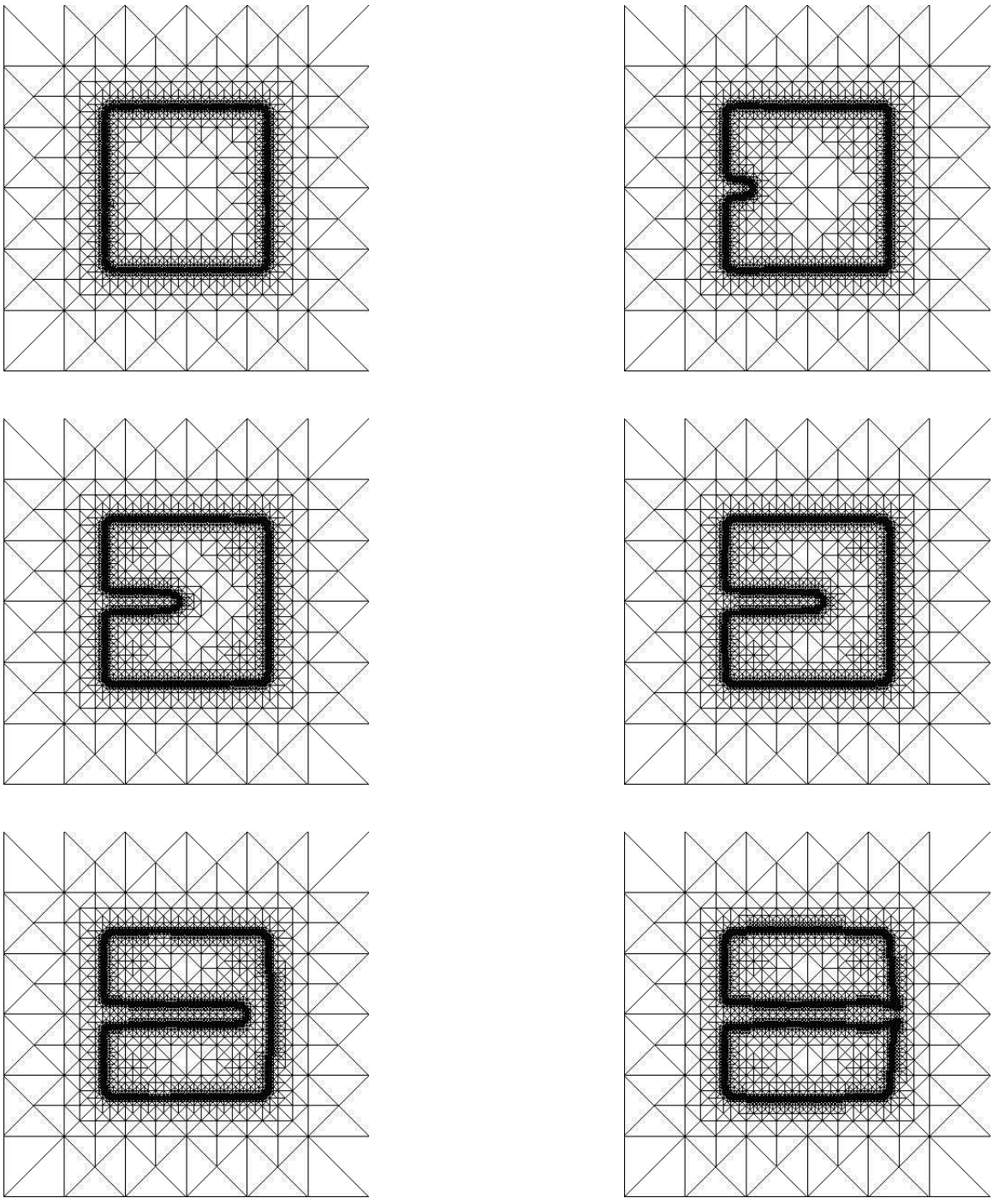

Figure 7.12: Adaptively refined mesh for cutting model.

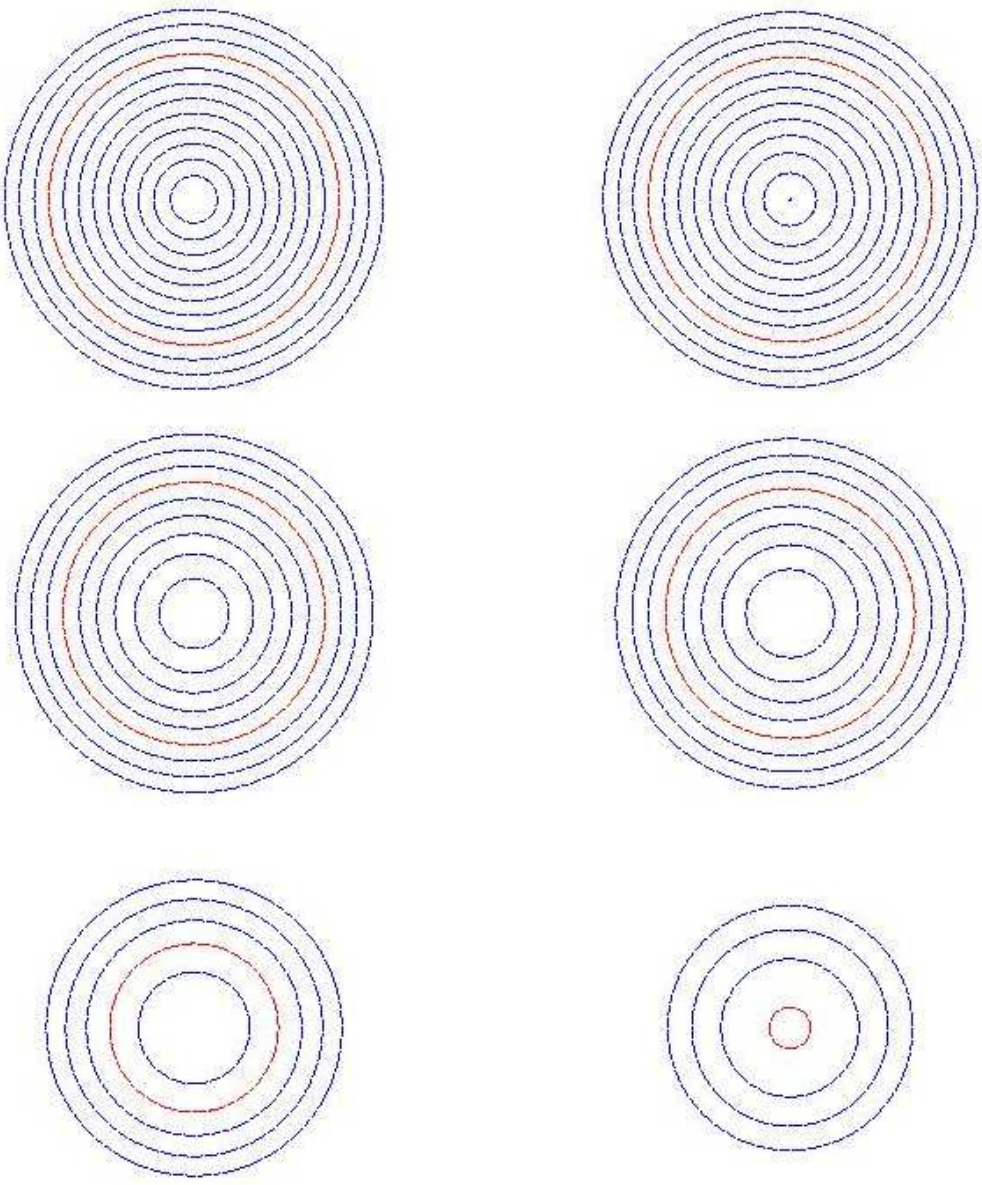

Figure 7.13: Shrinking level sets, red: zero level set, blue: other level sets.

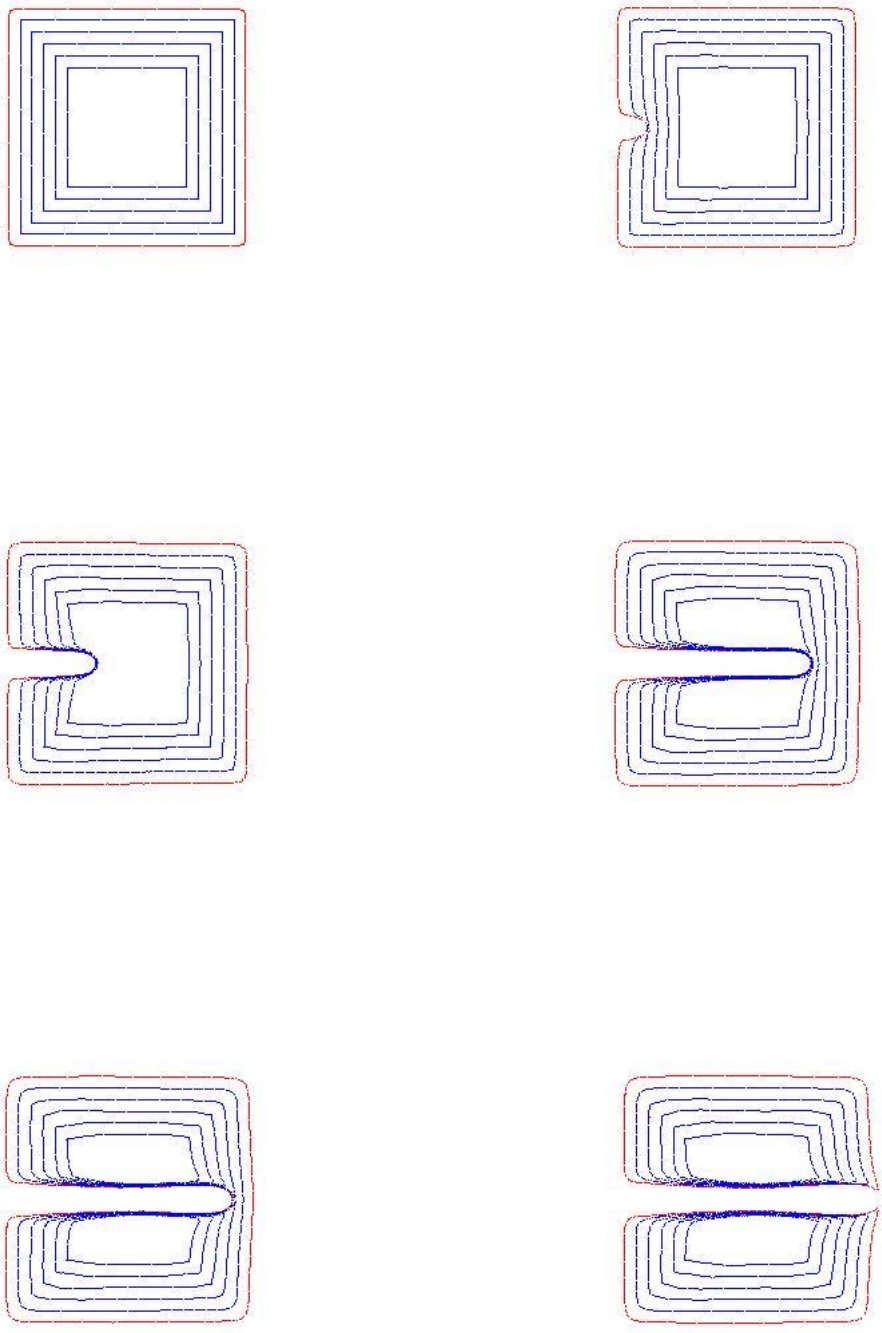

Figure 7.14: The behaviour of different non-zero level sets, red: zero level set, blue: other level sets.

ing the results and prioritizing the accuracy of calculations. Numerical modelling of cutting process includes input parameters such as the tolerance for adaptive method for variational inequality and the level of refinement for the level set based adaptivity. Therefore, we would like to investigate the sensitivity of calculated workpiece temperature and geometry to the above mentioned input parameters. Since the numerical parameters are related to the adaptive refinement methods, the combined adaptivity procedure should be used for the calculations.

We start by fixing the tolerance and varying the level of refinement for level set equation. Recall that in level set based refinement we implement the recursive refinement process by refining all elements that are not far than a given distance from the zero level set and have a size less than some parameter δ. By the size of the element we mean the length of the longest edge of the triangle. Our aim is to investigate the sensitivity of the numerical calculations to this parameter δ. Therefore, we take different values for δ and run the program keeping the tolerance for variational inequality fixed. The results for $\delta = 0.004,\ 0.005,\ 0.007,\ 0.008$ are shown in Figure 7.15. The figure shows how the changes in the triangle size parameter affect the temperature distribution in the material, workpiece geometry and the corresponding mesh. It is worth mentioning that no essential changes in results are observed by further variations of δ, but an increase of the parameter δ above some value leads to occurrance of big errors in the calculations of zero level set.

We continue our experiments by tracing the effect of the parameter *tol* entering the a posteriori error estimate for heat equation. Therefore, we fix the parameter δ and do experiments with different values of *tol*. Calculation results for $tol = 10^{-3},\ 5 \times 10^{-3},\ 10^{-4},\ 5 \cdot 10^{-4}$ are plotted in Figure 7.16. As expected, as the parameter *tol* decreases, the mesh inside the solid region becomes finer, while the larger values of *tol* lead to a coarser mesh inside the workpiece.

7.5.4 Sensitivity to model parameters

The cutting model involves two important parameters representing the heat amount emitted by the plasma beam and the velocity of the heat source. An interesting question arises, therefore, how the simulations results change if we vary those parameters, and do they correspond to the real situation. For the calculations of this section, we employ the level set based adaptive refinement procedure.

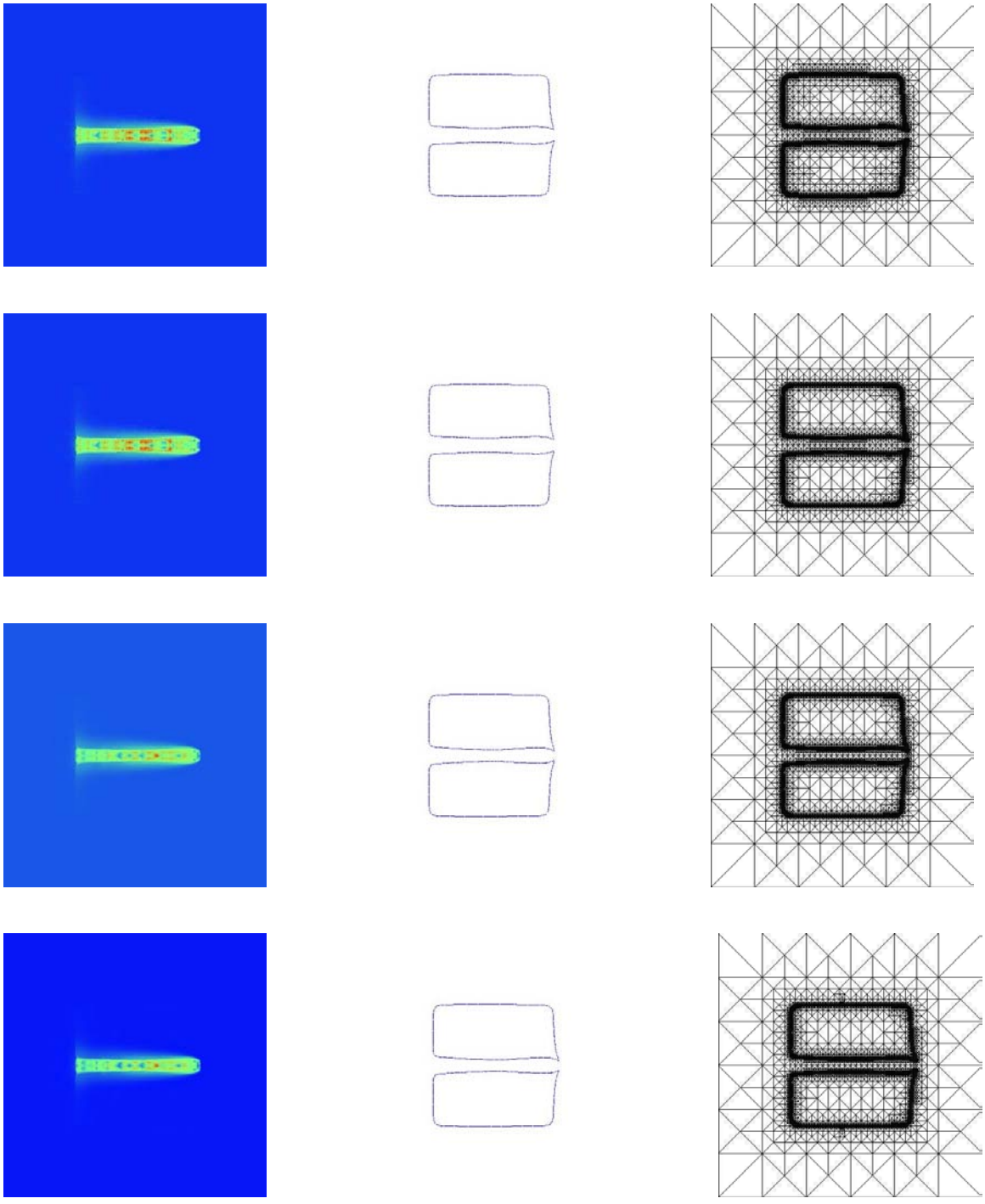

Figure 7.15: Sensitivity to numerical parameter δ. Simulations results of cutting process with fixed tolerance and increasing parameter $\delta = 0.004, 0.005, 0.007, 0.008$.

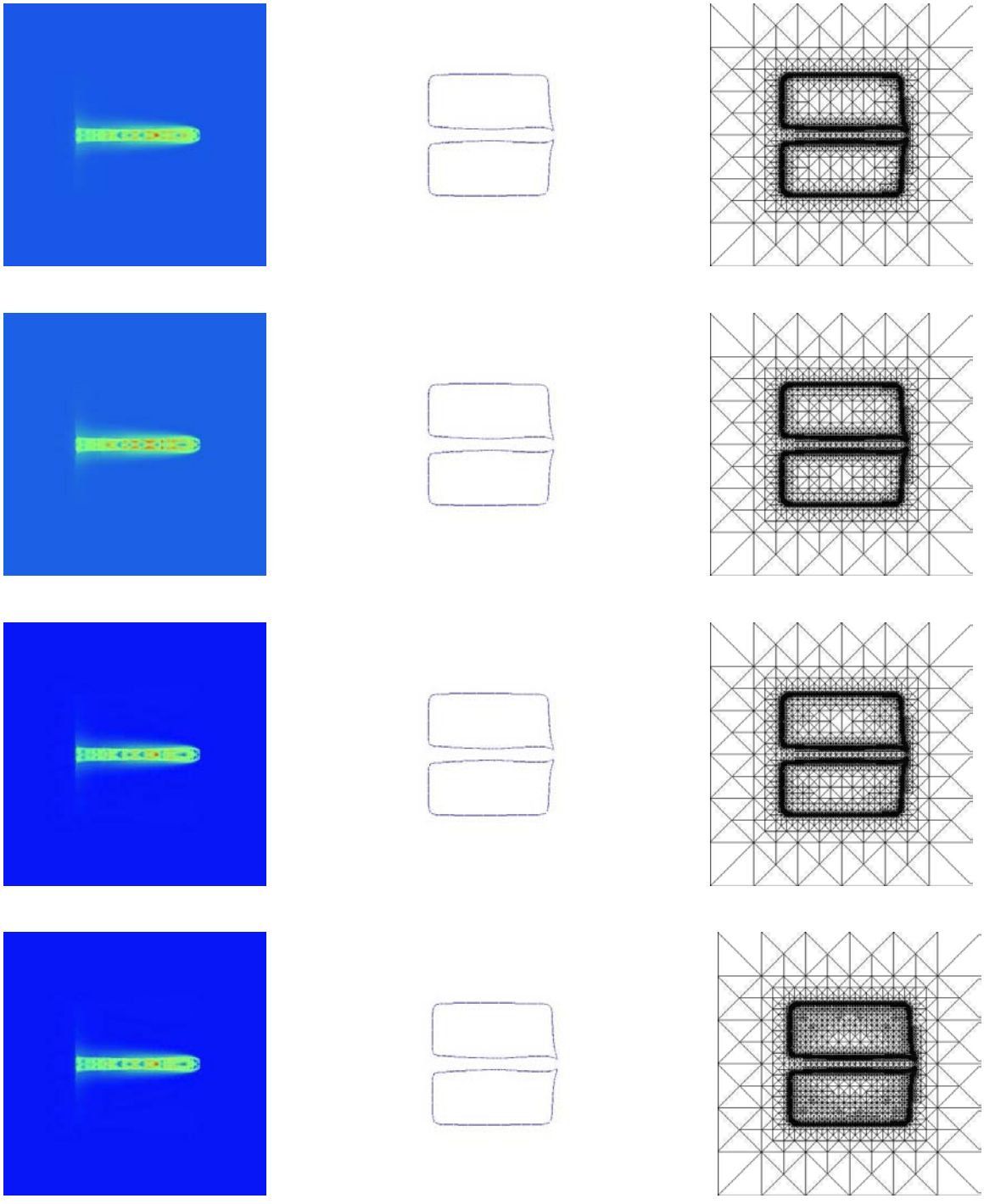

Figure 7.16: Sensitivity to numerical parameter *tol*. Simulations results of cutting process with fixed parameter δ and decreasing parameters $tol = 10^{-3},\ 5 \cdot 10^{-3},\ 10^{-4},\ 5 \cdot 10^{-4}$.

First, let us discuss the influence of the emitted heat flux density j_e. For a fixed velocity parameter $v = 160$, we run our program for different heat input parameters starting from a low value and increasing it subsequently during each further simulation. It is clear that increasing the heat input on the surface of the material will result in a widening of the cutting kerf. The bigger is the emitted heat flux density, the greater is the heating area and, therefore, the wider is the cut cavity. Figure 7.17 verifies our considerations. Starting with $j_e = 4.0$, we then increase its value to 5.8, 6.8 and 8.8. We stop our simulations at some time instant and illustrate the results for each case in Figure 7.17. The widening effect is easily observable. Another way to decrease the width of the cutting cavity is to increase the velocity of the plasma beam. Therefore, we repeat the calculations again with $j_e = 5.8$, but now with plasma device moving with higher velocity $v = 240$. We compare the results with the ones obtained earlier for $v = 160$ and plot them together in Figure 7.18. One can also observe better cut quality (squareness of edges, narrow band of temperature variation, etc.) by cutting with high speed plasma beam.

7.5.5 Topological changes

One of the main advantages of level set method is the way it handles complicated interfacial geometries. Topological changes in the evolving front associated with merging and breaking of the domain are handled naturally. The position of the melting front at any time t is given via the zero level set $\phi(x, t) = 0$ of the level set function ϕ. This zero level set need not be a single curve. In our problem it breaks at the end of the cutting process resulting in two separate domains with non-intersecting boundaries. The key fact is that although the final curve is not a single one anymore, the level set function ϕ remains single-valued. The picture in the last row of Figure 7.11 shows the break curves after the cut.

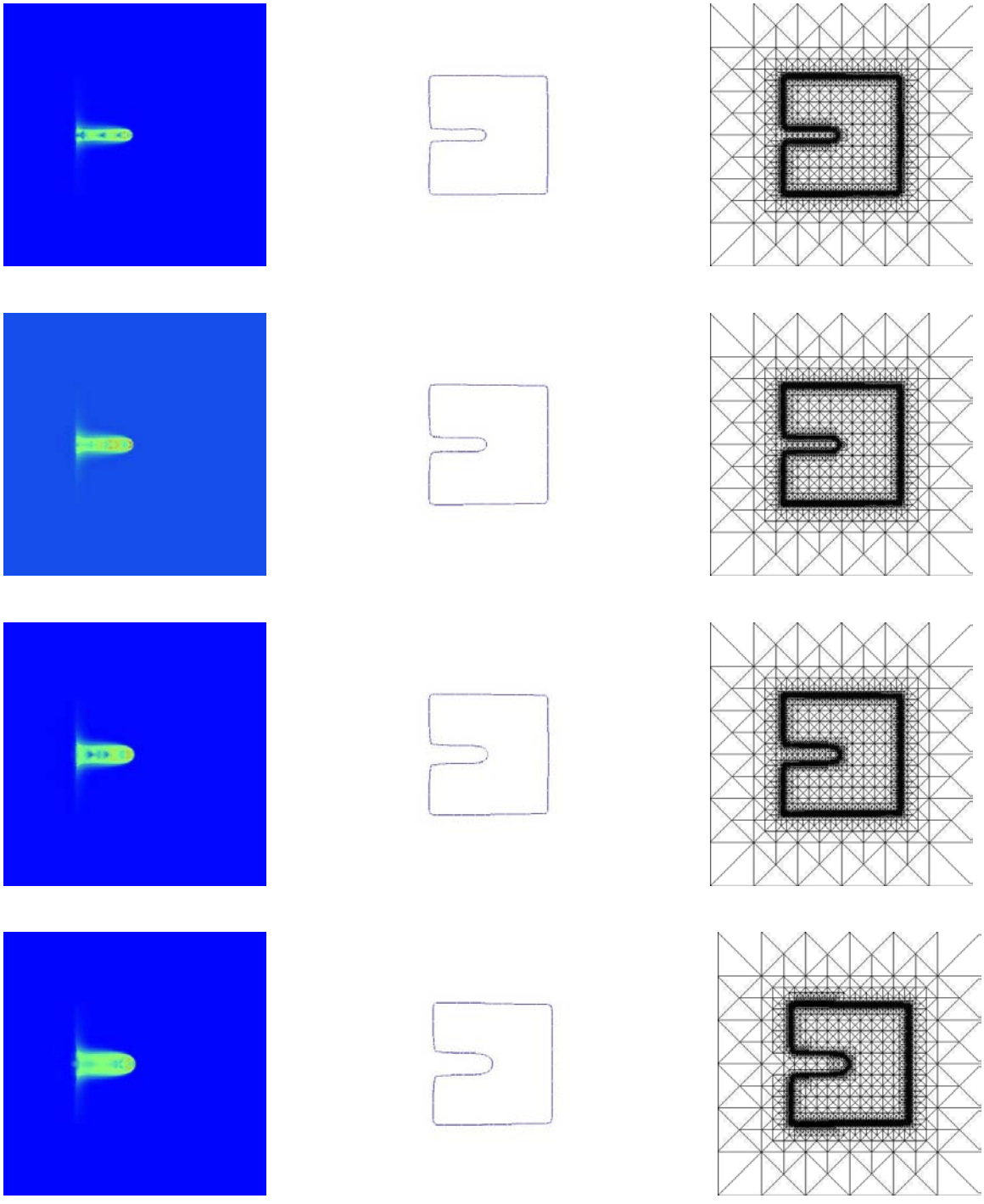

Figure 7.17: Sensitivity to heat input parameter. Simulations results of cutting process with fixed velocity and increasing heat input. The cut cavity widening is easily observable.

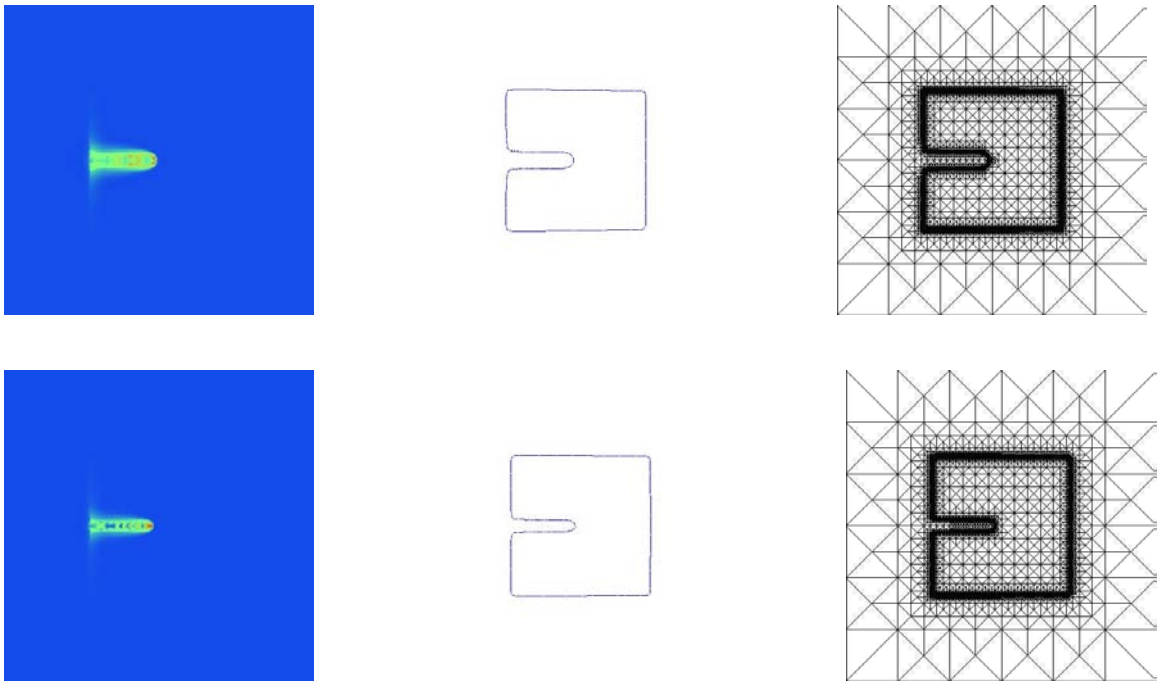

Figure 7.18: Sensitivity to velocity parameter. Results of two computations with fixed heat input and different device velocities. Above: $v = 160$, below: $v = 240$.

Chapter 8

Conclusions

Let us now conclude this work with a short presentation of main results and some recommendations for further investigations.

8.1 Summary of the work

The starting point for this study is a real-life problem coming from the steel industry[1], namely, a problem occurring during the plasma cutting of a workpiece. In this study we have focused our attention on the following main aspects:

- Description of thermal plasma cutting process and physical modelling of different effects taking place in the workpiece during the cutting.
- Mathematical modelling of the metal piece cut with plasma via Stefan-Signorini moving boundary approach.
- Reformulation of the classical model into a weak model using the concepts of theories on variational inequalities and level sets.
- Mathematical analysis of the weak model, establishment of existence and uniqueness results.
- Convergence of numerical algorithms, numerical results and computer simulations.

[1]The problem in its real form was stated by colleagues from Bremen Steel Company.

Summarizing, our investigations cover physical and mathematical modelling of the problem, mathematical analysis of the model and numerical results. The model allows us to get several qualitative results on the process, but is still open for further modifications.

8.2 Remarks on further developments

Because of the complexity of the cutting process and the wide range of different thermal effects occurring in the workpiece we could not give exhaustive answers to all problems. There are a lot of modifications possible and, for sure, desirable for the cutting model. The natural way to modify and improve any model is to get rid of as many assumptions and simplifications as possible. We give an outline of few of them.

1. A very important issue interesting for engineers concerning the plasma cutting is, of course, the deformations taking place on the cutting edge. Besides the temperature, the residual stresses in the pieces after the cut are another responsible for the deformations resulting in poor edge squareness. Therefore, an additional condition (e.g., equations of thermo-elasticity, elasticity, etc.) computing the deformations/stresses in the resulting pieces should be included in the model. We consider this as an extension of the model, which has to be done priorly.

2. There are several parameters in the cutting model. An interesting question would be the optimization of these parameters. In other words, one seeks an optimal set of parameters entering the model which may strongly influence the whole cutting process. One way of solving this problem would be to insert the set of parameters into an optimization problem and try to solve the resulting optimal control problem.

3. We did not consider the solid-solid phase changes in the material occurring during the heating of the workpiece to melting temperature. This can be included in the model by adding another condition (system of equations) describing the solid-solid phase change in the material. Some earlier publications by Schmidt, Boehm, Wolff and Dachkovski, [11], [44], [45] are a very nice starting point for the modification of the model in that direction.

4. We have neglected the heat lost by radiation as well as the energy used for chemical reactions taking place on the cutting surface. While the consideration of the radiation

of heat from the surface results in modifying the model by imposing appropriate nonlinear boundary conditions, the situation with chemical reactions on the surface is more complicated. We refer to [35], for one dimensional model of concrete carbonation, where the boundary conditions on the interface include the effects of chemical reaction.

5. Last, but not least, we expect better results of numerical simulations as soon as adaptive procedures for both variational inequalities and level set equations are applied. We hope to be able to successfully develop corresponding error estimators and come out with finer results which will satisfy engineers at the industry dealing with the problem as well as us, mathematicians, trying to make our small contributions in the process of solving real-life problems.

Appendix A

Viscosity solution method

The standard classical analysis of the Problem 6.2.3 by the method of characteristics shows that in general there can be no smooth solution for all times $t \geq 0$. The solution of Problem 6.2.3 may be discontinuous with a jump across a characteristic. There is also a lack of an appropriate notion of solution for which the existence and uniqueness results can be proved. We are going to utilize another approach known as *method of vanishing viscosity*. The idea is to add a viscosity term to the level-set equation (6.33) and consider the approximate problem:

Problem A.0.1. *Find the function* $\phi_\varepsilon(x,t) : \mathbb{R}^n \times (0,T) \to \mathbb{R}$, $n = 2, 3$, *such that*

$$\frac{\partial \phi_\varepsilon}{\partial t} + w \cdot \nabla \phi_\varepsilon = \varepsilon \Delta \phi, \tag{A.1}$$

$$\phi_\varepsilon(x,0) = \phi_0(x),$$

where ε *is a positive constant.*

The advantage of the method is that equation (A.1) is an initial-value quasi-linear parabolic equation, which can be shown to have a smooth solution. The viscosity term $\varepsilon\Delta\phi$ plays a role of a regularizer of the level-set equation (6.33). The limit of the smooth solution ϕ_ε as ε vanishes provides us with some sort of weak solution of (6.33).

Crandal, Evans and Lions [10] define a weak solution of (6.33) as follows:

Definition A.0.1. *A bounded, uniformly continuous function* ϕ *is said to be a* viscosity solution *of Problem A.0.1, if for all test functions* $\varphi \in \mathbb{C}^\infty(\mathbb{R}^n \times (0,T))$ *the following holds:*

1. *If $\phi - \varphi$ has a local maximum at a point (x_0, t_0), then*

$$\varphi_t(x_0, t_0) + w(x_0, t_0)\nabla\varphi(x_0, t_0) \leq 0, \tag{A.2}$$

and

if $\phi - \varphi$ has a local minimum at a point (x_0, t_0), then

$$\varphi_t(x_0, t_0) + w(x_0, t_0)\nabla\varphi(x_0, t_0) \geq 0. \tag{A.3}$$

2. *ϕ satisfies the initial condition*

$$\phi = \phi_0 \quad on\ \mathbb{R}^n \times \{t = 0\}. \tag{A.4}$$

Remark A.0.1. *In the definition no derivatives of the viscosity solution ϕ_ε appear; everything is written in terms of the smooth function φ. Our goal will be to pass from (A.1) to (6.33) as ε goes to zero by first moving all the derivatives onto the test function in order to avoid the "ugly" derivatives of the viscosity solution.*

Let us check whether the notion of viscosity solution is reasonable in the sense of its consistency with the classical solution. To be proved are the following statements:

1. If ϕ is a classical solution of level-set equation (6.33), then it is also a viscosity solution, i.e. any bounded and uniformly continuous function $\phi \in \mathbb{C}^1(\mathbb{R}^n \times [0, T))$ which solves (6.33), satisfies the two inequalities in the above definition.

2. If a viscosity solution ϕ of (6.33) is differentiable at some point (x_0, t_0), then it delivers the same result as the classical level-set equation at the same point.

Proof of 1. Let φ be a smooth function and assume that $\phi - \varphi$ attains a local maximum at some point (x_0, t_0). Then

$$\nabla(\phi - \varphi)(x_0, t_0) = 0,$$

and

$$\frac{\partial(\phi - \varphi)}{\partial t}(x_0, t_0) = 0.$$

Thus, using the fact that ϕ solves (6.33), we obtain

$$\frac{\partial\varphi}{\partial t}(x_0, t_0) + w(x_0, t_0)\nabla\varphi(x_0, t_0) = \frac{\partial\phi}{\partial t}(x_0, t_0) + w(x_0, t_0)\nabla\phi(x_0, t_0) = 0.$$

Analog discussions can be done for the case when $\phi - \varphi$ has a local minimum at (x_0, t_0).

Proof of 2. We will need the following result [13].

Lemma A.0.1. *Assume a function $f : \mathbb{R}^n \to \mathbb{R}$ is continuous and differentiable at some point x_0. Then there exists a function $g \in \mathbb{C}^1(\mathbb{R}^n)$ such that*

$$f(x_0) = g_(x_0) \tag{A.5}$$

and

$$f - g \text{ has a strict local maximum at } x_0. \tag{A.6}$$

Applying the lemma above we obtain that there exists a function $\varphi \in \mathbb{C}^1(\mathbb{R}^n \times [0,T))$ such that

$$\phi - \varphi \text{ has a strict local maximum at } (x_0, t_0). \tag{A.7}$$

Now denote by J_ε the mollifier in x and t and set $\varphi^\varepsilon := J_\varepsilon \varphi$. Then, thanks to the properties of the mollifier, we get the following uniform convergences near the point x_0, t_0

$$\varphi^\varepsilon \to \varphi, \quad \nabla\varphi^\varepsilon \to \nabla\varphi, \quad \frac{\partial\varphi^\varepsilon}{\partial t} \to \frac{\partial\varphi}{\partial t}. \tag{A.8}$$

From (A.7) we obtain

$$\phi - \varphi^\varepsilon \text{ has a maximum at some point } (x_\varepsilon, t_\varepsilon), \tag{A.9}$$

where the point $(x_\varepsilon, t_\varepsilon)$ converges to (x_0, t_0) as $\varepsilon \to 0$.

We know that ϕ is a viscosity solution, therefore, φ^ε, being a C^∞ function, plays the role of a test function and must satisfy the inequality introduced in the definition of the viscosity solution:

$$\varphi_t^\varepsilon(x_\varepsilon, t_\varepsilon) + w(x_\varepsilon, t_\varepsilon)\nabla\varphi^\varepsilon(x_\varepsilon, t_\varepsilon) \leq 0.$$

Let $\varepsilon \to 0$ in above. Then $(x_\varepsilon, t_\varepsilon) \to (x_0, t_0)$, and combining this with (A.8) leads to

$$\varphi_t(x_0, t_0) + w(x_0, t_0)\nabla\varphi(x_0, t_0) \leq 0. \tag{A.10}$$

Now we use the fact that ϕ is differentiable at (x_0, t_0). Together with (A.7) this implies

$$\phi_t(x_0, t_0) = \varphi(x_0, t_0), \quad \nabla\phi(x_0, t_0) = \nabla\varphi(x_0, t_0).$$

The substitution of latter in (A.10) brings us to

$$\phi_t(x_0, t_0) + w(x_0, t_0)\nabla\phi(x_0, t_0) \leq 0. \tag{A.11}$$

What remains is to repeat the arguments above for a function $-\phi$ for which there exists a smooth function φ such that $\phi - \varphi$ has a strict minimum at (x_0, t_0). Implementing the similar steps as before, we arrive at

$$\phi_t(x_0, t_0) + w(x_0, t_0)\nabla\phi(x_0, t_0) \geq 0, \tag{A.12}$$

which means that ϕ satisfies the classical level-set equation at the point (x_0, t_0).
Our next goal is to establish the uniqueness of a viscosity solution of the level set equation. Let us assume that for $x, y, p, q \in \mathbb{R}^n$ the Hamiltonian $H(p, x) = H(\nabla\phi, x) := w \cdot \nabla\phi$ satisfies the conditions

$$|H(p, x) - H(q, x)| \leq C|p - q|, \tag{A.13}$$

$$|H(p, x) - H(p, y)| \leq C|x - y|(1 + |p|). \tag{A.14}$$

Theorem A.0.1. *(Uniqueness of viscosity solution)*
Under assumptions (A.13) the viscosity solution of level set equation (6.33) is unique.

Proof. The proof is based on an idea of "doubling the number of variables" and is accurately described in the book of Evans, see [13]. □

Appendix B

Finite element method

The finite element method was first conceived in 1943 in a paper by Courant, but the importance of this contribution was ignored at the time. Then the engineers independently re-invented the method in the early fifties. Nowadays the whole procedure of the finite element method is mathematically respectable and it has become the most popular technique for obtaining numerical solutions of differential equations arising from engineering problems.

The finite element method can be described in a few words. Suppose that the problem to be solved is in weak formulation. The idea of finite element method is simple. It starts by a subdivision of the structure, or the region of physical interest, into smaller pieces. These pieces must be easy for the computer to record and identify: they may be triangles or rectangles. Then within each piece the trial functions are given an extremely simple form–normally they are polynomials of arbitrary degree. Boundary conditions are easier to impose locally along the edge of a triangle or rectangle, than globally along a more complicated boundary.

Let us start from the first step: divide the domain into finitely many smaller pieces. These small pieces are called elements. There are several kinds of elements, which can be used for the decomposition of the domain and it is not clear whether to subdivide the region into triangles, rectangles or other types of elements. We will not discuss the advantages and disadvantages of each type of elements and will subdivide the region of interest into triangles.

If we decompose the given domain Ω by triangles (see Figure B.1), we will see that the

union of these triangles will be a polygon Ω_h and in general, if $\partial\Omega$ is a curved boundary, then there will be a nonempty region $\Omega \setminus \Omega_h$, which will later, of course, contribute to the error. So one of the main tasks when considering curved boundary, will be to make the nonempty region as small in area as possible. For simplicity we will consider only polygonal domains, i.e. the case when $\Omega_h = \Omega$.

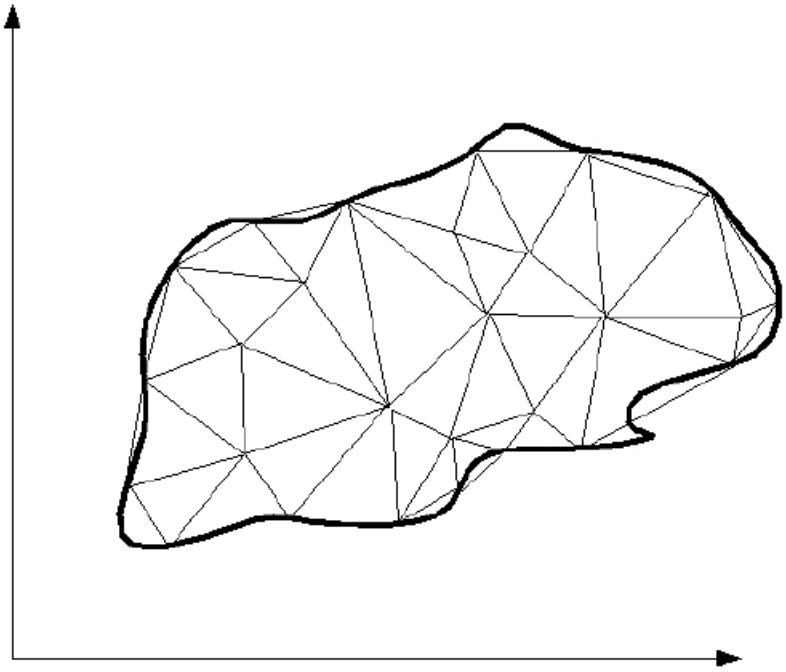

Figure B.1: A triangulation of a domain

Definition B.0.2. $\mathcal{T} := \{T_1, ..., T_{N_\mathcal{T}}\}$ *is called a (conforming)* triangulation *of* Ω*, if the following conditions are fulfilled: (see [8])*

1. T_i *are open triangles (elements) for* $1 \leq i \leq N_\mathcal{T}$*;*
2. T_i *are disjoint, i.e.* $T_i \cap T_j = \emptyset$ *for* $i \neq j$*;*
3. $\bigcup_{1 \leq i \leq N_\mathcal{T}} \overline{T_i} = \overline{\Omega}$*;*
4. *for* $i \neq j$ *the set* $\overline{T_i} \cap \overline{T_j}$ *is either*
    i. *empty, or*

ii. a common edge of T_i and T_j, or

iii. a common vertex of T_i and T_j.

Examples of conforming and non-conforming triangles are given in Figure B.2.

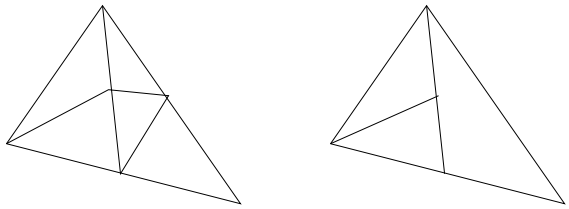

Figure B.2: Examples of conforming and non-conforming triangulation.

Let $\mathcal{T}_0$ be a triangulation of Ω. If we subdivide a subset of triangles of $\mathcal{T}_0$ into sub-triangles such that the resulting set of triangles is again a triangulation of Ω, then we call this a refinement of $\mathcal{T}_0$. Let the new triangulation be $\mathcal{T}_1$. If we proceed in this way, we can construct a sequence of triangulations $\{\mathcal{T}_k\}_{k\geq 0}$ such that $\mathcal{T}_{k+1}$ is a refinement of $\mathcal{T}_k$.

Let now $\mathcal{T}$ be a *conforming triangulation*. Our next task is to define a *finite element space* $\mathbb{X}_h$. For the moment we know only that $\mathbb{X}_h$ is a finite dimensional space of functions defined over the domain $\overline{\Omega}$. With the help of $\mathbb{X}_h$ we define the space

$$P_T = \{v_h|_T;\ v_h \in \mathbb{X}_h\}\,.$$

The members of this space are the restrictions of the functions $v_h \in \mathbb{X}_h$ to the elements (triangles) $T \in \mathcal{T}$. It is natural now to obtain some conditions guaranteeing that the inclusion $\mathbb{X}_h \subset \mathbb{H}^1(\Omega)$ holds (if you remember, our goal is to approximate solutions of problems belonging to the space $\mathbb{H}^1(\Omega)$).

Theorem B.0.2. *Assume that $\mathbb{X}_h \subset \mathbb{C}(\overline{\Omega})$ and $P_T \subset \mathbb{H}^1(T)$ for all $T \in \mathcal{T}$. Then*

$$\mathbb{X}_h \subset \mathbb{H}^1(\Omega),$$

$$\mathbb{X}_{h0} := \{v_h \in \mathbb{X}_h;\ v_h = 0 \text{ on } \partial\Omega\} \subset \mathbb{H}^1_0(\Omega)$$

Having in mind all previous considerations, we summarize the properties of a finite element space.

1. A finite element space is described by the underlying triangulation $\mathcal{T}$ of the domain $\overline{\Omega}$.

2. For each element T of the triangulation $\mathcal{T}$ the space

$$P_T = \{v_h|_T;\ v_h \in \mathbb{X}_h\}$$

   contains polynomials of certain degree.

3. There exists a canonical basis in the space $\mathbb{X}_h$, whose functions are easy to describe using the information on local elements.

Remark B.0.2. *In general, for our approximations we will use the finite element space $\mathbb{X}_{h0}$ for solving the second-order problems with homogeneous Dirichlet boundary and the space $\mathbb{X}_h$ if we are solving a second order Neumann problem.*

Remark B.0.3. *A common way to define the basis functions associated with the degrees of freedom is to take functions $\varphi_i \in P_1(T),\ i = 1, 2, 3$, such that*

$$\varphi_i(a_j) = \delta_{ij} = \begin{cases} 1 & \text{if} \quad i = j \\ 0 & \text{if} \quad i \neq j \end{cases}$$

for $i, j = 1, 2, 3$.

Note, that we can analogously define other finite element spaces using the spaces of higher degree polynomials. Here we state only a theorem on general Lagrange elements.

Theorem B.0.3. *Let the domain $\Omega \in \mathbb{R}^d$ be decomposed into triangles through the triangulation $\mathcal{T}$. Assume that the grid G_k is of order k, it means*

$$G_k := \bigcup_{T \in \mathcal{T}} G_k(T) = \{a_j,\ j = 1, 2, \cdots, N\}.$$

If the values of u_h on the grid G_k are known, then using these values we can uniquely determine a function $u_h \in \mathbb{X}_h \subset \mathbb{H}^1(\Omega)$ with

$$\mathbb{X}_h = \left\{u_h \in \mathbb{C}^0(\overline{\Omega});\ u_h|_T \in \mathbb{P}_k(T),\ T \in \mathcal{T}\right\}.$$

A basis of $\mathbb{X}_h$ is given as a collection of functions $\varphi_j \in \mathbb{X}_h$ such that

$$\varphi_j(a_i) = \delta_{ji}, \quad i, j = 1, 2, \cdots, N.$$

where δ_{ji} is the well known Kronecker delta function.
The basis functions on the given triangulation for linear, quadratic and 4th order finite elements are visualized in Figures B.3, B.4 and B.5.

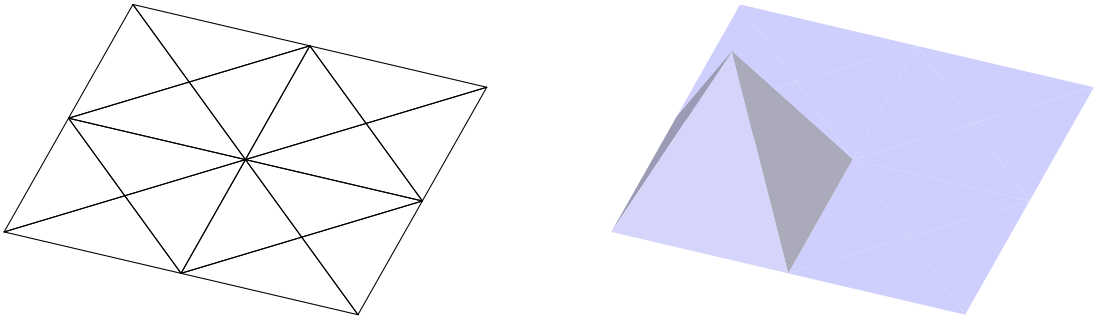

Figure B.3: Mesh and linear basis function.

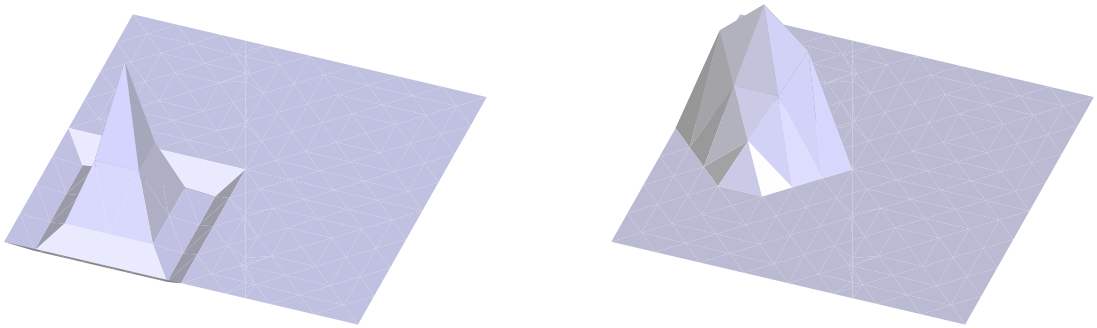

Figure B.4: Quadratic basis functions.

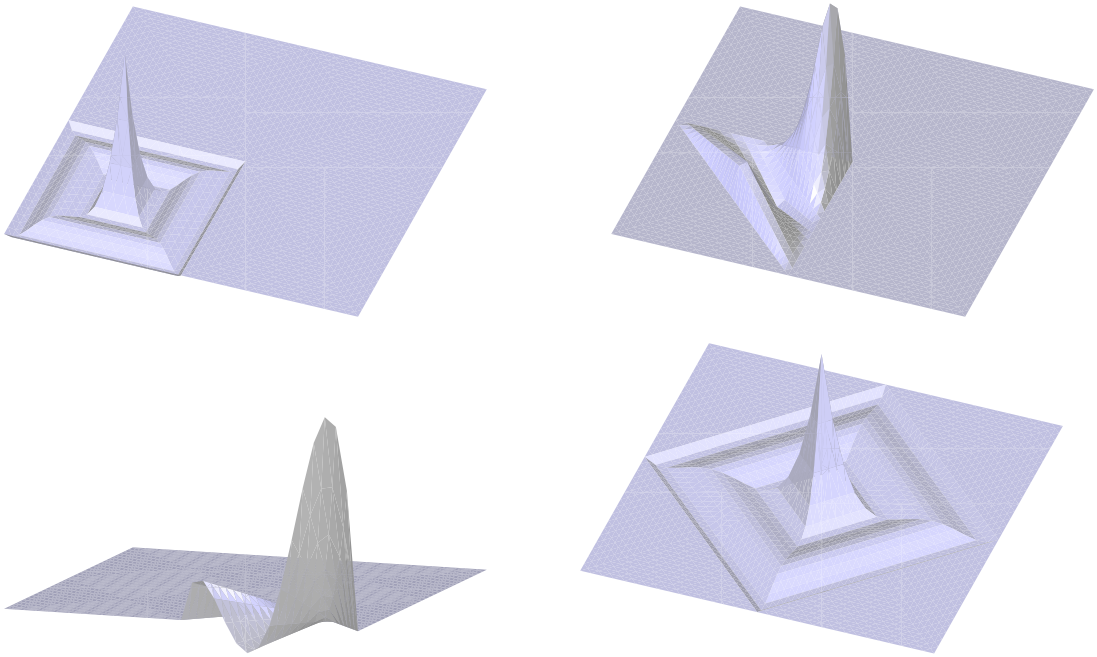

Figure B.5: 4th order basis functions.

B.0.1 Galerkin discretization

In the theory of classical solutions it is natural to use approximation procedures which are based on a point-wise evaluation of functions and differential operators. When dealing with weak solutions this approach cannot be taken over, because point values of functions in $\mathbb{H}^m(\Omega)$ are in general not defined, if $m - \frac{n}{2} \leq 0$ (m and n are the corresponding Sobolev numbers). The formulation of the original problem as weak problem suggests a different strategy to convert the infinite dimensional space into a finite dimensional one which then allows a numerical treatment.

Having in mind the old notations, let us again consider the following problem:

Problem B.0.2. *For a given $f \in \mathbb{X}^*$, find $u \in \mathbb{X}$ such that*

$$a(u, v) = \langle f, v \rangle \text{ for all } v \in \mathbb{X}.$$

Then discretization is obtained by replacing $\mathbb{X}$ with a finite dimensional subspace $\mathbb{X}_h$. To get a numerical approximation to the unknown function u, the idea of *Galerkin method* is to find $u_h \in \mathbb{X}_h$ such that

$$a(u_h, v) = \langle f, v \rangle \quad \text{for all } v \in V_h, \tag{B.1}$$

which is a finite dimensional problem.
We introduce a basis $\{\varphi_1, \varphi_2, ..., \varphi_n\}$ of V_h and taking into consideration the fact that (B.1) is satisfied for any $v \in V_h$, we replace v by basis functions:

$$a(u_h, \varphi_i) = \langle f, \varphi_i \rangle. \tag{B.2}$$

Now the desired approximate solution u_h is represented by means of chosen basis functions:

$$u_h = \sum_{j=1}^{n} U_j \varphi_j. \tag{B.3}$$

If this expression for u_h is now substituted into (B.2), we obtain the following system of equations:

$$\sum_{j=1}^{n} a(\varphi_j, \varphi_i) U_j = \langle f, \varphi_i \rangle \text{ for } i = 1, \ldots, n, \tag{B.4}$$

which must be solved for the unknowns $U_1, U_2, \cdots, U_n$. The equation (B.4) permits us to write it in the form

$$SU = B \tag{B.5}$$

with the matrix $S_{ij} = a(\varphi_j, \varphi_i)$, vector $B_i = \langle f, \varphi_i \rangle$ and U being the column vector of coefficients U_j. S is called the *stiffness matrix* and B is called the *load vector*.

For a given space $\mathbb{X}_h$, solving the corresponding discrete Problem (B.1) amounts to finding the coefficients U_j of the expansion (B.3) over the basis functions φ_j, $j = 1, 2, ..., n$. Thus, in order to obtain the numerical solution of any second order elliptic problem one has first, to compute the stiffness matrix S and load vector B for the specific problem, and second, to solve the algebraic system (B.5).

Appendix C

ALBERTA - An adaptive finite element toolbox

All proceeding calculations have been done using the finite element toolbox ALBERTA developed by Siebert and Schmidt, [46]. ALBERTA provides all needed tools for the efficient implementation and adaptive solution of general nonlinear problems in several space dimensions. It is a library with data structures and functions for adaptive finite element simulations in one, two and three dimension. Using these data structures, the finite element toolbox ALBERTA makes possible the usage of such abstract frameworks as finite element spaces and adaptive strategies, together with hierarchial meshes, routines for mesh adaption, administration of finite element spaces and corresponding degrees of freedom during mesh modification. Moreover, a wide range of tools for numerical quadrature, stiffness matrix and load vector assemblage, as well as diverse linear solvers for the system of algebraic equations, like conjugate gradient method, are available and easy to handle.
We ask the reader to consult [46] for the software and detailed documentation.

Bibliography

[1] R. Adams and J. Fournier *Sobolev spaces*, Academic press, 2003.

[2] N. Arai, A. Matsunami and S.W. Churchill *A Review of Measurements of Heat Flux Density Applicable to the Field of Combustion*, Experimental, Thermal and Fluid Science, 12, 1996, 452-460.

[3] T. Barth and J.A. Sethian *Numerical schemes for the Hamilton-Jacobi and level set equations on triangulated domains*, Journal of Computational Physics, 145, 1998, 1-40.

[4] E. Bänsch, A. Schmidt *Simulation of dendritic ctystal growth with thermal convection*, Interfaces and free boundaries, 2, 2000, 95-115.

[5] K.A. Bunting and G. Cornfield *Toward a General Theory of Cutting: A Relationship Between the Incident Power Density and the Cut Speed*, Transactions of the ASME, 116, 1975.

[6] J. Chessa, P. Smolinski and T. Belytschko *The extended finite element method for solidification problems*,Int. J. Numer. Methods Eng., 53, No.8, 2002, 1959-1977.

[7] D.L. Chop *Computing minimal surfaces via level set curvature flow*, J. Comput. Phys., 106, 1993, 77-91.

[8] P. G. Ciarlet, *The finite element method for elliptic problems*, North-Holland, 1987.

[9] M.G. Crandal and P-L. Lions *Viscosity solutions of Hamilton-Jacobi equations*, Transactions of AMS, 277, 1983,1-43.

[10] M.G. Crandal, L.C. Evans and P-L. Lions *Some properties of viscosity solutions of Hamilton-Jacobi equations*, Transactions of AMS, 282, 1984,487-502.

[11] S. Dachkovski, M. Böhm *Finite thermoplasticity with phase changes based on isomorphisms*, International Journal of Plasticity, 2o, 2004, 323-334.

[12] K. Eriksson and C. Johnson, *Adaptive finite element methods for parabolic problems I: A linear model problem*, SIAM J. Numer. Anal., 28 (1991), pp. 43–77.

[13] L.C. Evans *Partial Differential Equations*, Graduate Studies in Mathematics, vol. 19, AMS, 1998.

[14] A. Fichera *Problemi elastostatici con vincoli unilaterali: il problema di Signorini con ambigue condizioni al contorno*, Atti Accad. Naz. Lincei Mem. Cl. Sci. Fis. Mat. Natur. Sez. Ia, 7(8), 1964, 91-140.

[15] J.M. Fried *Niveauflächen zur Berechnung zweidimensionaler Dendrite*, Ph.D. thesis, Freiburg, 1999, 91-140.

[16] A. Friedman and L. Jiang *A Stefan-Signorini Problem*, J. Differential Equations, 51, 1984, 213-231.

[17] A. Friedman and D. Kinderlehrer *A one phase Stefan problem*, Indiana University Mathematics Journal, 24, No.11, 1975, 1005-1035.

[18] R. Glowinski,J.-L. Lions and R. Tremolier *Numerical Analysis of Variational Inequalities (Russian Translation)*, Mir, Moscow, 1979.

[19] H. Hafercamp,M. Niemeyer,J. Hoerner, J. Bosse,M. Kock,F. Knemann *Numerical Modelling of Thermal Plasma Cutting*, Thermal cutting conference, Timisoara, 1999.

[20] L. Jiang *Remarks on the Stefan-Signorini problem*, Free boundary problems. Theory and applications, vol. II, Research Notes in Math., 79, 1988.

[21] C. Johnson *Numerical solution of partial differential equations by the finite element method*, Cambridge University Press, 1994.

[22] J.-L. Lions *Quelques methodes de resolution des problemes aux limites non lineaires*, Dunod, Paris, 1969.

[23] R. Dautrey and J.-L. Lions *Mathematical analysis and numerical methods for science and technology*, vol. 3, Springer, 2000.

[24] R. Dautrey and J.-L. Lions *Mathematical analysis and numerical methods for science and technology*, vol. 5, Springer, 2000.

[25] J.-L. Lions, G. Stampacchia *Variational Inequalities*, Comm. Pure Appl. Math, 20, 1967, 493-519.

[26] S.L. Kamenomostskaya *On Stefan problem*, Matematicheskij Sbornik, vol.53(95), no.4, 1961, 489-514, (in Russian).

[27] M.L. Kim *Transient evaporative laser-cutting with boundary element method*, Journal of applied mathematical modeling, vol.25, 2000, 25-39.

[28] D. Kinderlehrer, G. Stampacchia *An introduction to Variational Inequalities and their applications*, SIAM, 2000.

[29] K. Matsuyama *Mathematical modelling of kerf formation phenomena in thermal cutting*, Welding in the world, vol.39, no.1, 1997, 28-34.

[30] A.M. Meirmanov *The Stefan Problem*, Walter de Gruyter, Berlin-New York, 1992.

[31] A.M. Meirmanov *The Stefan problem with surface tension in the three dimensional case with spherical symmetry: Non existence of the classical solution*, Euro. J. Appl. Math., vol. 4, 1993, 1-19.

[32] G. Minty *Monotone non linear operators in Hilbert space*, Duke Math. J., 29, 1962,341-346.

[33] W. Mitchell *A comparison of adaptive refinement techniques for elliptic problems*, ACM Trans. Math. Softw., 15, 1989,326-347.

[34] W. Mulder, S. Osher and J.A. Sethian *Computing Interface Motion in Compressible Gas Dynamics*, Journal of Computational Physics, 100(2), 1992, 209-228.

[35] A. Muntean *A Moving-Boundary Problem: Modeling, Analysis and Simulation of Concrete Carbonation* , Ph.D. thesis, ZeTeM, University of Bremen, 2006.

[36] V.A. Nemchinski *Dross formation and heat transfer during plasma arc cutting*, J.Phys. D:Appl. Phys., 30, 1997, 2566-2572.

[37] K. Ohmori *Numerical solution of two-fluid flows using finite element method*, Applied mathematics and computation, 92, 1998, 125-133.

[38] S. Osher and J.A. Sethian *Fronts Propogating with Curvature-Dependent Speed: Algorithms Based on Hamilton-Jacobi Formulations*, Journal of Computational Physics, 79, 1988, 12-49.

[39] D. Peng, B. Merriman, S. Osher, H. Zhao and M. Kang *A PDE-based fast local level set method*, Journal of Computational Physics, 155, 1999, 410-438.

[40] D. Rosenthal *Mathematical Theory of Heat Distribution During Welding and Cutting*, Welding J., 20, 1941,220-234s.

[41] J.A. Sethian *Level set methods and fast Marching methods*, Cambridge University Press,2003.

[42] J.A. Sethian and D. Adalsteinson *The fast construction of extension velocities in level set methods*, Journal of Computational Physics, 148, 1999, 2-22.

[43] A. Schmidt *Computation of three dimensional dendrites with finite elements*, Journal of Computational Physics, 125, 1996, 293-312.

[44] A. Schmidt, M. Wolff, M. Böhm and G. Löwisch *Modelling and testing of transformation-induced plasticity and stress-dependent phase transformations in steel via simple experiments*, Computational Materials Science, 32, 2005, 604-610.

[45] A. Schmidt, M. Wolff, M. Böhm *Phase transitions and transformation-induced plasticity of steel in the framework of continuum mechanics*,J. Phys. IV, 120, 2004, 145-152.

[46] A. Schmidt and K.G. Siebert *Design of adaptive finite element software: The finite element toolbox ALBERTA*, Lecture notes in computational science and engineering, vol.42, Springer, 2005.

[47] W. Schulz, V. Kostrykin, et al. *A Free Boundary Problem Related to Laser Beam Fusion Cutting:ODE Approximaton*, Int. J. Heat Mass Transfer, vol.40, no. 12, 1997, 2913-2928.

[48] Z. Shen, S. Zhang, J.Lu, X.Ni *Mathematical modelling of laser induced heating and melting in solids*, Optics and laser technology, vol.40, no. 8, 2001, 533-537.

[49] P.S. Sheng and V.S. Joshi *Analysis of Heat-affected Zone Formation for Laser Cutting of Stainless Steel*, J. Material Processing Technology, 53, 1995, 879-892.

[50] S.L. Sobolev *On a theorem of functional analysis*, Mat. Sb., 46, 1938, 471-496.

[51] S.L. Sobolev *Some applications of functional analysis in mathematical physics (Russian)*, Hauka, Moscow, 1988.

[52] J. Steinbach *A Variational Inequality Approach to Free Boundary Problems with Applications in Mould Filling*, Birkhäuser Verlag, Basel-Boston-Berlin, 2002.

[53] M. Storti *Numerical modeling of ablation phenomena as two-phase Stefan problems*, Int.J.Heat Mass Transfer, vol.38, no 15, 1995, 2843-2854.

[54] M. Sussman, P. Smereka and S. Osher *A level set approach for computing solutions to incompressible two-phase flow*, J. Comp. Phys., 114, 1994, 146-159.

[55] B.A. Ton *A Stefan-Signorini problem with set-valued mappings in Domains with intersecting fixed and free boundaries*, Bollettino U.M.I., 7, 1994, 231-249.

[56] J. Xi and A. Kar *Mathematical modelling of melting during laser materials processing* , Jornal of Applied Physics, vol.81, no 7, 1997, 3015-3022.

[57] W. Yu *A Stefan-Signorini problem with Gibbs-Thomson law* , Applicable Analysis, vol.61, 1996, 67-86.